ABSTRACT

Late Quaternary Alaskan Paleoclimate: Geoarchaeological Insights into the Pleistocene-Holocene Transition

Lyndsay M. DiPietro, Ph.D.

Mentor: Steven G. Driese, Ph.D.

Eastern Beringia is a region which has undergone dramatic changes since the end of the Last Glacial Maximum, environmentally and climatically. These changing conditions likely contributed to the changes in human behavior observed in the earliest human inhabitants who migrated into the region sometime within this time period. In order to better understand the relationship between shifting paleoenvironmental conditions and human behavior, it is crucial to have a detailed understanding of what those climatic changes looked like in the regions these early Beringians were inhabiting. To accomplish this goal, this dissertation uses modern pedological, micromorphological, and sedimentological analyses to reconstruct paleoclimate and the site formation history of three archaeological sites in Alaska: Dry Creek in the Nenana River Valley, Owl Ridge in the Teklanika River Valley, and Serpentine Hot Springs on the Seward Peninsula. This work reveals a progressive transition from cold, dry, open tundra conditions following the Last Glacial Maximum to cool, moist, boreal forest conditions in the middle to late Holocene, though this transition was not a smooth one.

Late Quaternary Alaskan Paleoclimate: Geoarchaeological Insights into the Pleistocene-Holocene Transition

by

Lyndsay M. DiPietro, B.S.

A Dissertation

Approved by the Department of Geosciences

_____

Stacy C. Atchley, Ph.D., Chairperson

Submitted to the Graduate Faculty of
Baylor University in Partial Fulfillment of the
Requirements for the Degree
of

Doctor of Philosophy

Approved by the Dissertation Committee

_____

Steven G. Driese, Ph.D., Chairperson

_____

Stephen I. Dworkin, Ph.D.

_____

Daniel J. Peppe, Ph.D.

_____

Katie M. Binetti, Ph.D.

_____

Kelly E. Graf, Ph.D.

_____

Ted Goebel, Ph.D.

Accepted by the Graduate School

December 2018

_____

J. Larry Lyon, Ph.D., Dean

Page bearing signatures is kept on file in the Graduate School.

TABLE OF CONTENTS

LIST OF FIGURES

LIST OF TABLES

ACKNOWLEDGMENTS

Science should be a collaborative endeavor. If there is anything I have learned throughout the course of my time in graduate school, it is this. There are many people, aside from myself, without whom this dissertation would not exist and many more without whom it would look very different than it does now. Now that I am nearing the end of this process, I would like to express my gratitude to these people.

First and foremost, perhaps, is my advisor, Dr. Steve Driese, who has been nothing but encouraging and supportive throughout this process. I know I have not been the easiest graduate student to mentor, nor has this project come together without much weeping and gnashing of teeth, but Dr. Driese has persevered throughout and has encouraged me to do the same. He has provided me with the academic and financial support to see this project through and for that, I thank him. Likewise, my committee members, those who are currently serving and those who have been willing to serve in this capacity in the past, Dr. Steve Dworkin, Dr. Dan Peppe, Dr. Lee Nordt, Dr. Joe Ferraro, and Dr. Katie Binetti, have been gracious in editing my work, giving guidance, and helping make this work better than it was before. I would especially like to thank Dr. Kelly Graf and Dr. Ted Goebel, both of whom have treated me like their own graduate student, supervising my field work, providing thorough and constructive feedback on my papers, and offering more help than I could have hoped for. Additionally, I would like to thank Dr. Mike Waters, who collected many of the samples used for this dissertation.

I also owe a debt of gratitude to my parents, who have supported me throughout my time at Baylor. I appreciate their willingness to give advice and help me keep my focus at the times when I needed it most. I would be remiss not to thank my friends as well, for putting up with me in these last stages of this process. Finally, I need to thank my dearest friend of all, who has been a constant source of encouragement, of good advice, and of thought-provoking conversation in the times when it seemed this project might not come together. It has, in large part because of your willingness to believe that it would even when I did not.

ATTRIBUTIONS

In addition to myself, several other people have contributed intellectually to this dissertation. Although the writing itself is almost entirely my work, my co-authors have made contributions to Chapters Two, Three and Four of this work.

Tyler Nelson and Dr. Jane Harvill from the Department of Statistics at Baylor University completed the numerical grain size partitioning discussed in Chapter Two. In addition to this work, the worked together to write the portion of the methods section relating to that statistical analysis and created Figures 2.4 and 2.7.

Dr. Ted Goebel contributed to the discussion of the lithics analysis in Chapter Three and provided the dates contained in table 3.1. He also edited the chapter for readability.

Dr. Kelly Graf contributed the excavation maps in Figures 4.1, 4.2, 4.3, and 4.4, in addition to sketching the soil profiles pictured in these same figures. She also edited much of the text. Dr. Gary Stinchcomb did preliminary analysis on the thin sections discussed in this paper and many of his observations are summarized in the results section of the chapter.

Dr. Steven Driese edited all three chapters for clarity.

CHAPTER ONE

Introduction

The late Quaternary is a time marked by rapidly shifting climatic conditions. The end of the Last Glacial Maximum (LGM) brought with it profound changes in atmospheric circulation, mean annual temperature and precipitation, and the distribution of floral, faunal, and human populations across the planet as ice sheets retreated. In few places has this dynamic climate had such a major effect on the landscape as it has in eastern Beringia, where this interval saw the decline of many tundra ecosystems, Pleistocene megafauna, and eventually the Bering Land Bridge itself and the migration of Paleolithic peoples from Siberia into Alaska and northern Canada.

This dynamic climate and the resultant landscape transformations during the late Quaternary, as well as the rich archaeological record in the area make eastern Beringia an ideal location to study the connections between changing climate and human behavior. To make these connections, however, the sequence and nature of these late Quaternary climate shifts must be well-defined and characterized. Much attention has been paid to this topic since around the 1970s and, as a result of lake core pollen studies and regional geological surveys, the general chronology of post-LGM climate events has been established for much of Alaska. What is less clearly understood, though, is the nature of these regional-scale climate events in more localized contexts that have clear evidence of late Pleistocene human occupants. Thankfully, the periglacial soils and sediments at many of these archaeological sites provides ample opportunity to begin addressing this

issue. This dissertation uses up-to-date analytical techniques to examine the site and soil formation processes at three Alaskan archaeological sites, two in central Alaska and one on the Seward Peninsula, in order to better understand the local climatic and environmental changes that occurred at these sites during the late Quaternary.

Chapter Two (DiPietro et al., 2017) of this dissertation focuses on the Dry Creek archaeological site, a well-stratified set of aeolian deposits with late Pleistocene occupational layers in the Nenana River Valley of central Alaska. The Nenana River Valley loess deposits are a nearly continuous record of climate following the LGM, making them an invaluable source of information about paleoatmospheric circulation. This chapter uses a numerical grain size partitioning technique to document a high-resolution record of wind intensity throughout the late Quaternary at Dry Creek.

Chapter Three (DiPietro et al., 2018) focuses on the Serpentine Hot Springs archaeological site in Bering Land Bridge National Park on the Seward Peninsula. The Serpentine Hot Springs site records the presence of fluted-point-making Paleolithic peoples in Beringia during the Younger Dryas (YD) climate event. This study uses micromorphological and geochemical data, coupled with scanning electron microscopy to reconstruct the depositional and pedogenic history of the profile at Serpentine Hot Springs.

Chapter Four (DiPietro et al., *in review*) returns its focus to central Alaska, discussing site formation and pedogenesis at the Owl Ridge archaeological site in the Teklanika River Valley. Owl Ridge is a key site for understanding the variability in late Pleistocene/early Holocene lithic assemblages in Alaska, but little geoarchaeological work from the site has been published. This chapter uses soil micromorphology, particle

size analysis, and organic and inorganic geochemical analyses to better understand the factors which shaped both the paleoenvironment and the way humans exploited the landscape during the late Pleistocene and early Holocene in the Teklanika River Valley.

CHAPTER TWO

Variations in Late Quaternary Wind Intensity from Grain-Size Partitioning of Loess Deposits in the Nenana River Valley, Alaska

This chapter published as: DiPietro, L. Nelson, T., Driese, S., Harvill, J., Variations in late Quaternary wind intensity from grain-size partitioning of loess deposits in the Nenana River Valley, Alaska, 2017. Quaternary Research, .87, 258-274.

Abstract

Continental loess is a rich record of paleoatmospheric data. A high-resolution column of 57 loess samples was collected from the Dry Creek archaeological site in the Nenana River Valley in central Alaska. Numerical grain-size partitioning using a mixed Weibull function was performed on grain-size distributions to obtain a reconstructed record of wind intensity over the last ~15,000 years. Two grain-size components were identified, one with a mode in the coarse silt range (C1) and the other ranging from medium- to very-coarse sand (C2). C1 dominates most samples and records regional northerly winds carrying sediment from the Nenana River. These winds were strong during cold intervals, namely the Carlo Creek glacial re-advance (14.2-14 ka) a late Holocene Neoglacial period (4.2-2.7 ka) and recent glacier expansion, weak during the Allerød (14-13.3 ka) and Younger Dryas (12.9-11.7 ka), and variable during the Holocene Thermal Maximum (11.4-9.4 ka). Deposition of C2 was episodic and represents locally-derived sand deposited by southerly katabatic winds from the Alaska Range. These katabatic winds occurred mainly prior to 12 ka, and after 4 ka. This study shows that numerical grain-size partitioning is a powerful tool for reconstructing paleoclimate and that it can be successfully applied to Alaskan loess

Introduction

Loess, or windblown silt, is one of the most useful sources of terrestrial paleoclimate information being studied today. It is widespread in the Quaternary, and can be correlated to marine foraminiferal oxygen isotope records (Kukla et al., 1988; Hovan et al., 1989; Begét et al., 1989). Loess deposition provides direct information about paleoatmospheric circulation and paleowinds (Lagroix and Banerjee, 2002; Muhs and Bettis, 2003; Muhs and Budahn, 2006) and can also serve as a proxy for paleoprecipitation and paleotemperature (Maher and Thompson, 1995; Deng et al., 2001).

Although loess studies have been commonplace in Alaska for over a century (e.g., Tarr and Martin, 1913), they are still fewer in number and scope than studies focusing on the Chinese Loess Plateau and other Asian dust deposits. Most Alaskan studies have focused on one of the following areas: 1) deposition (Begét and Hawkins, 1989); 2) loess origin and provenance (Pewe, 1955; Lagroix and Banerjee, 2002; Muhs and Budahn, 2006; Muhs et al., 2016); 3) chronology (Berger, 1987; Berger et al., 1996; Westgate et al., 1990; Preece et al., 1999; Berger, 2003); 4) magnetic properties (Begét et al., 1990; Liu et al., 1999; Vlag et al., 1999; Liu et al., 2001); and 5) paleosol significance (Muhs et al., 2003, 2004, 2008). The ultimate goal of these studies has been to determine the utility and implications of Alaskan loess records for paleoclimate reconstructions, largely by constraining atmospheric circulation patterns, wind intensities, and trends in precipitation and temperature change. In general, little has been written about the grain-size distribution of Alaskan loess and its implications for paleoclimate, despite the fact that such studies have been successfully conducted on Asian loess deposits. Such studies could provide crucial new insight into some of the most important topics in Alaskan

paleoclimate research, including high-latitude atmospheric circulation patterns and wind intensity during the last glacial-interglacial cycle and beyond.

Grain-size analysis provides information on depositional mechanisms of sediments as well as insight into spatio-temporal changes in deposition, which may be related to climate. Many strategies have been employed to gather paleoclimate information from grain-size data, particularly with regards to loess. Mass accumulation rates (MAR) have been used as indicators of continental or source-area aridity (Pye, 1995) and median grain diameter is commonly used as a proxy for mean wind intensity (An et al., 1991; Porter and An, 1995; Pye, 1995; Xiao et al., 1995). This latter measure has received much attention in the literature but is a less meaningful metric in polymodal sediments than in unimodal sediments. Recently, numerical grain-size partitioning has been employed to better describe changes in the distribution of polymodal (particularly aeolian) sediments (Sun et al., 2002, 2004; Lim and Matsumoto, 2006; Sun et al., 2008; Xiao et al., 2009; Park et al., 2014). The theoretical basis for this technique rests on the idea that different transport mechanisms produce unique modal grain-sizes in the sediment they deposit (Harding, 1949; Middleton, 1976; Ashley, 1978; Bagnold and Barndorff-Nielson, 1980). Thus, a polymodal grain-size distribution is the weighted sum of the modal distribution of all contributing sediment inputs and depositional processes. Numerical grain-size partitioning statistically models polymodal distributions as a mixture of unimodal distributions and quantitatively partitions the data into genetically distinct components (Sun et al., 2002). Changes in the relative proportions and modes of each component can then be interpreted in terms of changes in each depositional

mechanism. Although this technique has been widely applied to Asian dust sources, it has yet to be used in Alaska.

In this paper, we use a mixture of Weibull distributions to numerically partition the grain size of the aeolian deposits at the Dry Creek archaeological site, located in the Nenana Valley of central Alaska, into two primary components. The aim of this study is to provide a high-resolution record of late Pleistocene-Holocene wind intensities in the Nenana Valley and to demonstrate the applicability and utility of numerical grain-size modelling for Alaskan loess deposits.

Background

Study Site

The Dry Creek archaeological site is located north of Healy, Alaska in the central part of the state (Fig. 2.1). It is located on a south-facing bluff overlooking Dry Creek that is 3 km west from its confluence with the Nenana River (Fig. 2.2). Geographically, the site is in the northern foothills of the Alaska Range, about 10 km north of the Range proper. Dry Creek is noteworthy not only for its archaeological importance (Thorson and Hamilton, 1977; Graf et al., 2015) but also as a type-section for the late Quaternary stratigraphy of the Nenana River Valley. A nearly-continuous post-glacial loess mantle between 1 and 3 meters in thickness blankets the Nenana River Valley, absent only where the river exits the Alaska Range (Thorson and Bender, 1985). The Dry Creek site is perhaps the best-studied portion of this loess cap and its stratigraphy has been well-documented (Thorson and Hamilton, 1977). Stratigraphically, the site consists of 1-2 meters of aeolian deposits resting atop a Healy-age outwash terrace. Seven loess units, four sands, and five weakly-developed paleosols have traditionally been identified at the

site, capped by a modern cliff edge sand (Fig. 2.2). Mineralogically, the loess is quite uniform, consisting primarily of quartz, muscovite, and metamorphic rock fragments, reflecting the schistose nature of the regional bedrock.

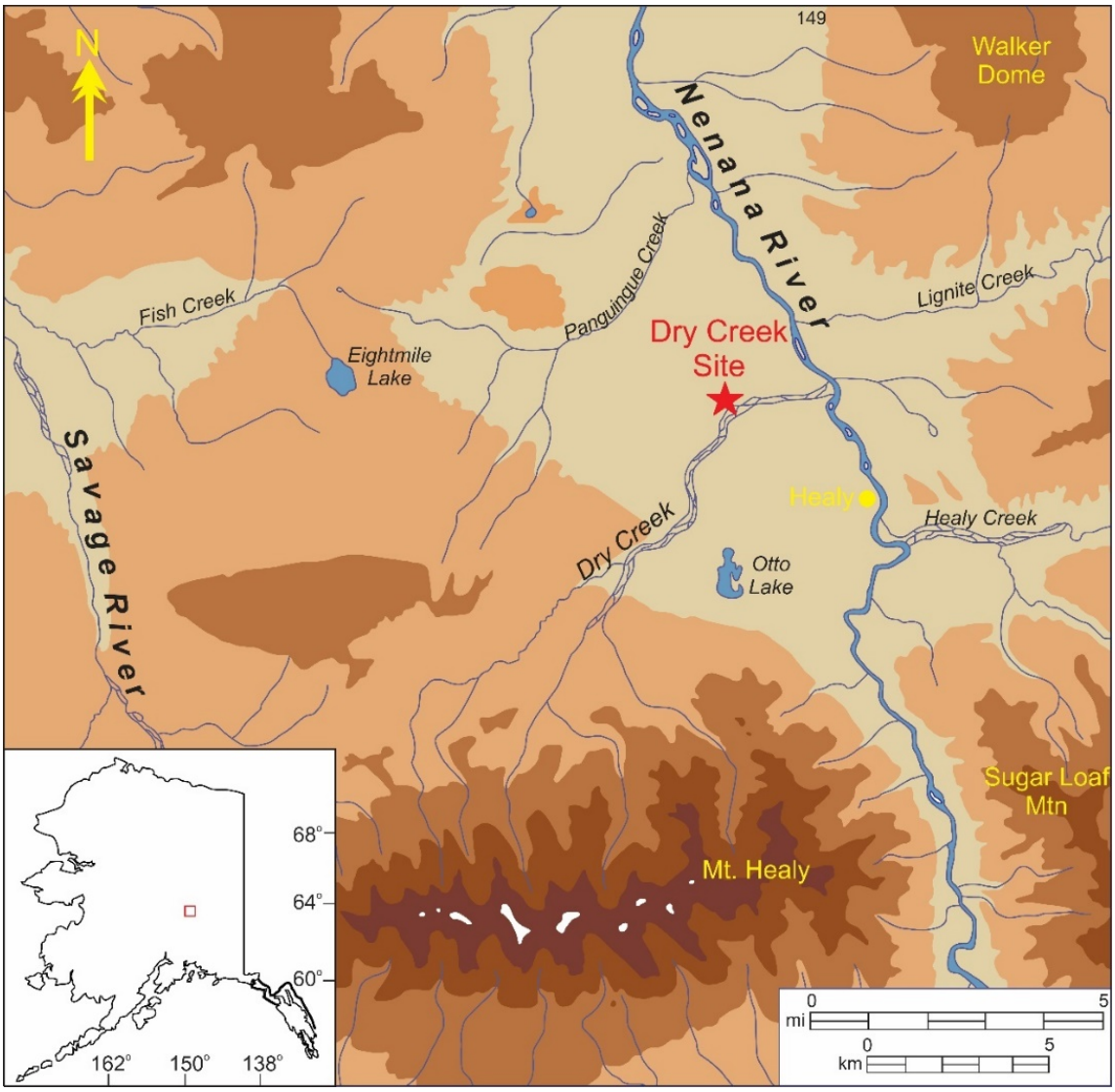

Figure 2.1. Location of the Dry Creek site in the Nenana River Valley, central Alaska.

Figure 2.2. a) Dry Creek site as viewed from the southern bank of Dry Creek; b) Photograph of the Dry Creek stratigraphic profile from the 2009-2011 excavation with locations and designations of loess units (blue) and paleosols (yellow) noted.

Because of its importance for early North American archaeology, the site's chronology has been well-established (Thorson and Hamilton, 1977; Powers et al., 1983; Bigelow and Powers, 1994; Graf et al., 2015). Radiocarbon dates suggest that the aeolian package preserved at the site began accumulating sometime prior to about 13.5 ka, and deposition has continued until recent times.

Regional Climatology

Modern Beringian climate patterns are the result of the interplay between four main pressure cells: the Siberian High, Canadian Low, Aleutian Low, and Pacific Subtropical High (Mock et al., 1998). During the winter, the Canadian and Siberian highs are well-developed to the northeast and west of Alaska, respectively, while the Aleutian Low dominates over the Bering Sea. This results in strong winds moving across central Alaska from the northeast, flowing from the Canadian High to the Aleutian Low (Fig. 2.3a). During the summer, the Aleutian Low and Canadian High-pressure cells are

diminished and the Pacific Subtropical High strengthens and migrates northward to affect southern and central Alaska, resulting in weaker winds blowing across central Alaska from the southwest (Fig. 2.3b). Winds capable of entraining and depositing loess occur during both seasons, following the prevailing directional trends described above, but dust storms are more commonly observed during the summer and fall months when snow and ice cover are absent from the major floodplains that serve as regional sediment sources. (Begét, 2001; Muhs, 2003; Muhs and Budahn, 2006; Hatfield and Maher, 2009; Graf and Bigelow, 2011; Muhs et al. 2016). In the Nenana Valley, modern winds have come predominantly from the north for the past decade, save for February, April, and July, which have southerly average winds (WRCC, 2017).

Beringia has seen major changes in boundary conditions since the end of the Last Glacial Maximum (LGM), namely a decrease in ice sheet size, reduction in glaciers, and the formation of the Bering Strait, which could have had significant implications for the fundamental workings of its climate system in the past. Some studies of paleowind have suggested marked shifts in wind patterns between interglacial and glacial times (Lagroix and Banerjee, 2002, 2004 ; Muhs and Budahn, 2006). During glacial times, 'winter-type' circulation may dominate, with winds coming predominantly from the northeast, whereas 'summer-type' circulation with weaker southwesterly winds may dominate during interglacial periods, although these findings are far from ubiquitous (Jensen et al., 2016). Katabatic winds were also common in the past and there is evidence for major post-LGM deflation by such high-velocity winds in the Nenana River Valley (Thorson and Bender, 1985). Such winds may run contrary to the prevailing wind directions at any given time.

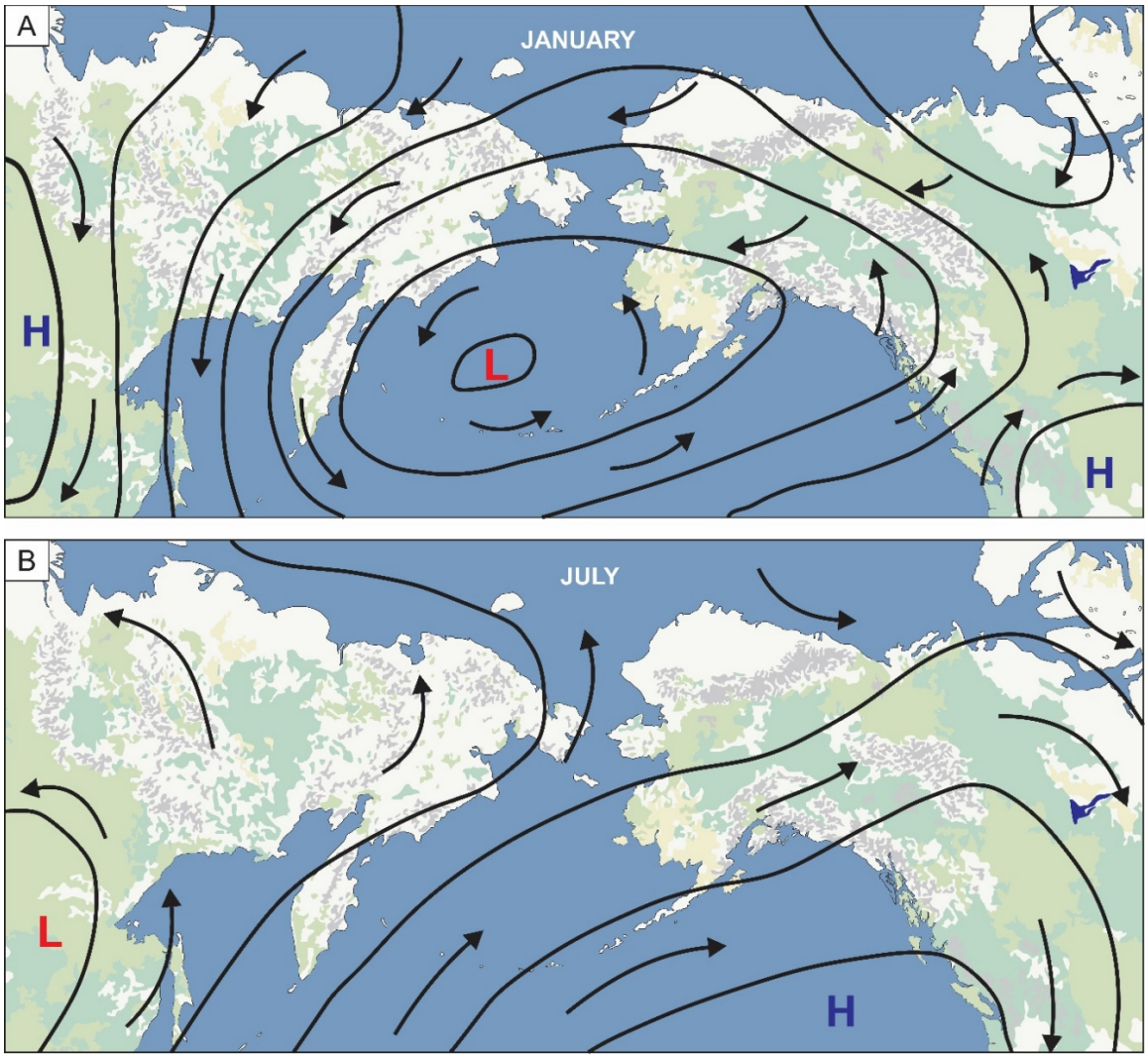

Figure 2.3 Synoptic-scale atmospheric circulation patterns over Beringia; a) January circulation, with the Aleutian Low dominating over the north Pacific, Canadian High to the east, Siberian High to the west and northerly-northeasterly winds in central Alaska; b) July circulation, with the Pacific Subtropical High dominating over the north Pacific and southerly-southwesterly winds in central Alaska. (Adapted from Mock et al., 1998).

Materials and Methods

Sample Collection, Grain-Size Distributions, and Geochemistry

The sediment samples analyzed in this study were collected approximately 20 m east of the Dry Creek excavation area during the summer of 2012. Bulk samples were taken every 2.5 cm, starting at the base of the outcrop and ending just beneath the modern

sand deposit, totaling to 57 samples over 1.6 meters. Prior to analysis, bulk samples were dried and random powder mounts were prepared from a subset of samples for x-ray diffraction (XRD) to determine mineralogy. Samples for particle size analysis were pre-treated with 30% H_2O_2 until reaction ceased to remove organic particles. X-ray analyses indicated that carbonates were absent, so HCl pre-treatment was unnecessary. Samples were then suspended in 1L of de-ionized water, dispersed with 10 mL of 10% $(NaPO_3)_6$ and sonicated for 3 minutes to ensure complete disaggregation. Particle-size analysis was performed using a Malvern MasterSizer 2000 with a Hydro MU dispersion unit. Data were collected in quarter-□increments and were converted to grain sizes using the Mie Theory. Duplicate analyses were performed periodically to ensure accuracy. Raw grain-size data are presented in Supplementary Table 1. Elemental concentrations of ten major oxides (SiO_2, Al_2O_3, CaO, Na_2O, K_2O, Fe_2O_3, MgO, MnO, TiO_2, and P_2O_5) and eighteen trace elements (As, Ba, Co, Cr, Cu, Mo, Nb, Ni, Pb, Rb, Sc, Sr, Th, U, V, Y, Zn, and Zr) were determined for each sample on a Rigaku ZSX-Primus 2 wavelength-dispersive X-ray fluorescence (XRF) spectrometer with a 4.0 kW rhodium target X-ray tube. Bulk samples were shatter boxed for 2 minutes, mixed with a cellulose binder in a 6:1 ratio, and prepared as pressed pellets for analysis. These data are included in Supplementary Table 2.

Data Analysis

Although there are several functions that may be used to numerically model grain-size distributions, the most commonly applied are the lognormal and the Weibull distributions. The Weibull distribution was chosen for this study for two primary reasons: first, because it is able to accommodate both symmetrical and positively and negatively

skewed distributions and second, because most wind speeds can be best modelled using a Weibull function and it logically follows that loess grain-size distributions should mimic those of their transport mechanism (Sun et al., 2004).

A Weibull distribution is defined by the probability density function

$$f(\delta, a, b) = \frac{a}{b^a}\delta^{a-1}e^{(\frac{\delta}{b})^a}, \delta > 0$$

where a and b are called the shape and scale parameters, respectively. Figure 2.4 illustrates three Weibull distribution shapes: extremely right skewed, for $a = b = 1$, moderately right skewed for $a = 1.5$ and $b = 1$, and nearly symmetric for $a = 5$ and $b = 1$. A mixture Weibull distribution is defined by the probability density function

$$f(\delta, a_1, b_1, a_2, b_2, p) = p\left(\frac{a_1}{{b_1}^{a_1}}\delta^{a_1-1}e^{\left(\frac{\delta}{b_1}\right)^{a_1}}\right) + (1-p)\left(\frac{a_2}{{b_2}^{a_2}}\delta^{a_2-1}e^{\left(\frac{\delta}{b_2}\right)^{a_2}}\right), \delta > 0$$

where a_1 and a_2 are the scale parameters, b_1 and b_2 are the shape parameters, and p, $0 < p < 0.5$ is a weight that estimates the proportion of observations that belong to the less-prevalent Weibull distribution.

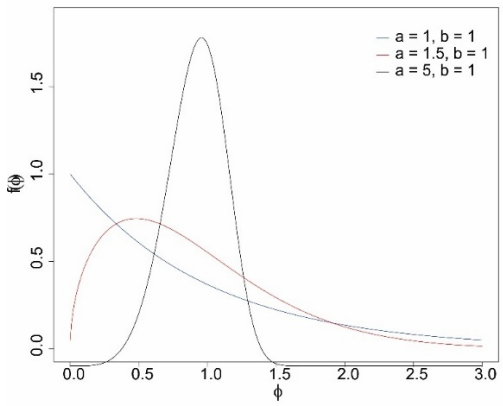

Figure 2.4. Weibull distributions with varying values of a and b: extremely right-skewed (blue), moderately right-skewed (red) and symmetrical (black).

For each of the 57 samples, it was of interest to model the distribution of the grain diameters (in μm). Grain diameters ranged from 0.2 to 2,380 μm, resulting in substantial axis compression. Consequently, grain diameter was transformed to a base-2 logarithm (φ) scale. Additionally, because some of the values of the φ increments were negative, 12.5 was added to all transformed values so that all were strictly positive, to adhere to the requirement that the values of a Weibull variable are strictly positive. We call this transformed variable δ. This one-to-one transformation preserves the integrity of the data and is easily reversed for interpretation back into the original grain diameters. Data analysis was performed on the transformed δ values. The open-source software R was used for all data analysis (*https://www.r-project.org/*). For each of the 57 samples, the first step was to determine the shape of the distribution of δ. This was accomplished via a histogram with a kernel density estimate superimposed on the histogram. The kernel density estimate was especially helpful in determining the shape, and in particular, whether the distribution was unimodal or bimodal. It was determined that 36 of the 57 samples had a unimodal distribution, and the remaining 21 bimodal. For those bimodal samples, a mixture distribution was used to model δ.

The function **mix** in the *mixdist* package was then used to fit either a single Weibull, or a mixture of Weibull distributions, to each of the 57 samples. Once the family of distributions is specified, the function **mix** uses a combination of a Newton-type method and the EM algorithm to find parameter estimates that provide the best fit of the specified distribution to the data. The resultant fit is the set of parameter estimates that minimizes the mean square error between the data and the fitted distribution. To ensure convergence of the algorithm, it was necessary to select starting values for the mean and

standard deviation individually for each of the 57 samples. Starting values were determined by visual inspection of the location of the peak (or peaks) in the data. These data are summarized in Supplementary Table 1.

Age-Depth Model

The Dry Creek archaeological site is an important, but often-debated, part of the late Pleistocene archaeological record in central Alaska. Although there is clear evidence of human populations in eastern Beringia following the LGM, the material remains left by these early Americans have been the subject of extensive debate in the archaeological community. Lithic assemblages dating between about 9 and 13 ka are commonly found at south-facing bluff localities such as Dry Creek, but there is both spatial and temporal variability in the types of artifacts found during this interval. Numerous explanations for this variability have been proposed but no true consensus has yet been reached on the issue. Dry Creek is, perhaps, the best known of the Pleistocene archaeological sites in central Alaska and, as such, has factored heavily in this debate. In order to better constrain the chronology of the two late Pleistocene archaeological components at the site, an abundance of radiocarbon dates have been obtained from the nearly 350 m^2 excavated since the 1970s. The original work at the site produced 18 radiocarbon dates (Thorson and Hamilton, 1977), many of which were deemed incongruent and dismissed as a result of contamination from locally-derived lignite dust. The site was re-visited in the mid-1990s by Bigelow and Powers (1994), resulting in six new AMS radiocarbon ages collected on wood charcoal from the lower part of the stratigraphy. Because none of these original 24 dates were from cultural features, but rather from natural charcoal, Graf et al. (2015) revisited the site in 2011 with the intention of dating hearths from the late

Pleistocene occupations in loess units 2 and 3. Their work resulted in an additional six dates.

Clearly, Dry Creek has been both extensively and securely dated over the past forty years of research. Although this is certainly a benefit for this study, the manner in which the dates have been recorded in the literature has led to some difficulties as well. Because the dates from the site were collected with the intention of dating paleosols, depositional units, and archaeological components, exact depths below surface remained unpublished for virtually all samples. Thorson and Hamilton (1977) display the stratigraphic location of each date, but Bigelow and Powers (1994) record only relative descriptions of the sampling locations. Because both ages and corresponding depths are crucial for the development of an age-depth model, this severely limited the number of ^{14}C ages that could be included in the model utilized in this study. The ten dates used to calculate the age model for this study are summarized in Table 1. The majority of dates used here are from Thorson and Hamilton (1977). Because the locations of their dates are presented graphically, it was only possible to approximate the position of each date within the individual stratigraphic units. However, many of Thorson and Hamilton's dates appear to come from the same stratigraphic location. In such instances, only one date was selected from each level. For instance, in their Figure 2.4, Thorson and Hamilton (1977) presented dates of 3430±75 and 3655±60 from the uppermost part of paleosol 4a in loess 6. Because individual depths could not be assigned to each date, only 3655±60 was included in the age model in this study for that stratigraphic level. This same difficulty led to a rejection of five of Thorson and Hamilton's (1977) 18 dates for this model, in addition to the five dates Thorson and Hamilton themselves dismissed.

Only one date was used from Bigelow and Powers (1994), also as a result of the lack of depth information. The one date included from this study comes from the upper portion of paleosol 1, which is thicker and more easily traceable from the original sampling locality to the sampling locality for this study. Finally, one date from Graf et al. (2015) was included to extend the age model to the lowermost portions of the profile. This sample is the only one of the ten used to develop the age model for this study that had measured depth data available (Graf, pers. comm. 2016). Only one of the six dates from the Graf et al. (2015) study was included in this model because their loess 2 dates were all derived from within two vertical centimeters of one another. It is also worth noting that the dates from Graf et al. (2015) are from cultural features, rather than from natural charcoal. Although the cultural dates do not appear to be discordant with natural dates obtained by Thorson and Hamilton (1977), the possibility remains that the lower part of the section may be older than is modeled here. Once the dates were selected and their corresponding depths in the original excavation block approximated, these locations were correlated across the 20 or so meters between the main excavation block and the sampling locality for this study. This is easily done using simple lithostratigraphic correlation methods because the thicknesses and character of the depositional units do not change significantly over this distance. Although cryoturbation is present at the site, soil micromorphology suggests that this primarily affects the upper portion of the profile (generally above loess 4) and results in less-than-cm-scale disruptions (Graf et al. 2015). Micromorphology also indicates that no major hiatuses in deposition are present at the site. Furthermore, the organic stringers and upper sand units in the profile are largely continuous, easily followed across tens of meters distances, and serve as marker positions

for the locations of radiocarbon dates. The extrapolated positions of each date are noted in Figure 2.5. This method of extrapolation, although necessary due to the absence of charcoal in the section from which grain size samples were collected, introduces inherent errors, which must be addressed. However, we believe that errors have been minimized as much as possible and that the age model presented here is a reasonable one given the expressed uncertainties.

All radiocarbon dates were calibrated using the program CLAM v2.2 (Blaauw, 2010) within the open-source statistical environment R v3.1.2 (R Development Core Team 2014). All dates are given in calibrated years before present (cal yr BP) weighted by the calibrated probabilities of the dates, using the IntCal 13.14 calibration curve (Reimer et al., 2013). These calibrated dates were then used to generate an age-depth model at increments of 0.5 cm, using a third-order polynomial regression (Fig. 2.6). The resulting calendar age point estimates for each depth are based on the weighted average of 100,000 iterations calculated within the CLAM program.

Results

Bulk grain-size distributions are presented in Figure 2.5. Samples are composed of 3-7% clay (<4μm), 40-75% silt (4-62.5 μm), and 22-56% sand (62.5-2000 μm). Median grain-size ranges from 37-89 μm, modal grain-size from 43 to 72 μm, and mean grain-size from 31-75 μm, all typical size ranges for Alaskan loess, which tends to be somewhat sandier and less-clayey than loess deposits elsewhere (Muhs et al., 2003). Visual examination of the distribution histograms for each sample reveals that, broadly, the grain-size distributions of the Dry Creek samples fall into one of two categories: unimodal distributions, or bimodal distributions with one fine component similar to the

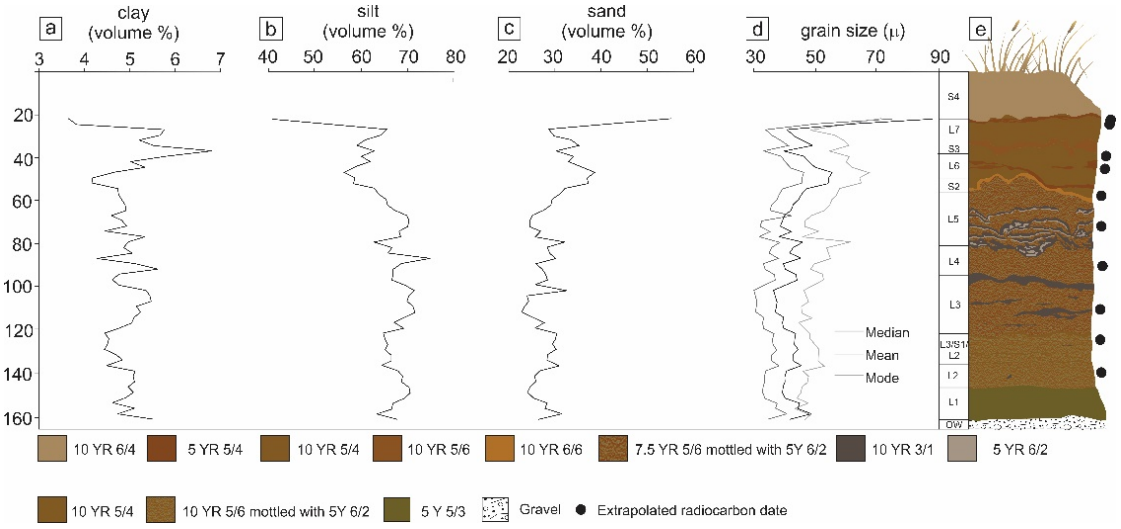

Figure 2.5. Grain-size distribution vs depth; a) volume percent clay (less than 4□m); b) volume percent silt (4-62.5□m); c) volume percent sand (62.5-2000□m); d) mean, median, and mode; e) schematic illustration of the Dry Creek stratigraphy at the sampling location for this study (OW-outwash; S-sand units; L-loess units) with locations of radiocarbon dates shown. Paleosols are dark colored "stringers" located mainly within loess units. Cryoturbation has affected loess units 5-7, resulting in folding of paleosols. Colors correspond to field moist Munsell colors of each unit.

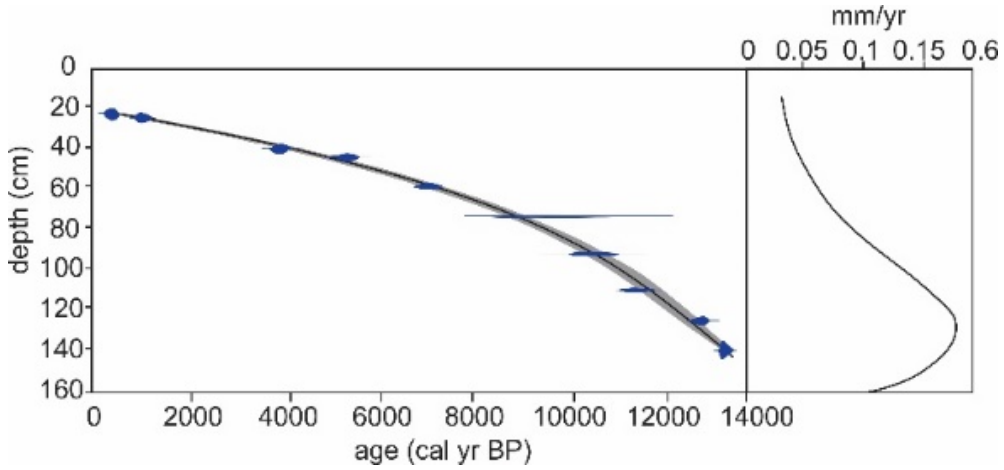

Figure 2.6. Age-depth model and mass accumulation rates calculated using CLAM for the Dry Creek section. Estimated errors denoted with bars. Uncertainty in the model is shown in grey. Sources of radiocarbon dates include Thorson and Hamilton (1977), Bigelow and Powers (1994) and Graf et al. (2015).

Table 2.1 Selected Dry Creek radiocarbon dates used for age model development.

Stratum	Depth (cm)	Material	Age Estimate	Calibrated	Reference
L7	22.1	charcoal	375 ± 40	315-507	Thorson and Hamilton, 1977
L7	24.4	charcoal	1145 ± 60	934-1229	Thorson and Hamilton, 1977
L6	39.8	charcoal	3655 ± 60	3835-4150	Thorson and Hamilton, 1977
L6	44	charcoal	4670 ± 95	5054-5597	Thorson and Hamilton, 1977
L6	58.5	charcoal	6270 ± 110	6930-7424	Thorson and Hamilton, 1977
L5	73.5	charcoal	8600 ± 460	8537-11,070	Thorson and Hamilton, 1977
L4	92.2	charcoal	9340 ± 195	10,188-11,182	Thorson and Hamilton, 1977
L3	110	charcoal	10060 ± 75	11,286-11,963	Bigelow and Powers, 1994
L2	125.3	charcoal	11120 ± 85	12,774-13,131	Thorson and Hamilton, 1977
L2	140	hearth charcoal (*Salix sp.*)	11635 ± 40	13,380-13,570	Graf et al., 2015

unimodal samples described above and one coarse component. Both types of distributions are represented throughout the section, though unimodal distributions dominate, comprising 63% of the samples analyzed. Samples with a unimodal distribution were fit using a single Weibull distribution, whereas those with a bimodal distribution were fit using a two-component mixed Weibull distribution (Fig. 2.7).

The fine component (component 1, C1) at Dry Creek is present in all samples. It has a modal size between 33.5 and 62.5 μm, with an average value of 39 μm (4.68 ϕ) and is fine-skewed. Modal size is large near the base of the section, decreases gradually over the lower 100 cm, and increases again above 80 cm, with a highly variable interval

between 80 and 100 cm depth (Fig. 2.8a). Largest modal sizes occur at 14.1 ka, 13.3 ka, 12.9 ka, 10.3 ka, 6.3 ka, and 0.4 ka and smallest modal sizes occur at 13.9 ka, 11.1 ka, 3.7 ka, and 1.6 ka. The coarse component (component 2, C2) is not uniformly distributed throughout the section. It is more common near the base and top of the profile, but can be found sporadically throughout. The mode of the C2 component ranges from 481 to 1304 μm, with an average value of 1055 μm (-0.77 ϕ). Maxima for the C2 component occur at 12.7 ka, and 4.2ka, and minima at 13 ka and 0.4 ka (Fig. 2.8b). The C1 component dominates all samples, accounting for at least 85% of each, but commonly as much as 100% (Fig. 2.8c).

Elemental concentrations were determined for each sample in an effort to identify geochemical indicators of provenance change throughout the profile. Both major and trace element concentrations in the bulk sediment were found to either be remarkably consistent throughout, or to vary primarily in conjunction with the abundance of the C2 component (Fig. 2.9, Supplement 2). There is a moderately strong positive relationship between the abundance of the C2 component and the concentration of Si, and a moderately strong negative relationship between C2 and Ti, Al, Mg, K, Zr, and Th. The good correlation between elemental concentration and abundance suggests that the chemistry of these elements is largely being driven by the abundance of C2 additionally appears to be enriched in quartz and depleted in Ti, Al, Mg, K, Zr, and Th, as compared to C1.

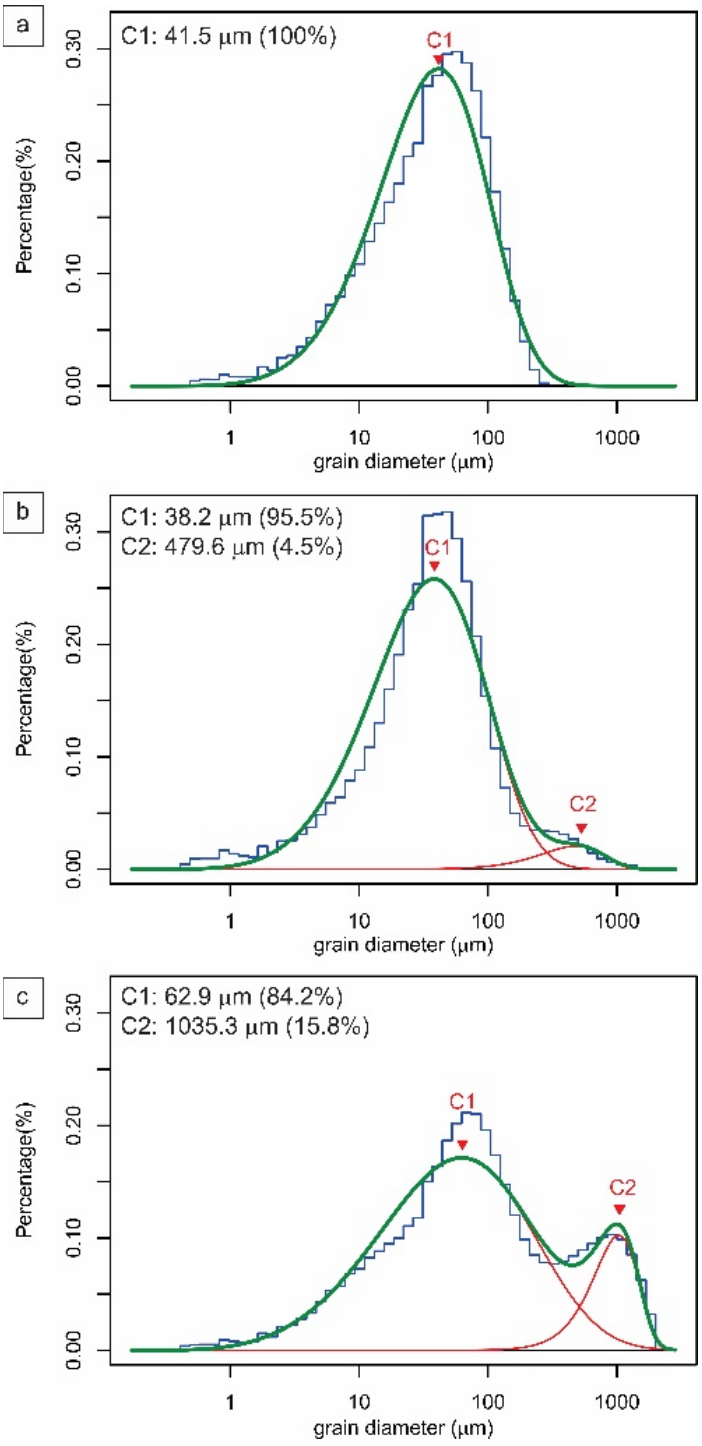

Figure 2.7. Examples of grain-size distributions and Weibull-partitioned components from Dry Creek; a) unimodally distributed sample with only C1 present (sample DCb-31); b) bimodally distributed sample with a small proportion modal size of C2 (sample DCb-3); c) bimodally distributed sample with a large proportion and modal size of C2 (sample DCb-57). Raw data indicated by blue histogram, C1 and C2 shown in red, and fitted curve in green.

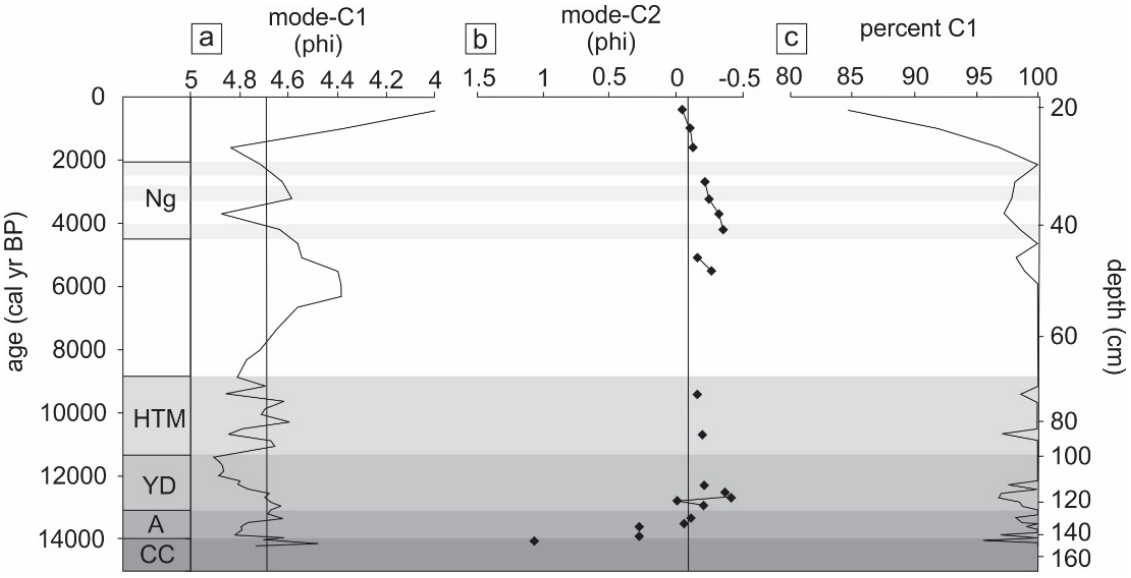

Figure 2.8. Results of grain size partitioning using the mixed Weibull distribution; a) modal size of C1 in microns with average value (39.2) denoted by line; b) modal size of C2, where present, in microns with average value (1075.1) denoted by line; c) proportion of C1 in each sample. Results are plotted against time in cal yr BP and depth in cm. CC = Carlo Creek; A = Allerød; YD = Younger Dryas; HTM = Holocene Thermal Maximum; Ng= Neoglacial.

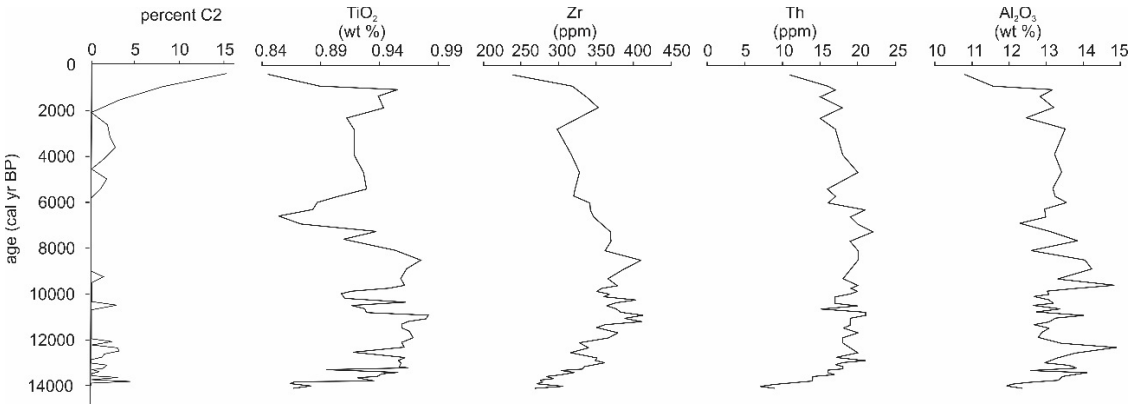

Figure 2.9. Plots showing the relationship between the abundance of C2 (in volume percent) and elemental concentrations of a) SiO_2; b) TiO_2; c) Al_2O_3; d) Fe_2O_3; e) MnO; f) MgO; g) CaO; h) Na_2O; i) K_2O; j) P_2O_5; k)ZrO_2; l) Th and associated R-squared values. All major element concentrations are given in weight percent, trace elements in ppm.

Discussion

Interpretation of grain-size components

The Dry Creek site is located in the northern foothills of the Alaska Range, overlooking Dry Creek about 3 km from its confluence with the Nenana River (Fig. 2.1). Given this geographic position, there are a number of potential sediment sources that could have contributed to deposition of the loess package at the site over the last several thousand years. Most proximal is the glaciofluvial outwash terrace upon which the latest Pleistocene and Holocene loess cap has accumulated. This terrace rises at least 25 m above the current floodplain of Dry Creek and is poorly-sorted and conglomeratic, composed primarily of cobble- to boulder-sized clasts of quartz, quartz-muscovite schist, and other lithic fragments. The unlithified outwash deposit fines near the top and has been subjected to extensive physical and chemical weathering since the late Pleistocene, when it is inferred to have been deposited during the Healy glaciation (Péwé et al., 1965; Ritter, 1982; Dortch et al. 2010) . The silty-sandy matrix of the outwash could have easily been entrained by southerly winds and deposited atop the bluff. Dry Creek itself is another potential sediment source. The creek is a braided stream that originates in the northern flank of the Alaska Range. Bedload in its shallow channels is similar lithologically to the glaciofluvial outwash deposits in the region, largely consisting of igneous and meta-sedimentary cobbles (Thorson and Hamilton, 1977). Suspended sediment is predominantly silt derived from the Birch Creek Schist (also called the Fairbanks Schist) and tends to be mainly quartz and muscovite, although appreciable amounts of chlorite, lithic fragments, rutile, and magnetic minerals have been reported (Thorson and Hamilton, 1977). The modern braid plain is commonly subaerially exposed,

particularly during dry summers and in the fall (Fig. 2.2), leaving silt and sand available for entrainment and aeolian transport. Perhaps the most obvious source for aeolian sediment in the area surrounding Dry Creek is the Nenana River. The Nenana River exits the Alaska Range approximately 10 km south of its confluence with Dry Creek and flows northward as a narrow braided river where it has incised through several outwash terraces of varying late Quaternary ages (Wahrhaftig and Black, 1958). Sediment from the Nenana River is dominated by quartz, muscovite, and rock fragments (primarily metamorphic and metasedimentary), though chlorite, epidote, rutile, magnetics, and zoisite/clinozoisite are reported as common mineral constituents (Thorson and Hamilton, 1977). Historic dust entrainment from the Nenana River during wind storms has been reported, and Muhs and Budahn (2006) cited it as an important source for loess in the Fairbanks area to the north. Broadly speaking, both the Tanana and Yukon Rivers to the north of Dry Creek are important regional loess sources as well. The Yukon is separated from Dry Creek by nearly 300 km as well as by the Yukon Tanana Uplands, so its importance as a sediment source at Dry Creek is likely negligible, but the Tanana, only about 100 km to the northeast, could reasonably contribute sediment to the site. Geochemical surveys of Nenana, Tanana, and Yukon River silts have been performed by Muhs and Budahn (2006), but the elemental concentrations in that study were determined only for sediment in the 2-53 □m size fraction. The loess at Dry Creek is much coarser than this and small sample sizes prevented the analysis of particle-size separates. As a consequence, our bulk geochemical analyses performed on sediment with a wider range of grain sizes did not plot on the provenance diagrams constructed by Muhs and Budahn

(2006). However, given the regional importance of the Tanana River, it seems reasonable to consider it a possible source at Dry Creek.

The grain size of an aeolian deposit is dependent upon three factors: the grain-size distribution of the sediment source, the distance the sediment has been transported, and wind intensity. We suggest that neither the grain-size distribution of the sediment sources described above, nor their distance from Dry Creek, have changed significantly since the LGM. Vegetation also plays a major role in loess deposition in two major ways: 1) vegetation height can affect surface roughness, and therefore wind velocity, and 2) certain types of vegetation (e.g. spruce forest) serve as more effective sediment traps than others (e.g., herb tundra) and all types of vegetation serve as better traps than no vegetation (Muhs et al., 2003). Following the LGM, central Alaska was covered by sparse herb tundra vegetation, which transitioned to shrub tundra, and finally boreal forest by 9-10 ka (e.g., Graf and Bigelow, 2011, and references therein). Because changes in vegetation occur throughout the time interval of this study, vegetation must be ruled out as a factor influencing grain-size distributions in order to ascribe any sort of climatic meaning to those distributions. To some extent, this is impossible to do. Vegetation likely plays at least some role in loess accumulation at Dry Creek. However, if vegetation were the driving force behind grain-size variations at Dry Creek, one might expect to see broad changes in particle size that correspond to vegetation transitions. This does not appear to be the case here. Additionally, spruce forest has been present at Dry Creek for at least the past 9,000 years or so, during which time variations in the grain-size distribution of the loess at Dry Creek are observed. If grain-size variations were solely the result of changes in vegetation, this would not be the case, so some additional factor must be at play.

Moreover, spruce forest is a more effective sediment trap than tundra vegetation (Muhs et al., 2003). Therefore, sediment accumulation rates should be higher during times when the surface vegetation is dominated by spruce, rather than by herb or shrub tundra. Instead, the reverse is true at Dry Creek. Sediment accumulation rates are highest in the late Pleistocene and drop during the Holocene. This suggests that, although loess accumulation probably started at Dry Creek as a result of the herb/shrub tundra transition during the late Pleistocene, subsequent changes in vegetation type have had little effect on the character of the loess at the site. Thus, we may interpret changes in the modal size of C1 and C2 of the loess to represent changes in competence of sediment-transporting winds. In order to do this, however, it is necessary to identify the provenance of each component. C1 has a modal size almost entirely in the coarse silt category, save for the most recently deposited loess. Loess with a modal size in this range is the most common component in Asian dust and has thus been widely studied (Vandenberghe, 2013). It is interpreted to have been transported in low to near-surface suspension clouds during seasonal dust storms (Tsoar and Pye, 1987) over a distance of tens of km (Vandenberghe, 2013). In one instance a transport distance of nearly 100 km was recorded for this size subgroup (Pendea et al., 2009), but this seems to be the exception rather than the rule. Sources for this subgroup are most commonly glaciofluvial deposits and alluvial plains (Smalley et al., 2009). At Dry Creek, C1 is interpreted to represent deposition of Nenana River silt by northerly-northeasterly winds. Southerly sources are likely too close to Dry Creek to result in sediment this fine, particularly when it is easily possible for most wind to entrain and transport grains as large as fine sand for distances of several km. It is possible that input from the Tanana River is responsible for the fine-skewed nature of C1,

which would also suggest northerly winds, but this remains to be tested at additional sites. The loess cap at Dry Creek thickens and coarsens slightly to the north (Thorson and Hamilton, 1977), also supporting an interpretation of dominant northerly winds. Maximum and minimum wind velocities associated with the deposition of C1 range between 0.07 and 0.095 m/s (Fig. 2.10), estimated from laboratory experiments (Thorson and Bender, 1985).

C2 has a modal size in the range of medium- to very-coarse sand. Sediment of this size is uncommon in loess deposits and is generally transported via saltation or, in the case of medium sand, very short-term suspension (Vandenberghe, 2013 and references therein). As such, the source of C2 must have been quite proximal. The sands at the Dry Creek site have long been interpreted as derived from Dry Creek itself, or perhaps from the outwash at the base of the aeolian profile (Thorson and Hamilton, 1977; Bigelow et al., 1990), and we concur with this interpretation. These sediment sources would require strong southerly winds, perhaps the katabatic winds flowing off of the Alaska Range as suggested by Thorson and Bender (1985) and Bigelow et al. (1990). Wind velocities necessary to deposit C2 range from 0.3 to 0.45 m/s (Fig. 2.10), which are comparable to the katabatic wind velocity in the Nenana River Valley calculated by Thorson and Bender (1985) for the late glacial period. As vegetation transitioned from grass-dominated to shrub-dominated to tree-dominated (Bigelow and Powers, 2001) and surface roughness increased, the velocity of these winds may have decreased during the Holocene, but, assuming Thorson and Bender's (1985) assertion that actual katabatic wind velocities lie between their maximum and minimum estimates, they likely would still have been

competent to entrain and deposit C2, particularly given that the modern cliffhead sand at the site falls into the C2 size category.

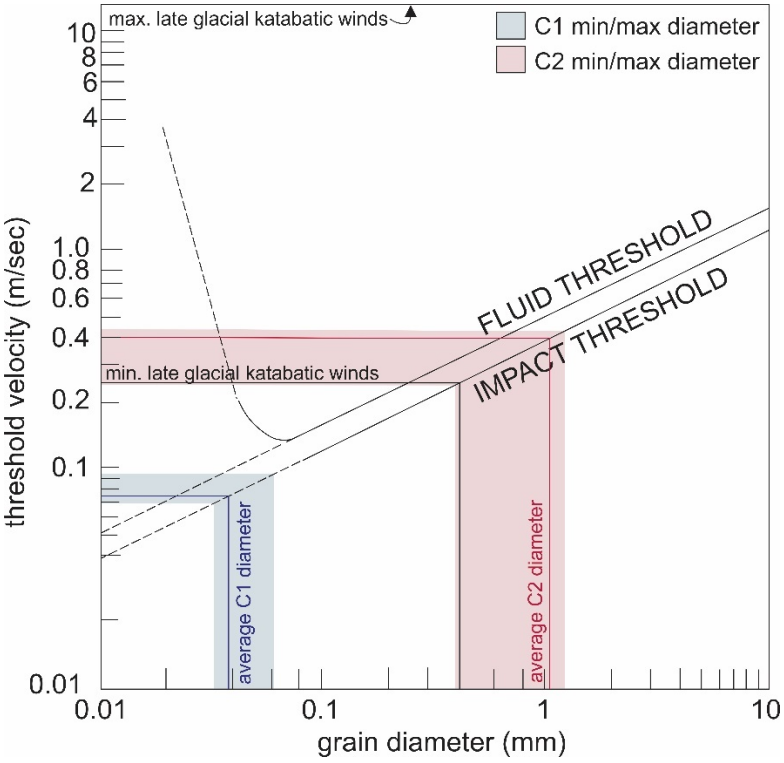

Figure 2.10. Estimated minimum threshold velocities for entrainment (fluid threshold) and deposition (impact threshold) for Weibull-partitioned components C1 (in blue) and C2 (in red). Shaded areas denote minimum and maximum threshold velocities for deposition based on minimum and maximum modal sizes of C1 and C2, red and blue lines represent average modal size of each component. Modified from Thorson and Bender (1985) with their estimated minimum and maximum calculated late glacial katabatic wind velocities marked in black.

This interpretation of wind regimes follows the model proposed by Muhs and Budhan (2006) for central Alaska, wherein primary winds come from the north and katabatic winds occasionally transport from the south, leading to the formation of aeolian deposits, which are a mixture of sediment from northerly and southerly sources. Because of the proximity of Dry Creek to the southerly sediment sources, there is a disparity in grain size between the sediment deposited by katabatic winds and regional winds.

Because of this disparity, the use of grain-size partitioning on this suite of samples is possible and allows for the analysis of what are essentially two separate grain-size records at Dry Creek: one recording the intensity of regional northerly winds carrying C1 over the past 15,000 years and another recording the occurrence and intensity of episodic southerly katabatic winds carrying C2 over the same time interval.

This study is not the first to use grain size as a proxy for wind intensity in central Alaska, nor even at Dry Creek. Bigelow, Beget and Powers published a study in 1990 (Bigelow et al., 1990) asserting that the sand 1 layer identified at the site by Thorson and Hamilton (1977) represented increased wind intensities related to katabatic winds and a rapid, short-lived environmental shift during the Younger Dryas. Their assertion was challenged by Waythomas and Kaufman (1991), who argued that sand 1 was not as ubiquitous throughout the Nenana Valley as Bigelow et al. (1990) had suggested, and that the stratigraphy of the Nenana Valley showed little regional regularity. They furthermore argued that such coarse-grained deposits need not be the result of hundreds or thousands of years of sedimentation but, instead, they might have been produced from hour- to day-long events. Additionally, they argued that the presence of additional sand layers at Dry Creek, which are not addressed by Bigelow et al. (1990), indicate that a single climate event cannot be the cause of what appears to be a repeating sedimentological feature. Instead, they proposed that the variable presence of unvegetated bluffs created by downcutting rivers are responsible for variations in the particle size at Dry Creek. Waythomas and Kaufman (1991) raise the additional point that, at that time, the evidence for any time interval of climatic change associated with the Younger Dryas in the interior of Alaska was spotty at best. To some extent, this is still the case; evidence for a Younger

Dryas climate reversal abounds in southern Alaska but is less straightforward in the interior, perhaps indicating moisture, but not temperature responses (Graf and Bigelow, 2011). Begét et al. (1991) responded to Waythomas and Kaufman's (1991) concerns, citing Wahrhaftig (1958), Thorson (1975) and Thorson and Hamilton (1977) as evidence that some degree of continuity does exists in the Nenana Valley loess. Although Begét et al. (1991) does not cite this work, Powers and Hoffecker (1989) and Hoffecker et al. (1988) presented additional evidence that there is a consistent stratigraphy in the region. A regional stratigraphy suggests that the patterns observed in grain-size distributions are the result of regional-scale processes, rather than short-term, local variations in sediment availability. Begét et al. (1991) also argued that sand 1 is too laterally extensive to have been derived from transient bluff exposures or blowouts along Dry Creek.

The model proposed by Bigelow, Begét, and Powers (1990) does not precisely mirror that proposed in our study. They suggested that the winds transporting sand 1 and transporting the loess units were one and the same, whereas in our study we argue that they come from different directions and represent sediment derived from different sources. Nevertheless, Bigelow et al.'s (1990) interpretations for a valley-wide stratigraphy and against the importance of ephemeral sediment sources have bearing on the work presented here. Furthermore, the model proposed in our study may, in fact, help to resolve some of the additional issues raised by Waythomas and Kaufman (1991). Southerly katabatic winds driven by glaciation in the northern Alaska Range provide a more effective mechanism for repeating sand-rich layers in the stratigraphy in a way that the Younger Dryas model proposed by Bigelow et al. (1990) does not. It also explains the high proportion of silt in the sand layers at the site. Silt and sand deposition were

concurrent at Dry Creek; if silt and sand are deposited by different mechanisms, an increase in the proportion of one need not correspond with an absence of the other.

Late Quaternary wind intensities

The modal sizes of C1 and C2, as well as the relative proportions of C1 and C2, were plotted against calibrated radiocarbon ages in order to examine the chronology of late Quaternary changes in wind strength in the Nenana River Valley (Fig. 2.8). Variations in the modal size of C1 broadly correspond with six major climatic events over the last ~15,000 years. Modal sizes are higher than average, suggesting intensification of northerly winds and, thus, the Aleutian Low during three time intervals: 14.2-14 ka, 7.5-4 ka, and ~2.5-1.6 ka. The first of these intervals coincides with dates usually assigned to the Older Dryas, a brief cold period identified in some parts of North America between the Bolling and Allerød warm intervals, but records of the Older Dryas are scarce in this part of Alaska. Instead, we suggest that the oldest part of the profile at Dry Creek represents high velocity winds associated with the Carlo Creek glacial readvance in the Nenana Valley, which is generally dated between 14 and 16 ka (Dortch et al., 2010). The latter two intervals correspond broadly with proposed Neoglacial re-advances during the Holocene between 7.6 and 5.8 ka and after 3 ka (Calkin, 1988; Powers and Hoffecker, 1989; Anderson et al., 2001). Weaker winds are indicated by minima in the modal size of C1, specifically from 14-13.3 ka, 12.6-11 ka, 9.7-8 ka, 3.9-2.5 ka, and 1.5-0.9 ka. The first of these intervals corresponds the Allerød warm period. Of interest are the relatively weak wind intensities recorded here during the Younger Dryas, commonly dated from 12.9-11.7 ka in central Alaska. The effects of the Younger Dryas in central Alaska have long been debated; some climate records indicate cool

and/or dry conditions during this interval (Hu et al., 1993; Abbott et al., 2000; Bigelow and Edwards, 2001), whereas others indicate little to no deviation from previous conditions (Anderson et al., 1994; Bigelow and Powers, 2001). Younger Dryas perturbations appear to be most intense along the southern coast of Alaska and it has been suggested than increased insolation and the geographic isolation of central Alaska from the northern Pacific are causes of the variability observed (Bigelow and Edwards, 2001). For the Dry Creek record, increased summer insolation during this interval (Bartlein et al., 1991) may have resulted in a weakening of the Aleutian Low and decreases in regional northerly wind strength and lower C1 modal sizes. Variable wind strength is indicated between 11.4 and 9.4 ka, roughly coinciding with the expression of the Holocene Thermal Maximum (HTM) in central Alaska (Kaufman et al., 2004). Kaufman et al. (2016) find that that the early Holocene (11.7-8.2 ka) in eastern Beringia was marked by fluctuating temperatures, rather than a prolonged period of warmth as has been previously suggested. Their evidence of fluctuating temperature combined with the findings of fluctuating wind intensity in our study suggest that the HTM in Alaska was a time of rapid oscillations in climate, rather than protracted warmth as is seen elsewhere in the world. The largest increase in C1 modal size occurs near the top of the section, just below the modern cliff-edge sand. Here the mode of C1 reaches its maximum of 62.5 μm. Although the geochemical data did not indicate a major provenance shift throughout the profile (Supplement 2), we suggest that this coarsening represents a transition towards southerly prevailing winds and a much closer sediment source, such as occur at the site today. This sediment would likely have come from the Nenana River as well, but the

portion of the river to the south of the site rather than to the north, thus accounting for the uniformity of the geochemical data throughout the section.

We interpret the occurrence and modal size of C2 to indicate the prevalence and strength of higher-velocity, katabatic southerly winds in the Nenana River Valley, and it may therefore be used as a record of glacier extent in the northern Alaska Range. C2 is observed most commonly prior to ~12 ka and after 4 ka at Dry Creek, suggesting increased katabatic windstorm frequency and expanded glaciers during these intervals. Higher storm frequency before 12 ka is likely the result of expanded glaciers and the retreating Cordilleran ice sheet in the Alaska Range following the LGM. Higher ice volume in the mountains would have led to intense density-driven katabatic winds, particularly as the foothills and lowlands warmed comparatively during deglaciation. Glaciation controlled the character of C2 during the late glacial period, but it is noteworthy that the largest modal sizes of C2 are not associated with this time period when there is no record of large alpine glaciers in the Alaska Range. Rather, the largest modal size in C2 is observed at 12.9 ka, at the onset of the Younger Dryas chronozone. As discussed previously, evidence for a climatic reversal associated with the Younger Dryas in central Alaska is somewhat convoluted. It has been argued that cooler sea-surface temperatures in the northern Pacific caused an increase in southerly wind strength during the Younger Dryas. As migrating air currents move over chilled air resting atop a glacier or ice sheet, potential for displacement of the chilled air mass exists, even if ice volume is relatively low, provided that the prevailing winds are strong enough (Thorson and Bender, 1985). This means that, during the Younger Dryas, strong southerly winds directed against the Alaska Range may have displaced cold air atop mountain glaciers

down into the Nenana River which, according to the model proposed in this study, would have resulted in a proposed valley-wide increase in sand deposition (Bigelow et al., 1990) without necessitating an increase in the modal size of C1. This also may explain why there is such variability in proxy records in interior Alaska during the Younger Dryas: sites which are located nearer the southern coast of Alaska or proxies which might record changes in southerly winds (such as the modal size of C2) should show increased Younger Dryas effects, whereas sites further from the coast or which were not sensitive to changes in southerly wind intensity (such as the modal size of C1) should not. The C2 peak between 5.5 and 5.1 ka is somewhat more puzzling, because it occurs during what has widely been recognized as a period of glacial retreat during the middle Holocene (Ten Brink and Waythomas, 1985; Levy et al., 2004; Daigle and Kaufman, 2009; Kaufman et al., 2016; LaBrecque and Kaufman, 2016) and thus cannot be explained simply in terms of ice volume, but it does not occur during a widely-recognized climate reversal, such as the Younger Dryas. It is possible that this peak is the result of error in the age model used in this study and that the three C2 peaks near the top of the profile actually correspond to the three Neoglacial periods described above, although this is a somewhat dissatisfying explanation and perhaps not a likely one, given the apparently good correlation between the rest of the profile and existing climate records. This peak may be the result of a short-lived, previously undescribed glacial advance during the middle Holocene, which would seem a bold interpretation to make given the abundance of work that has been performed on Nenana Valley glaciation over the last several decades. A final explanation may be that this particular peak is not, in fact, related to ice volume but to another factor affecting katabatic wind frequency and intensity, namely,

regional wind patterns. As northern hemisphere temperatures increased following the LGM, southerly regional winds caused by the Pacific Subtropical High in the northern Pacific likely began to prevail in southern Alaska (Hopkins, 1982). These southerly regional winds, weaker but more consistent than those that dominated during the Younger Dryas, could have displaced cold air sitting atop reduced glaciers in the Alaska Range that would not otherwise have been displaced. The weaker regional southerly winds would have resulted in weaker katabatic winds and explains why the modal size of C2 during this interval is smaller than during the Younger Dryas, despite their similar cause. Three late Holocene periods of Neoglacial expansion have been recorded across Alaska at 4.5-4 ka, 3.3-2.9 ka, and 2.2-2.0 ka (Kaufman et al., 2016.; Solomina et al., 2015), which broadly correspond with the late Holocene C2 record at Dry Creek. The Dry Creek record does not show three distinct events during this time interval, perhaps as a result of decreasing deposition rates throughout the Holocene (Fig. 2.6), but it is likely that the abundance of C2 in the upper part of the profile reflects Neoglacial cooling and glacier expansion from the late Holocene until the recent.

Paleosol development and landscape stability

In periglacial settings dominated by loess, soil development and silt deposition are competing processes (Muhn and Bettis, 2003). Pedogenesis may only occur when the rate of silt deposition slows to such a point that chemical weathering and humification may take place. Soil development also requires some degree of landscape stability so that freshly weathered material remains in place, rather than being eroded away. Geochemically, soil development is generally associated with changes in the concentrations of three types of elements: 1) base cations (Ca, Na, K, Mg); 2) redox-

sensitive elements (Fe, Mn); and 3) organic compounds (C, P). When the concentrations of these elements deviate in a predictable from the mean values present in loess, pedogenesis is indicated. Ca, Na, and K become depleted as a result of the weathering of unstable primary minerals, such as feldspars, amphiboles, pyroxenes, or micas. Ca and Mg can become enriched when carbonate precipitation occurs in a soil. Redox-sensitive elements are lost under reducing (poorly-drained) conditions, gained under oxidizing (well-drained) conditions, and re-mobilized when drainage is variable. Organic matter increases in soils as plants, fungi, and microbes colonize, increasing C and causing a surface depletion/sub-surface enrichment pattern in P. Thus, from examining the geochemistry of paleosols-loess sequences, it should be possible to reconstruct many characteristics of a buried soil that is no longer actively forming.

Thorson and Hamilton (1977) identified five paleosols in the stratigraphic sequence at Dry Creek: three Cryepts in the lower part of the section (paleosols 1,2, and 3), an Ochrept (paleosol 4a) and an Orthod (paleosol 4b). They described the paleosols as having well-developed A horizons, commonly overlying B horizons, and labelled several of the paleosol intervals up to 35 cm thick. Thorson (2005) identified the lower paleosols as well-drained grassland soils with bioturbation soil carbonate, lepidocrocite, and 12-14% clay. Hoffecker et al. (1988) referred to the paleosols as ‘well-developed’. Such well-developed paleosols should show clear geochemical evidence, then, for protracted periods of landscape stability in the past and would represent major hiatuses in deposition at the site. There is, however, little if any evidence in the major element concentrations gathered in this study indicating that this is the case. As discussed previously, base cation concentrations at the site correlate somewhat well with the abundance of the C2

component (Fig. 2.9 f-j), which suggests that very little chemical weathering and re-mobilization of elements has occurred in the profile. The poor correlation of redox-sensitive elements with C2 (Fig. 2.9 d, e) is likely the result of remobilization, although this could just as likely be from drainage changes resulting from modern freeze-thaw processes and overprinting from the modern surface soil as from relict soil development. Both soil color and elemental analysis indicate increasing organic C concentrations in paleosols, but the characteristic P depletion/enrichment is lacking. In fact, aside from the organic C, there is not one instance in which trends in elemental concentrations at Dry Creek correlate with the location of one of the 'well-developed' buried soils. Additionally, soil micromorphology performed at the site (Graf et al., 2015) shows a complete lack of weathering-related pedofeatures. These findings would indicate that the paleosols at Dry Creek are not nearly so well-developed as they have been described in the past. A quick examination of the soil profile in Fig. 2.2 suggests that this should not be so surprising a finding. Rather than 35-cm thick 'paleosol intervals', it is clear that the paleosols at Dry Creek generally consist of little more than 1-2 cm thick generally discontinuous accumulations of organic matter. Paleosol 1 is the most discontinuous of the five buried soils, consisting of less-than-1-cm thick lenses of organic matter. This morphology, combined with the lack of chemical evidence for weathering, could indicate that what has been referred to as a paleosol is actually simply the accumulation of organic matter along relict permafrost table positions during the late glacial period, when permafrost may have been quite close to the ground surface and sedimentation was likely rapid. Paleosol 2 is somewhat better developed, is 3-4 cm thick, and is continuous across the site, but still lacks any evidence for chemical weathering. Paleosol 3 is the most

developed but would be better characterized as a complex of cm-scale, dark organic-rich and white to grey leached couplets, with little mixing between or within couplets that it is one cohesive buried soil. Paleosol 4a is certainly better developed than paleosols 1 and 2 but is still represented by a 3-4 cm-thick discrete accumulation of organic matter in loess that is generally reddened, again likely a result of spodic processes occurring in paleosol 4b near the surface today. Paleosol 4b is the thickest and best developed buried soil at the site and, based on the radiocarbon chronology, may represent a few hundred years of stability. Certainly, none of the other paleosols at the site attest to any longer-term landscape stability.

However, that is not to say that the paleosols do not represent short periods of landscape stability at Dry Creek. They almost certainly do, and there is evidence in the grain-size data to support this. If paleosols formed as a result of reduced deposition, they should be associated with accompanying decreases in wind intensity and, consequently, with lower modal sizes in the C1 component. This is, in fact, exactly what is observed (Fig. 2.8). Minima in C1, indicating weaker winds and probably less deposition, coincide with the location of paleosols throughout the profile. Paleosol 2 corresponds to a minimum in the C1 component following the Younger Dryas interval, and paleosols 4a and 4b to minima between the Neoglacial events of the late Holocene. Paleosol 3 is perhaps the most intriguing. The light-dark couplets of paleosol 3 seem to coincide with fluctuations in wind intensity during the HTM and probably indicate very short periods of landscape stability in a rapidly fluctuating climate. No single couplet is well-developed, but the paleosol 3 complex as a whole could suggest a protracted interval of climate fluctuation between conditions that were ideal for soil development and those that were

not. It is likely that the paleosols at Dry Creek represent minor depositional hiatuses or, more likely, periodic slowing (but not cessation) of silt deposition and that the actual rate of deposition is likely more variable than is depicted in Fig. 2.6. These hiatuses are impossible to incorporate into the site's sedimentation model, however, given the current resolution of the site's radiocarbon chronology, but the largely un-weathered state of each paleosol suggests that the effects of this on the age model are likely minor. Nevertheless, the paleosols do provide important information regarding landscape stability in the Nenana Valley since the LGM.

Conclusions

1) Using a mixture of Weibull distributions to numerically partition grain size distributions, we observe two grain size components in the late Quaternary loess cap at the Dry Creek site: C1, a fine-skewed component with modal size between 33.5 and 62.5 □m, and C2, a symmetrical component with modal size between 481 and 1304 □m. We attribute the deposition of C1 to regional-scale northerly winds carrying silt from the Nenana and possibly the Tanana Rivers, and C2 to deposition of locally-derived medium- to very-coarse sand by southerly katabatic winds.

2) The modal size of Weibull-partitioned component C1 is proportional to the strength of regional winds. Northerly winds associated with the Aleutian Low were intense during the Carlo Creek glacial readvance, during three late Holocene Neoglacial expansions, and within the last 1000 years. Wind strength was low during the Allerød and Younger Dryas, suggesting a weakened Aleutian Low during warmer climatic intervals. The Holocene Thermal Maximum in the Nenana River Valley was marked by variable wind intensities, likely resulting from variable temperatures across Beringia.

3) Weibull-partitioned component C2 is present in just under half of the samples collected from the site. The presence and modal size of this component reflect the frequency and intensity of southerly katabatic winds in the Nenana River Valley. Such winds were episodic and common prior to 12 ka, likely as a result of expanded glaciers and the retreating Cordilleran ice sheet in the northern Alaska Range, as well as after 4 ka, in association with late Holocene Neoglacial events. There is evidence for intense southerly winds between 5.5 and 5.1 ka, perhaps as a result of a longer residence time of the Pacific Subtropical High further northward. The velocity of these winds did not vary significantly over this time period.

4) This study provides compelling evidence that grain-size partitioning techniques may be applied to Alaskan loess as a way to reconstruct paleoatmospheric circulation and regional-scale paleoclimate. Application of this technique to the Alaskan loess record at other key sites could yield valuable, high-resolution information about Quaternary climate across the region.

References

Abbott, M.B., Finney, B.P., Edwards, M.E., Kelts, K.R., 2000. Lake-level reconstruction and paleohydrology of Birch Lake, central Alaska, based on seismic reflection profiles and core transects. Quaternary Research 53, 154–166.

An, Z., Kukla, G., Porter, S.C., Xiao, J., 1991. Late Quaternary dust flow on the Chinese loess plateau. Catena 18, 125–132.

Anderson, L., Abbott, M.B., Finney, B.P., 2001. Holocene climate inferred from oxygen isotope ratios in lake sediments, central Brooks Range, Alaska. Quaternary Research 55, 313–321.

Anderson, P.M., Lozhkin, A.V., Eisner, W.R., Kozhevnikova, M.V., Hopkins, D.M., Brubaker, L.B., Colinvaux, P.A., 1994. Two late Quaternary pollen records from south-central Alaska. Géographie physique et Quaternaire 48, 131–143.

Ashley, G.M., 1978. Interpretation of polymodal sediments. The Journal of Geology 411–421.

Bagnold, R.A., BARNDORFF-NIELSEN, O., 1980. The pattern of natural size distributions. Sedimentology 27, 199–207.

Bartlein, P.J., Anderson, P.M., Edwards, M.E., McDowell, P.F., 1991. A framework for interpreting paleoclimatic variations in eastern Beringia. Quaternary International 10, 73–83.

Begét, J.E., 2001. Continuous Late Quaternary proxy climate records from loess in Beringia 20, 499–507.

Begét, J.E., Bigelow, N., Powers, W.R., 1991. Reply to the Comment of C. Waythomas and D. Kaufmann. Quaternary Research 36, 334-338.

Begét, J.E., Hawkins, D.B., 1989. Influence of orbital parameters on Pleistocene loess deposition in central Alaska.

Begét, J.E., Stone, D.B., Hawkins, D.B., 1990. Paleoclimatic forcing of magnetic susceptibility variations in Alaskan loess during the late Quaternary. Geology 18, 40–43.

Berger, G.W., 2003. Luminescence chronology of late Pleistocene loess-paleosol and tephra sequences near Fairbanks, Alaska. Quaternary Research 60, 70–83.

Berger, G.W., 1987. Thermoluminescence dating of the Pleistocene Old Crow tephra and adjacent loess, near Fairbanks, Alaska. Canadian Journal of Earth Sciences 24, 1975–1984.

Berger, G.W., Péwé, T.L., Westgate, J.A., Preece, S.J., 1996. Age of Sheep Creek tephra (Pleistocene) in central Alaska from thermoluminescence dating of bracketing loess. Quaternary Research 45, 263–270.

Bigelow, N., Begét, J., Powers, R., 1990. Latest Pleistocene increase in wind intensity recorded in eolian sediments from central Alaska. Quaternary Research 34, 160 168.

Bigelow, N.H., Edwards, M.E., 2001. A 14,000 yr paleoenvironmental record from Windmill Lake, Central Alaska: Lateglacial and Holocene vegetation in the Alaska range. Quaternary Science Reviews 20, 203–215.

Bigelow, N.H., Powers, W.R., 2001. Climate, vegetation, and archaeology 14,000–9000 cal yr BP in central Alaska. Arctic Anthropology 171–195.

Bigelow, N.H., Powers, W.R., 1994. New AMS dates from the Dry Creek Paleoindian site, central Alaska. Current Research in the Pleistocene 11, 114–116.

Blaauw, M., 2010. Methods and code for "classical"age-modelling of radiocarbon sequences. quaternary geochronology 5, 512–518.

Calkin, P.E., 1988. Holocene glaciation of Alaska (and Adjoining YUKON Territory, Canada). Quaternary Science Reviews 7, 159–184.

Daigle, T.A., Kaufman, D.S., 2009. Holocene climate inferred from glacier extent, lake sediment and tree rings at Goat Lake, Kenai Mountains, Alaska, USA. Journal of Quaternary Science 24, 33–45.

Deng, C., Zhu, R., Jackson, M.J., Verosub, K.L., Singer, M.J., 2001. Variability of the temperature-dependent susceptibility of the Holocene eolian deposits in the Chinese loess plateau: a pedogenesis indicator. Physics and Chemistry of the Earth, Part A: Solid Earth and Geodesy 26, 873–878.

Dortch, J.M., Owen, L.A., Caffee, M.W., Li, D., Lowell, T.V., 2010. Beryllium-10 surface exposure dating of glacial successions in the Central Alaska Range. Journal of Quaternary Science 25, 1259–1269.

Graf, K.E., Bigelow, N.H., 2011. Human response to climate during the Younger Dryas chronozone in central Alaska. Quaternary International 242, 434–451.

Graf, K.E., DiPietro, L.M., Krasinski, K.E., Gore, A.K., Smith, H.L., Culleton, B.J., Kennett, D.J., Rhode, D., 2015. Dry Creek Revisited: New Excavations, Radiocarbon Dates, and Site Formation Inform on the Peopling of Eastern Beringia. American Antiquity 80, 671–694.

Harding, J.P., 1949. The use of probability paper for the graphical analysis of polymodal frequency distributions. Journal of the Marine Biological Association of the United Kingdom 28, 141–153.

Hatfield, R.G., Maher, B.A., 2009. Fingerprinting upland sediment sources : particle size specific magnetic linkages between soils , lake sediments and suspended sediments.

Hoffecker, J.F., Waythomas, C. F., Powers, W.R., 1988. Late Glacial Loess Stratigraphy and Archaeology in the Nenana Valley, Central Alaska. Current Research in the Pleistocene 5, 83-86.

Hopkins, D.M., 1982. Aspects of the paleogeography of Beringia during the late Pleistocene. Paleoecology of Beringia 3–28.

Hovan, S.A., Rea, D.K., Pisias, N.G., Shackleton, N.J., 1989. A direct link between the China loess and marine δ18O records: aeolian flux to the north Pacific.

Hu, F.S., Brubaker, L.B., Anderson, P.M., 1993. A 12 000 year record of vegetation change and soil development from Wien Lake, central Alaska. Canadian Journal of Botany 71, 1133–1142.

Jensen, B.J., Evans, M.E., Froese, D.G., Kravchinsky, V.A., 2016. 150,000 years of loess accumulation in central Alaska. Quaternary Science Reviews 135, 1–23.

Kaufman, D.S., Ager, T.A., Anderson, N.J., Anderson, P.M., Andrews, J.T., Bartlein, P.J., Brubaker, L.B., Coats, L.L., Cwynar, L.C., Duvall, M.L., 2004. Holocene thermal maximum in the western Arctic (0–180 W). Quaternary Science Reviews 23, 529–560.

Kaufman, D.S., Axford, Y.L., Henderson, A.C.G., McKay, N.P., Oswald, W.W., Saenger, C., Anderson, R.S., Bailey, H.L., Clegg, B., Gajewski, K., Hu, F.S., Jones, M.C., Massa, C., Routson, C.C., Werner, A., Wooller, M.J., Yu, Z., n.d. Holocene climate changes in eastern Beringia (NW North America) – A systematic review of multi-proxy evidence. Quaternary Science Reviews.

Kukla, G., Heller, F., Ming, L.X., Chun, X.T., Sheng, L.T., Sheng, A.Z., 1988. Pleistocene climates in China dated by magnetic susceptibility. Geology 16, 811 814.

LaBrecque, T.S., Kaufman, D.S., 2016. Holocene glacier fluctuations inferred from lacustrine sediment, Emerald Lake, Kenai Peninsula, Alaska. Quaternary Research 85, 34–43.

Lagroix, F., Banerjee, S.K., 2004. The regional and temporal significance of primary aeolian magnetic fabrics preserved in Alaskan loess. Earth and Planetary Science Letters 225, 379–395.

Lagroix, F., Banerjee, S.K., 2002. Paleowind directions from the magnetic fabric of loess profiles in central Alaska. Earth and Planetary Science Letters 195, 99–112.

Levy, L.B., Kaufman, D.S., Werner, A., 2004. Holocene glacier fluctuations, Waskey Lake, northeastern Ahklun Mountains, southwestern Alaska. The Holocene 14, 185–193.

Lim, J., Matsumoto, E., 2006. Bimodal grain-size distribution of aeolian quartz in a maar of Cheju Island, Korea, during the last 6500 years: Its flux variation and controlling factor. Geophysical Research Letters 33.

Liu, X.M., Hesse, P., Beget, J., Rolph, T., 2001. Pedogenic destruction of ferrimagnetics in Alaskan loess deposits. Soil Research 39, 99–115.

Liu, X.M., Hesse, P., Rolph, T., Begét, J.E., 1999. Properties of magnetic mineralogy of Alaskan loess: evidence for pedogenesis. Quaternary International 62, 93–102.

Maher, B.A., Thompson, R., 1995. Paleorainfall reconstructions from pedogenic magnetic susceptibility variations in the Chinese loess and paleosols. Quaternary Research 44, 383–391.

Middleton, G.V., 1976. Hydraulic interpretation of sand size distributions. The Journal of Geology 405–426.

Mock, C.J., Bartlein, P.J., Anderson, P.M., 1998. Atmospheric circulation patterns and spatial climatic variations in Beringia. International Journal of Climatology 18, 1085–1104.

Muhs, D., 2003. Stratigraphy and palaeoclimatic significance of Late Quaternary loess palaeosol sequences of the Last Interglacial–Glacial cycle in central Alaska. Quaternary Science Reviews 22, 1947–1986.

Muhs, D.R., Ager, T.A., Bettis, E.A., McGeehin, J., Been, J.M., Begét, J.E., Pavich, M.J., Stafford, T.W., De Anne, S.P., 2003. Stratigraphy and palaeoclimatic significance of Late Quaternary loess–palaeosol sequences of the Last Interglacial–Glacial cycle in central Alaska. Quaternary Science Reviews 22, 1947–1986.

Muhs, D.R., Ager, T.A., Skipp, G., Beann, J., Budahn, J., McGeehin, J.P., 2008. Paleoclimatic significance of chemical weathering in loess-derived paleosols of subarctic central Alaska. Arctic, Antarctic, and Alpine Research 40, 396–411.

Muhs, D.R., Bettis, E.A., 2003. Quaternary loess-paleosol sequences as examples of climate-driven sedimentary extremes. Special Papers-Geological Society of America 53–74.

Muhs, D.R., Budahn, J.R., 2006. Geochemical evidence for the origin of late Quaternary loess in central Alaska. Canadian Journal of Earth Sciences 43, 323–337.

Muhs, D.R., Budahn, J.R., Skipp, G.L., McGeehin, J.P., 2016. Geochemical evidence for seasonal controls on the transportation of Holocene loess, Matanuska Valley, southern Alaska, USA. Aeolian Research 21, 61–73.

Muhs, D.R., McGeehin, J.P., Beann, J., Fisher, E., 2004. Holocene loess deposition and soil formation as competing processes, Matanuska Valley, southern Alaska. Quaternary Research 61, 265–276.

Park, C.-S., Hwang, S., Yoon, S.-O., Choi, J., 2014. Grain size partitioning in loess paleosol sequence on the west coast of South Korea using the Weibull function. Catena 121, 307–320.

Pendea, I.F., Gray, J.T., Ghaleb, B., Tantau, I., Badarau, A.S., Nicorici, C., 2009. Episodic build-up of alluvial fan deposits during the Weichselian Pleniglacial in the western Transylvanian Basin, Romania and their paleoenvironmental significance. Quaternary International 198, 98–112.

Pewe, T.L., 1955. Origin of the upland silt near Fairbanks, Alaska. Geological Society of America Bulletin 66, 699–724.

Péwé, T.L., Hopkins, D.M., Giddings Jr, J.L., 1965. Quaternary geology and archaeology of Alaska.

Porter, S.C., Zhisheng, A., 1995. Correlation between climate events in the North Atlantic and China during the last glaciation.

Powers, W.R., Guthrie, R.D., Hoffecker, J.F., 1983. Dry Creek: Archeology and paleoecology of a late Pleistocene Alaskan hunting camp. .

Powers, W.R., Hoffecker, J.F., 1989. Late Pleistocene settlement in the Nenana valley, central Alaska. American Antiquity 263–287.

Preece, S.J., Westgate, J.A., Stemper, B.A., Péwé, T.L., 1999. Tephrochronology of late Cenozoic loess at Fairbanks, central Alaska. Geological Society of America Bulletin 111, 71–90.

Pye, K., 1995. The nature, origin and accumulation of loess. Quaternary Science Reviews, Aeolian Sediments in the Quaternary Record 14, 653–667.

Reimer, P.J., Bard, E., Bayliss, A., Beck, J.W., Blackwell, P.G., Bronk Ramsey, C., Buck, C.E., Cheng, H., Edwards, R.L., Friedrich, M., 2013. IntCal13 and Marine13 radiocarbon age calibration curves 0-50,000 years cal BP.

Ritter, D.F., 1982. Complex river terrace development in the Nenana Valley near Healy, Alaska. Geological Society of America Bulletin 93, 346–356.

Smalley, I., O'Hara-Dhand, K., Wint, J., Machalett, B., Jary, Z., Jefferson, I., 2009. Rivers and loess: the significance of long river transportation in the complexevent-sequence approach to loess deposit formation. Quaternary International 198, 7–18.

Solomina, O.N., Bradley, R.S., Hodgson, D.A., Ivy-Ochs, S., Jomelli, V., Mackintosh, A.N., Nesje, A., Owen, L.A., Wanner, H., Wiles, G.C., Young, N.E., 2015. Holocene glacier fluctuations. Quaternary Science Reviews 111, 9–34.

Sun, D., Bloemendal, J., Rea, D.K., An, Z., Vandenberghe, J., Lu, H., Su, R., Liu, T., 2004. Bimodal grain-size distribution of Chinese loess, and its palaeoclimatic implications. Catena 55, 325–340.

Sun, D., Bloemendal, J., Rea, D.K., Vandenberghe, J., Jiang, F., An, Z., Su, R., 2002. Grain-size distribution function of polymodal sediments in hydraulic and aeolian environments, and numerical partitioning of the sedimentary components. Sedimentary Geology 152, 263–277.

Sun, D., Su, R., Bloemendal, J., Lu, H., 2008. Grain-size and accumulation rate records from Late Cenozoic aeolian sequences in northern China: Implications for variations in the East Asian winter monsoon and westerly atmospheric circulation. Palaeogeography, Palaeoclimatology, Palaeoecology 264, 39–53.

Tarr, R.S., Martin, L., 1913. Glacial Deposits of the Continental Type in Alaska. The Journal of Geology 21, 289-300

Ten Brink, N.W., Waythomas, C.F., 1985. Late Wisconsin glacial chronology of the north-central Alaska Range: A regional synthesis and its implications for early human settlements. (No. 19), National Geographic Society Research Reports. North Alaska Range Early Man Project.

Thorson, R.M., Bender, G., 1985. Eolian deflation by ancient katabatic winds: a late Quaternary example from the north Alaska Range. Geological Society of America Bulletin 96, 702–709.

Thorson, R.M., Hamilton, T.D., 1977. Geology of the Dry Creek Site; a stratified Early Man site in interior Alaska. Quaternary Research 7, 149–176.

Tsoar, H., Pye, K., 1987. Dust transport and the question of desert loess formation. Sedimentology 34, 139–153.

Vandenberghe, J., 2013. Grain size of fine-grained windblown sediment: A powerful proxy for process identification. Earth-Science Reviews 121, 18–30.

Vlag, P.A., Oches, E.A., Banerjee, S.K., Solheid, P.A., 1999. The paleoenvironmental magnetic record of the Gold Hill steps loess section in central Alaska. Physics and Chemistry of the Earth, Part A: Solid Earth and Geodesy 24, 779–783.

Wahrhaftig, C., Black, R.F., 1958. Quaternary geology of the Nenana River valley and adjacent parts of the Alaska Range; Engineering geology along part of the Alaska Railroad.

Waythomas, C.F., Kaufman, D.S., 1991. Comment on: "Latest Pleistocene Increase in Wind Intensity Recorded in Eolian Sediments from Central Alaska," by N. Bigelow, J.E. Begét, and W.R. Powers. Quaternary Research 36,329-333.

Westgate, J.A., Stemper, B.A., Péwé, T.L., 1990. A 3 my record of Pliocene-Pleistocene loess in, interior Alaska. Geology 18, 858–861.

Xiao, J., Chang, Z., Si, B., Qin, X., Itoh, S., Lomtatidze, Z., 2009. Partitioning of the grain-size components of Dali Lake core sediments: evidence for lake-level changes during the Holocene. Journal of Paleolimnology 42, 249–260.

Xiao, J., Porter, S.C., An, Z., Kumai, H., Yoshikawa, S., 1995. Grain size of quartz as an indicator of winter monsoon strength on the Loess Plateau of central China during the last 130,000 yr. Quaternary Research 43, 22–29.

CHAPTER THREE

Deposition and Pedogenesis of Periglacial Sediments and Buried Soils at the Serpentine Hot Springs Archaeological Site, Seward Peninsula, AK

This chapter published as: DiPietro, L., Driese, S., and Goebel, T., 2018. Deposition and pedogenesis of periglacial sediments and buried soils at the Serpentine Hot Springs archaeological site, Seward Peninsula, AK. Catena, 170 204-223.

Abstract

Soil micromorphology is an excellent tool for relating quantitative laboratory data to soil development in complex pedogenic settings. This study utilizes micromorphology, scanning electron microscopy, bulk soil geochemistry, clay mineralogy, and particle-size analysis to reconstruct the depositional and pedogenic history of the Serpentine Hot Springs fluted point site on the Seward Peninsula, Alaska. Sediment deposition occurred via colluviation, which dominated during the late glacial period and early- to middle Holocene, and aeolian processes, which dominated during the Younger Dryas (YD) and late Holocene. Two buried soils are present: one dating to the Holocene Thermal Maximum (HTM) and the other dating just before the Neoglacial period. Pedofeatures fall into four categories: 1) cryogenic features; 2) clay illuviation features; 3) podzolization/redox features; and 4) anthropogenic features. The spatial relationships among these features provides insight into the pedogenic history of the soil. The HTM soil is characterized by clay illuviation, suggesting warm, mildly acidic, well-drained soil conditions. The pre-Neoglacial soil is characterized by incipient placic horizon development and podzolization, indicative of moist, acidic, variably drained conditions. Cryogenic features associated with late Holocene Neoglaciation dominate the modern

soil. Despite cryogenic activity and the presence of permafrost, the cultural stratigraphy of the site remains intact.

Introduction

Micromorphology, the microscopic examination of soils in their undisturbed states (Stoops, 2003), is concerned with the genesis, classification, and characterization of sediments, soils, and paleosols as well as the interaction of soils with the landscapes and climatic conditions which shape them (Kubiëna, 1938). It is a tool long used in paleopedology and, more recently, in geoarchaeology to better understand the processes by which soils form and change over time. Most commonly, micropedological techniques are applied to answer questions about deposition, site and soil formation, and paleoenvironment (Courty, 1991; Douglas et al., 1990; Ringrose-Voase et al., 1994; Rutherford, 1974).

Since the 1970s, micromorphology has been applied as a tool to better understand complex temporal and spatial relationships within soil profiles. It has been used in paleoenvironmental studies to help address interpretive difficulties resulting from the superposition of pedogenic features associated with one set of climatic or environmental conditions on top of features associated with a different set of conditions, often referred to as pedogenic overprinting (e.g. Bronger et al., 1993; Driese and Ashley, 2016; Kemp, 1999, 1998; McCarthy et al., 1998). From an archaeological perspective, micromorphological studies have been used to address concerns about the stratigraphic integrity of the archaeological record at sites in ‘active’ soils, such as Vertisols and Gelisols which can displace artifacts (e.g. Bertran, 1994; Bertran et al., 2010; Bertran and Texier, 1995; Driese et al., 2013; Gilbert, 2011; Todisco and Bhiry, 2008).

The periglacial soils and sediments at the Serpentine Hot Springs archaeological site on the Seward Peninsula offer an ideal opportunity to demonstrate the utility of micromorphology in geoarchaeological and paleoenvironmental contexts. The Serpentine Hot Springs site represents the first well-documented occurrence of fluted points in a buried, well-dated context in Alaska and, as such, plays an important role in understanding the migration of modern *Homo sapiens* into North America (Goebel et al., 2013; Smith et al., 2013). The place of Alaska's fluted point sites within the broader context of early human occupations of North America has long been debated (Goebel et al., 2013; Goebel and Potter, 2016; Smith et al., 2013; Solecki, 1950). Fluted points are diagnostic of Clovis technology, the first widespread and well-documented Paleoamerican archaeological complex in North America. Although the presence of modern humans in the Americas prior to the Clovis culture has gained increasing acceptance in recent years, a viable predecessor for Clovis technology has yet to be identified. When first discovered in the 1950s, Alaskan fluted points appeared to be a promising candidate for such an antecedent technology, but these first-discovered points were not recovered from contexts that could be dated reliably. Since that time, however, Alaskan fluted points have been recovered from buried contexts and a very different picture of their role in North American prehistory has emerged. Rather than representing a progenitor of Clovis technology, recent work suggests that Alaskan fluted points may instead represent a so-called 'reverse' migration of Clovis peoples from the northwestern United States and Canada back into Alaska (Smith and Goebel, 2018). Thus, understanding the integrity of the archaeological record at Serpentine, a key fluted point site in Alaska, is critical. However, the site is in a periglacial setting, where disruptive

processes such as cryoturbation and solifluction are a major concern for the stratigraphic integrity of the archaeological record. Micromorphology allows for a more detailed assessment of the degree of site disturbance and can help identify problem areas for interpreting archaeological data.

Understanding the paleoenvironmental history of the Serpentine soil is also important, because climate research has begun to predict the magnitude and effects of future climate change, and the models have suggested that the high-latitudes exhibit amplified responses to warming (Flato and Boer, 2001). Understanding amplified warming in the northern latitudes is especially important because it operates as a positive feedback mechanism-warming causes permafrost melting, which, in turn, leads to the oxidation of previously-sequestered organic matter and the release of CO_2 and CH_4. This process is a complex one (Davidson and Janssens, 2006) that highlights the need for real-world paleoclimate case studies to 'field check' the validity of model predictions. Paleoenvironmental studies of high-latitude soils are far fewer in number than studies of their temperate and tropical counterparts and micromorphological analysis of soils like those at Serpentine can provide an important, albeit qualitative, record of how these sensitive soils have responded to the dynamic climate shifts of the late Quaternary. This study integrates classical micromorphological analysis with scanning electron microscopy, detailed particle size analysis, and geochemical methods to determine the depositional and pedogenic history of the soils at the Serpentine site and the integrity of the important archaeological record it contains.

Background

Geographic Setting

The Serpentine Hot Springs fluted point site, BEN-192, is located on the Seward Peninsula in northwest Alaska within the confines of Bering Land Bridge National Preserve (Fig. 3.1). Although the regional bedrock primarily consists of meta-sedimentary rocks and chlorite schists, the site itself sits at the edge of one of a series of tin ore-bearing, shallowly emplaced Late Cretaceous biotite granite stocks, locally known as the Oonatut Granite complex (Hudson, 1977). The landscape surrounding the site is characterized by granite tors, ridges, and rolling hills, separated by broad upland valleys. The bluff upon which the site is located overlooks the hot springs for which it is named to the southeast and a small, unnamed creek that flows into Hot Springs Creek to the south.

Non-acidic shrub tundra species, including dwarf birch, various blueberry species, lowbush cranberry, bear berry, crowberry, lichens, and mosses, dominate the modern upland vegetation. Stands of *Salix sp.* (willow) are commonly found along creek margins and floodplains in the valley. Mean annual precipitation (MAP) at the site is ~400 mm/yr, about 60% of which falls during the summer months (Rupp et al., 2000). The area receives approximately 150 mm/yr snowfall during the winter. Winters are cold and long with temperatures reaching -30°C on average, and temperatures are below freezing between October and May (Hopkins, 1959; Rupp et al., 2000). Summers (June-September) are generally cool, with an average temperature near 7°C (Rupp et al., 2000), giving a mean annual temperature of -6°C (Hopkins, 1959). Although it is located just south of the Arctic Circle, the site and surrounding area were not glaciated during the

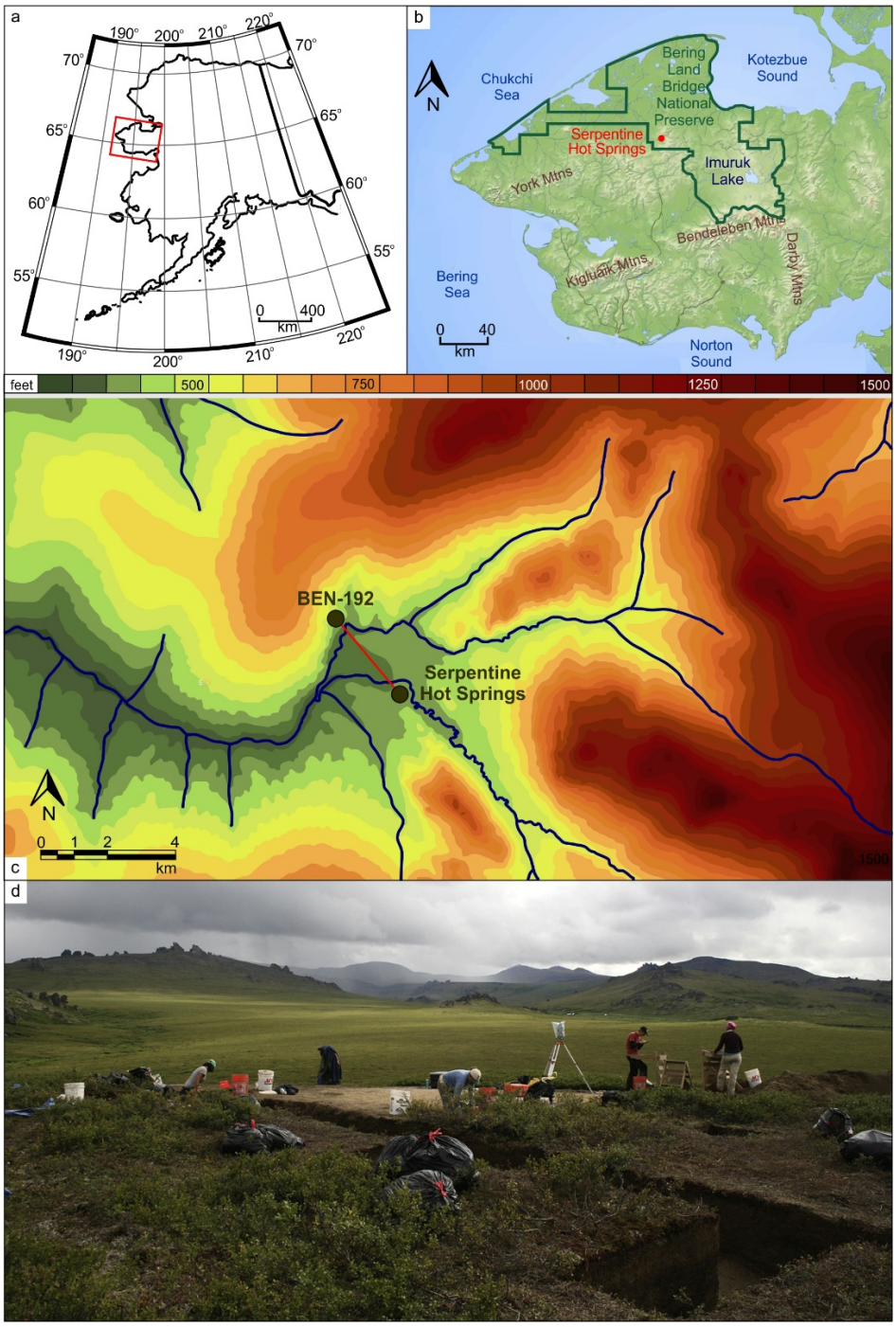

Figure 3.1 A) Map showing the location of the Seward Peninsula in northwest Alaska, and the Bering Sea; B) Location of the Serpentine Hot Springs archaeological site, BEN-192, on the Seward Peninsula, northwest Alaska; C) Topographic map showing position of the Serpentine Hot Springs archaeological site D) Photograph of Serpentine Hot Springs archaeological site looking towards the bunkhouse at Serpentine Hot Springs (white buildings visible in the midground) to the southeast. Line of sight is marked in red in Fig. 3.1C.

Last Glacial Maximum. Instead, glaciation was restricted to the Kigluaik, Darby, York, and Bendeleben Mountains (Calkin, 1988; Kaufman and Hopkins, 1986; Kaufman and Manley, 2004).

Site Stratigraphy

Three major colluvial stratigraphic units were identified at Serpentine during excavation (Fig. 3.2). These units were differentiated primarily based on field textural analysis and were identified independently of soil horizons. Each of the three strata, designated as units 1, 2, and 3 from oldest to youngest, were interpreted as colluvial in origin, having washed down the gentle slope behind the site. The bedrock surface upon which the sediment package rests unconformably has irregular topography and is variably weathered across the landform. In most places, a thick layer of gruss or gravelly, saprolitized granite overlies fresh bedrock and forms the base of the profile (Unit 0). Colluviation of this grussy material from upslope was interpreted as the primary depositional mechanism for units 1, 2, and 3 (Goebel et al., 2013). A large blowout is located along the bluff edge directly adjacent to the site, and it is likely that this and other similar areas have contributed aeolian silt to the soil as well, although in lesser quantities than the colluvium.

Unit 1 is the basal sedimentary unit. It is a poorly-sorted, angular to subangular, brown, clayey to silty gravel with abundant silty and clayey matrix. Gravel clasts are primarily granite lithic fragments 3-5 mm in diameter. Coarse material (sand and gravel) is, in some instances, concentrated in lenses. Unit 2, a clayey silt, overlies Unit 1. The contact between the two depositional units is irregular to wavy. Unit 2 is more clay-rich and better sorted than Unit 1, although abundant sand and gravel are still present. Its

color is much darker, and abundant charcoal is present. Overlying Unit 2 is Unit 3, another silty gravel that is texturally like Unit 1. The thickness of Unit 3 is variable, ranging from about 20-70 cm. All three units appear to have been affected by cryoturbation, because the boundaries between them are irregular and highly undulatory in places. It is important to note, however, that all three units are easily distinguishable from one another and readily identifiable across the site.

Materials and Methods

Field Description and Sampling

Block excavation of 33 m^2 was conducted at Serpentine over the course of three summer field seasons between 2009 and 2011 (Fig. 3.2). During excavation, the three lithostratigraphic units described above were identified. Since the textural and morphological differences between the three units were easily recognized during excavation, these lithostratigraphic designations were used by most excavators when taking field notes and logging artifact provenance. Once excavation was finished and work on the soil profile itself began, the profile was described and mapped by Michael Waters and Kelly Graf (Texas A & M Univ.) in accordance with NRCS soil-description protocols. Samples were taken from the geologic trench excavated at the site. Bulk sediment samples were taken from each depositional unit: two samples from units 1 and 3, one sample from Unit 2, and one sample from the grussy saprolite (Fig. 3.2). Two

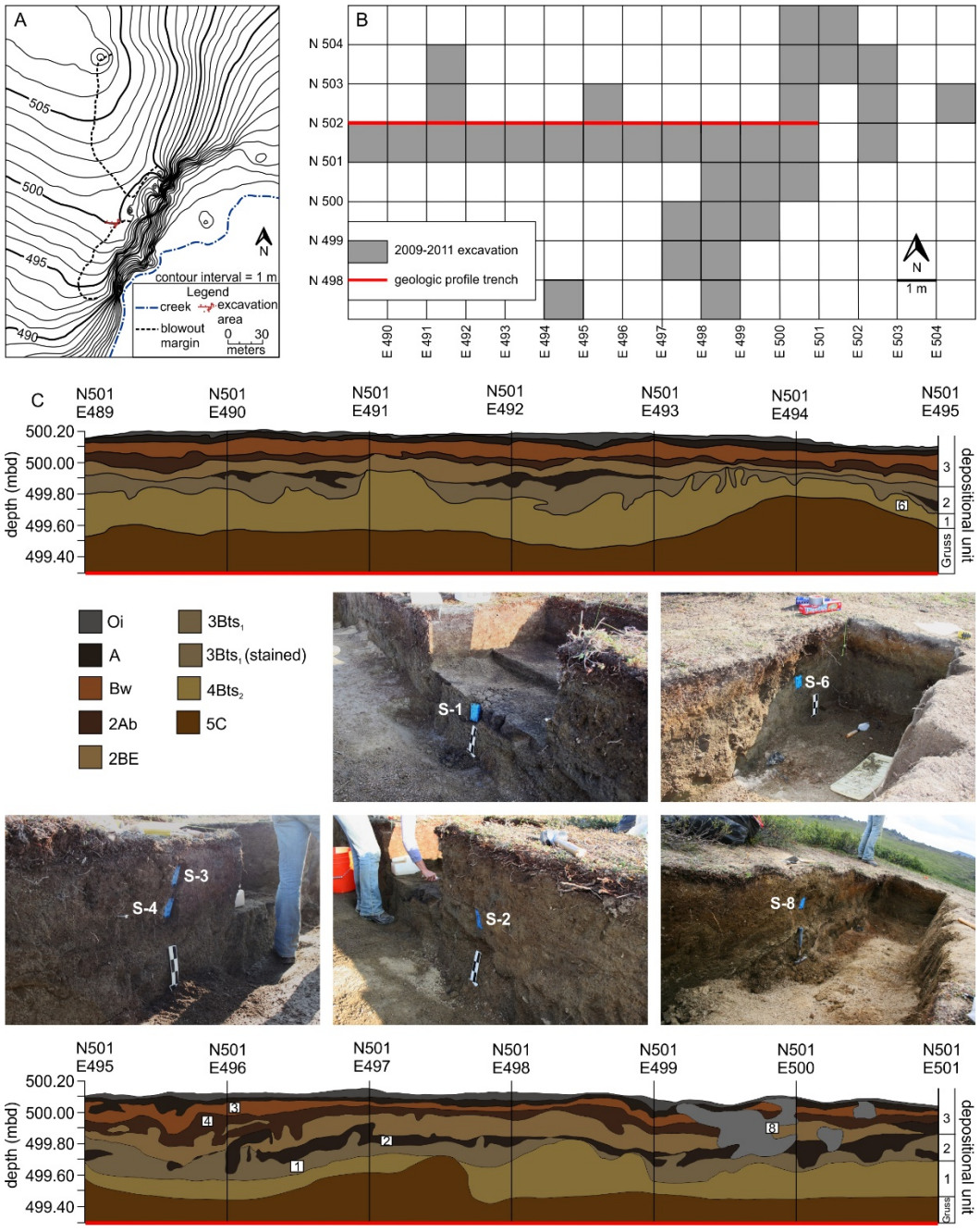

Figure 3.2. A) Topographic map showing location of the Serpentine Hot Springs archaeological excavation near the edge of a granite bluff and location of blowout margin; B) Map of the excavation block, showing location of the geologic profile trench; C) Schematic profile drawing of the north wall of the geologic trench, including depositional units 1-3 soil horizons, rodent burrow in gray, and locations of thin section samples. Photographs are included showing the locations from which each thin section was collected within the excavation trench. Depth for the schematic profiles is indicated in m below the arbitrary site datum

oriented samples for micromorphological analysis were collected in plastic electrical conduit boxes from each unit.

During excavation, trend and plunge were measured for all large-sized artifacts (those whose size was great enough that the measuring process would not disturb their orientation) using a Brunton pocket transit. Of the 1,512 pieces of debitage and tools recovered from the site, plunge was scored for 62 artifacts and trend for 50. Orientations of these artifacts were separated into 20° bins for trend and 10° bins for plunge and plotted on polar histograms. Pearson's chi-squared goodness of fit tests were performed on the data (plunge: $\chi^2 = 18.1$, d.f. = 8, p = 0.020; trend: $\chi^2 = 11.2$, d.f. = 16, p = 0.797) to test for random distributions (Fig. 3.3).

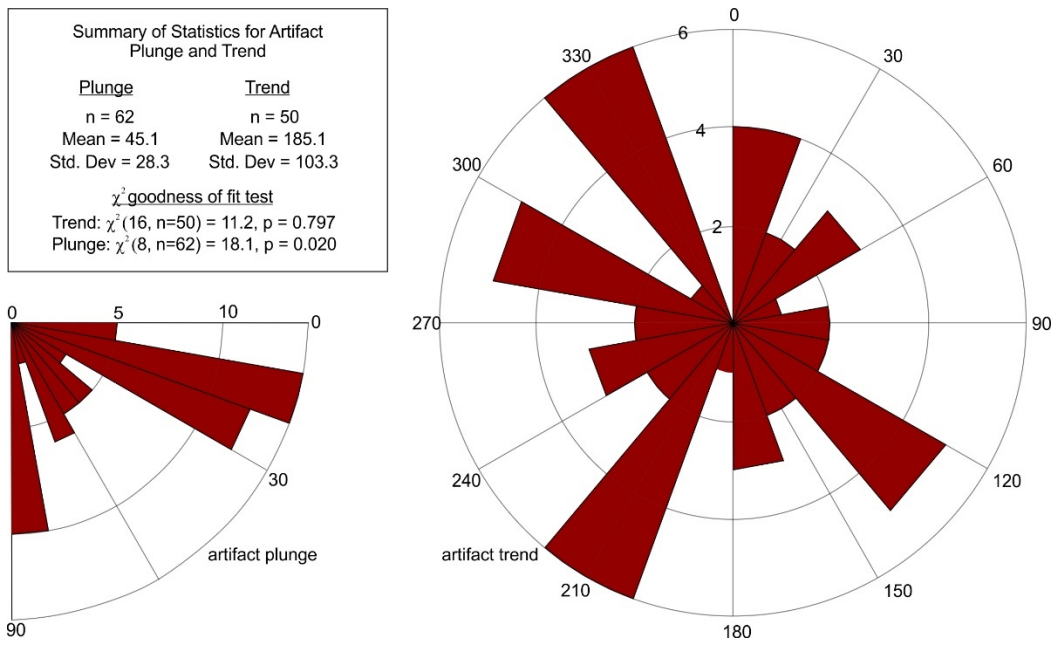

Figure 3.3. Frequencies of artifact plunge and trend with statistical results from the analysis of each variable. Concentric circles represent the number of artifacts with orientations in each range. Plunge data suggest some vertical re-orientation of large artifacts. Trend data indicate random orientation of artifacts and do not support colluvial reworking of the archaeological materials.

Laboratory and Analytical Methods

Two radiocarbon dates on bulk humates were obtained for this study, in addition to the many dates presented in Goebel et al. (2013). Aliquots of the bulk soil samples from the uppermost Bw and the buried A horizon were sent to Beta Analytics for dating (Table 1).

Oriented samples collected for soil micromorphology were air-dried, surface impregnated with Hillquist thin-section epoxy, and sent to Spectrum Petrographics for vacuum impregnation and thin-section preparation. Prepared slides were 5x7 cm (Fig. 3.4). Microscopy was performed on an Olympus BX51 binocular polarizing microscope, and photomicrographs were taken using a 12.5 MPx Leica digital camera attachment. Thin sections were described using soil-micromorphology terminology following Stoops (Stoops, 2003).

Additional 1” x 2” microprobe polished thin sections were prepared from each billet by National Petrographic Service Inc. for scanning electron microscopy. Thin sections were mounted on aluminum stubs using carbon tape and then sputter-coated with 20 nm of carbon (EM ACE 600, Leica Microsystems). Specimens were observed in a Versa 3D scanning electron microscope (FEI, Hillsboro, OR, USA) by using a backscattered electron detector. Electron dispersive spectroscopy (EDS) was performed with an Octane Pro Silicon Drift Detector (EDAX, Mahawah, NJ, USA) at 20kV, spot size 7, and at a working distance of 10mm.

Table 3.1 Radiocarbon chronology for Serpentine Hot Springs archaeological site.

Previously Reported Radiocarbon Dates (Goebel et. al., 2013)

Unit	Sample Number	Age, ^{14}C BP	Age, cal BP[a] (1 σ range)	Material dated
2	UCIAMS-90959	10,295 ± 25	12,030-12,120	cf. *Salix* sp. charcoal
2	UCIAMS-90960	10,290 ± 25	12,010-12,109	cf. *Salix* sp. charcoal
2	UCIAMS-90961	10,370 ± 25	12,132-12,379	cf. *Salix* sp. charcoal
2	UCIAMS-90962	10,320 ± 25	12,045-12,210	cf. *Salix* sp. charcoal
2	UCIAMS-90963	10,275 ± 25	11,998-12,083	cf. *Salix* sp. charcoal
2	UCIAMS-77097	9940 ± 25	11,267-11,358	charcoal[b]
2	UCIAMS-77098	9375 ± 25	10,567-10,655	charcoal[b]
2	UCIAMS-90953	10,270 ± 25	11,993-12,078	*Betula* sp. charcoal
2	UCIAMS-90954	9985 ± 25	11,321-11,598	cf. Ericaceae charcoal
2	UCIAMS-90955	9900 ± 25	11,247-11,305	*Betula* sp. charcoal
2	UCIAMS-90956	10,015 ± 25	11,398-11,603	cf. Ericaceae charcoal
2	UCIAMS-90957	8875 ± 25	9914-10,147	cf. Ericaceae charcoal
2	UCIAMS-90958	9930 ± 25	11,250-11,390	*Betula* sp. charcoal
2	UCIAMS-90965	10,375 ± 30	12,142-12,379	charcoal[b]
2	UCIAMS-90966	10,325 ± 35	12,046-12,372	charcoal[b]
2	UCIAMS-106037	10,075 ± 50	11,408-11,763	cf. Ericaceae charcoal
2	UCIAMS-106038	10,440 ± 40	12,169-12,521	cf. *Salix* sp. charcoal
2	UCIAMS-106036	9370 ± 35	10,524-10,658	*Betula* sp. charcoal
2	UCIAMS-106039	9335 ± 35	10,501-10,587	*Betula* sp. charcoal
2	UCIAMS-106040	9360 ± 35	10,520-10,651	*Betula* sp. charcoal
2	UCIAMS-106041	8920 ± 35	9937-10,178	*Betula* sp. charcoal
2	UCIAMS-106042	9345 ± 35	10,510-10,645	*Betula* sp. charcoal
2	UCIAMS-77095	9920 ± 25	11,256-11,325	charcoal[b]
2	UCIAMS-77096	9960 ± 25	11,285-11,396	charcoal[b]
1	UCIAMS-90967	12,760 ± 50	14,950-15,148	charcoal[b]

Published dates come from Goebel et al. (2013).

New Dates from the Current Study

Unit	Sample Number	Age, ^{14}C BP	Age, cal BP (1 σ range)	Material dated
3	Beta-409065	5690 ± 30	6405-6535	organic sediment (S-3b)
3	Beta-409064	3820 ± 30	4100-4115 4145-4295 4345-4335	organic sediment (S-3a)

[a] Calibrated using OxCal v4.2.3 Bronk Ramsey (2013); r:5 IntCal13 atmospheric curve (Reimer et al. 2013)

[b] Sample too small to be identified

Clay mineralogy was determined at Baylor University for each sample by means of x-ray diffraction using a Siemens D-5000 x-ray diffractometer with Cu-Kα radiation at an accelerating potential of 40 kV and a tube current of 30 mA. Oriented aggregates were

prepared for determination of clay mineralogy. The clay size fraction (less than 2 microns) was separated via centrifugation, vacuum-oriented and applied to glass slides following the Millipore transfer method outlined by Moore and Reynolds (1989). Four oriented aggregates were prepared from aliquots of each sample and each aggregate subjected to a different treatment: 1) K-saturation; 2) K-saturation and heat treatment at 550°C for 5 hours; 3) Mg-saturation; and 4) Mg-saturation and solvation with a 4:1 solution of glycerol and de-ionized water. Oriented aggregates were scanned over a range of 2-30° 2θ with a step size of 0.04° and a dwell time of 2 seconds.

Samples for particle-size analysis were sieved to remove grains larger than 2 mm in diameter. Once sieved, the remaining material was pre-treated with 30% H_2O_2 until reaction ceased to remove particulate organic matter. X-ray analyses indicated that carbonates were absent, so HCl pre-treatment was unnecessary. Samples were then suspended in 1L of de-ionized water, dispersed with 10 mL of 10% $(NaPO_3)_6$ and sonicated for 3 minutes to ensure complete disaggregation. Particle-size analysis was performed using a Malvern MasterSizer® 2000 with a Hydro MU dispersion unit. Data were collected in quarter-phi increments and were converted to grain sizes using the Mie Theory. Duplicate analyses were performed periodically to ensure accuracy.

Aliquots of the greater-than-2 mm and less-than-2 mm fractions from each sample were then powdered and sent to ALS Chemex to determine bulk elemental chemistry. Samples were put into solution using a four-acid, near-total digestion process and analyzed for the concentrations of 48 major and trace elements via combination ICP-MS/ICP-AES. Raw data are provided in Supplement 1. Carbon and nitrogen content was determined using a Thermo Finnegan Flash 1112 Series elemental analyzer at Baylor

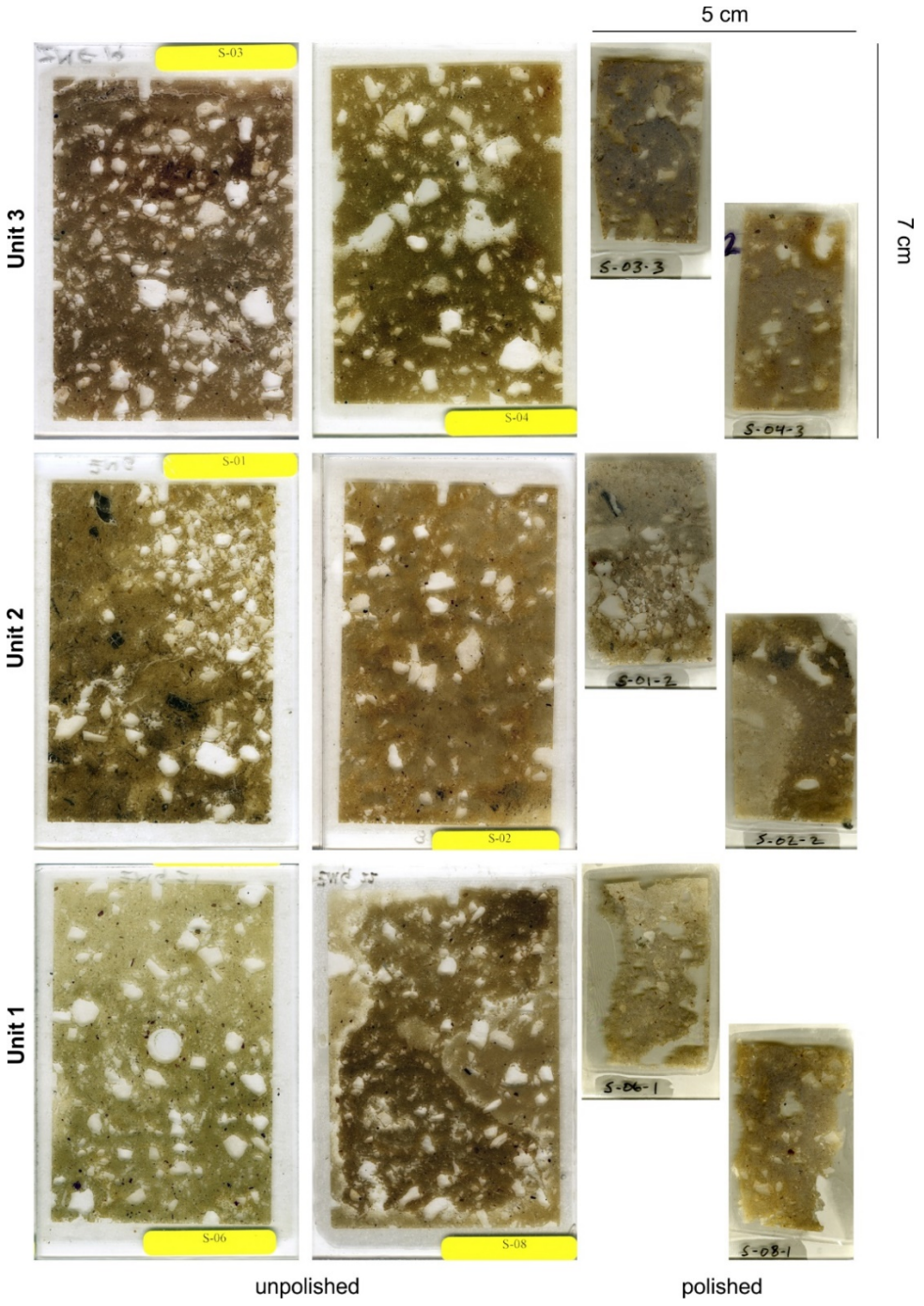

Figure 3.4. Scans of the six large (5x7 cm) unpolished thin sections used for micromorphological analysis and six small (2x4.5 cm) polished thin sections used for scanning electron microscope (SEM) analysis. Both sets of thin sections were prepared from the same billets and the sample numbers correlate to the sample numbers from Fig 3.2.

University. Prior to analysis, the sediments were found to be non-calcareous, so acidification of samples was not needed.

Results

Soil Morphology

Seven soil horizons were identified at Serpentine, based on a combination of field description and laboratory characterization (Fig. 3.2). Laboratory data and field descriptions are summarized in Table 2. At the top of the soil profile is a thick organic mat, identified as the modern Oi horizon of the soil. In places, an A horizon underlies it, although this is not present universally across the excavation block. Beneath the A horizon is a thin Bw horizon with platy ped structure. A buried soil complex underlies this, consisting of an Ab horizon and a BE horizon. These horizons overlie a second buried soil complex, consisting of upper and lower Bts horizons, which show evidence for both podzolization and clay illuviation. Technically, this combination of horizon subscripts is not allowed within the USDA soil taxonomic system, because the illuviation of clay and sesquioxides occurs in non-compatible soil environments. Nevertheless, evidence for both processes is clearly present within the horizon in question, likely as the result of overprinting. This is not to suggest that the clay illuviation and podzolization were contemporaneous, but instead, that there is evidence for both processes having acted upon the horizon at some point during the history of the soil. Below this is the C horizon of the soil, composed of the gruss described in section 2.2. The ‘f’ subscript is not added to the soil horizons as designated in this paper because the soil was not frozen during the period of excavation, but it is likely that the soil is frozen for most of the year.

Site Chronology

Goebel et al. (2013) developed an initial chronology for the site using radiocarbon dates from wood charcoal (Table 1). The samples were identified where possible and were found to be either willow (*Salix*), birch (*Betula*), or Ericaceae, three common plants near the site today (Goebel et al., 2013). Twenty-four of the 25 dates obtained during excavation were from Unit 2, which is the main archaeological horizon at the site. These dates place its deposition between 12,500 and 10,000 BP, during and just after the Younger Dryas. One charcoal sample was collected from the underlying Unit 1. This sample, whose species was unidentifiable, did not come from the excavation block proper, but from a test pit to the north of the site, further up the ridge. It places the deposition of Unit 1 sometime between 14,950 and 15,400 BP. No wood charcoal was found in Unit 3.

This study contributes two new radiocarbon ages for Unit 3 (Table 1). Because wood charcoal was lacking for this unit, the decision was made to date the soil organic matter from the buried A horizon and the upper Bw horizon. These new dates suggest that the upper buried soil at the site dates to between 6400 and 6500 BP and the Bw horizon dates to 4100-4350 BP.

Soil Micromorphology and Microscopy

Texture and Composition. All samples analyzed are very poorly sorted (Fig. 3.5A, 9). The coarse mineral fraction is dominated by angular to subangular sand-to granule-sized quartz, plagioclase and potassium feldspars, biotite, and igneous rock fragments. The relative proportions of these minerals are consistent throughout all depositional units, although units 1 and 3 have considerably more sand and gravel than does unit 2. Both

Table 3.2. Soil laboratory characterization data, sample numbers, and descriptions.

Horizon	Unit	Sample	Clay[b]	Silt[b]	Sand[b]	Gravel	C/N	Description
Oi/A	3	-	-	-	-	-	-	fine to medium, weak, granular to platy ped structure, broken upper boundary, many very fine to medium roots, very dark grey (2.5Y 3/1)
Bw	3	S-3a	13.45 (16.40)	61.21 (74.65)	7.34 (8.95)	18	31.38	fine to medium, weak, granular to platy ped structure, broken upper boundary, many very fine to medium roots, dark brown (10 YR 3/3)
2Ab	3	S-3b	11.75 (15.26)	49.08 (62.44)	17.17 (22.30)	23	19.93	fine to medium, weak, granular to platy ped structure, wavy upper boundary, many very fine to medium roots, very dark greyish brown (10 YR 3/2)
2BE	3	-	-	-	-	-	-	fine to medium, weak, massive to platy ped structure, wavy upper boundary, many very fine to medium roots, brown (10 YR 5/3)
$3Bts_1$	2	S-2	16.65 (17.91)	69.25 (73.39)	8.09 (8.70)	7	7.89	fine to medium, moderate to strong platy to granular ped structure (platy near top of horizon, granular near base), wavy to broken upper boundary, common clay cutans, abundant charcoal and organic staining (2.5 Y 3/1), greyish brown (2.5 Y 5/2)
$4Bts_2$	1	S-1a, S-1b[a]	12.31 (14.66)	54.02 (64.31)	17.67 (21.03)	16	8.83	fine to medium, weak to moderate, platy ped structure, wavy to broken upper boundary, few clay cutans, organic staining (2.5 Y 3/1), light olive brown (2.5 Y 5/3)
5C	Gruss	Gruss	1.43 (6.52)	11.30 (51.36)	9.97 (42.11)	78	7.17	poorly-sorted, gravelly granitic saprolite with abundant clay coatings and iron oxide accumulations

[a]Particle size and carbon/nitrogren concentrations given here represent an average of the value for these two samples.

[b] Values in parentheses are calculated on a gravel-free basis

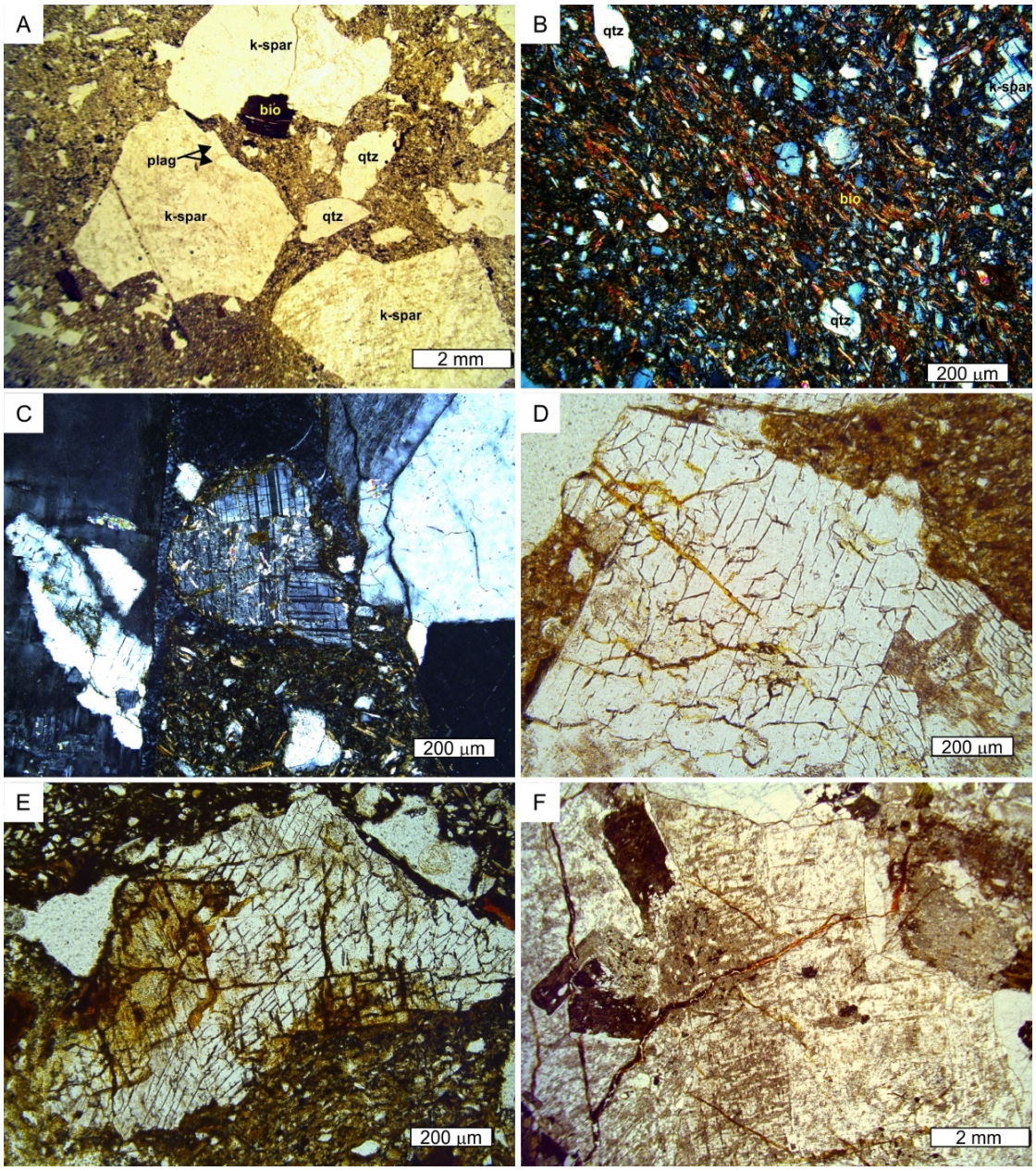

Figure 3.5. Photomicrographs illustrating the general character of skeletal grains and matrix. A) Major skeletal constituents of the soil (qtz-quartz, k-spar-potassium feldspar, plag-plagioclase feldspar, bio-biotite) and their distribution within the soil matrix (plane-polarized light (PPL), S-03, unit 3); B) Composition of the fine soil matrix, including silt-sized quartz and biotite (cross-polarized light (XPL), S-01, unit 2)); C) Sericitized potassium feldspar in igneous rock fragment (XPL, S-04, unit 3); D) and E) Plagioclase feldspar with alteration to orange-yellow clay along randomly-oriented fractures and unaltered, orthogonal fractures along cleavage planes (PPL, S-01, unit 2); F) Randomly-oriented, clay-filled fracture in a potassium feldspar in the gruss (PPL).

units 1 and 2 have increased matrix relative to unit 3. The groundmass is composed of quartz silt, micas, and clays (Fig. 3.5B). Both muscovite and biotite are observed, are generally slightly larger than the silt-sized quartz and appear to be oriented roughly parallel to the ground surface. Units 1 and 3 have a single-spaced to open porphyric coarse/fine distribution, whereas unit 2 has a double-spaced to open porphyric coarse/fine distribution, indicating lower sand and gravel content. There is evidence for intense chemical alteration of feldspars throughout the soil profile. Nearly all feldspar grains, regardless of mineralogy, are sericitized, some of them heavily so. Sericite occurs randomly within the feldspar grains and is not associated with fractures or cleavage traces (Fig. 3.5C). Two fracture networks have been identified in the sand and gravel clasts (Fig. 3.5D, E). The first occurs regardless of mineralogy and cross-cuts grains at apparently random orientations. In the feldspars, alteration to orange-yellow clay minerals and Fe-oxide precipitation has occurred along these fractures. This fracture network is present in coarse clasts in the soil profile as well as in the underlying gruss (Fig. 3.5F). The second set of fractures is unique to the feldspar grains in the soil and occurs at right angles following cleavage traces. Fe-oxides are rarely observed along this fracture network, but never is there alteration to clay minerals.

Cryogenic Features. Cryogenic features are easily recognized throughout all three depositional units, though the nature of these features changes with depth. Unit 3 at the top of the profile shows a classic assemblage of freeze-thaw related pedofeatures. Laminated silt caps are common atop large igneous rock fragments in the upper horizons of the soil (Fig. 3.6A). Wavy or platy microfabric and lenticular pores, indicative of ice lens formation during repeated freeze-thaw cycles (Dumanski and St. Arnaud, 1966;

McMillan and Mitchell, 1953; Van Vliet-Lanoë et al., 2004; Van Vliet-Lanoë, 2010) are prevalent throughout the groundmass (Fig. 3.6B,C). Microgranular aggregates are common (Fig. 3.6D). Nearly all feldspars in this uppermost horizon show evidence of fractures likely related to frost-shattering along cleavages (Fig. 3.6E), and many large biotite grains show evidence of de-lamination and exfoliation (Fig. 3.6F). Elongated grains are commonly vertically oriented (Fig. 3.6G), suggesting the occurrence of frost-jacking, a process by which ice lenses grow beneath elongated grains, forcing them to rotate over time (Kaplar, 1965; Van Vliet-Lanoë et al., 2004; Van Vliet-Lanoë, 2010).

In contrast, units 2 and 1 show relatively little evidence for cryogenic activity. Wavy and lenticular microfabrics are virtually absent from the lower portions of the soil profile, as are silt- capped grains and microgranular aggregates. The fractures observed along cleavage planes in feldspars throughout the profile are likely the result of frost shatter, a phenomenon that occurs when moisture accumulates along planes of weakness within a grain and subsequently expands during freezing (Van Vliet-Lanoe et al., 2004; Van Vliet-Lanoë, 2010). The soil matrix of units 2 and 1 is characterized by the presence of oriented clays, often occurring as granostriated b-fabrics (Fig. 3.6H), a common result of intra-soil stress caused by ice formation (Bunting, 1983; Fox, 1983; Miedema, 1987; Tarnocai and Smith, 1989; Van Vliet-Lanoë, 1985). Granostriated b-fabric is also a commonly-observed feature in colluvial deposits, however, and it is possible that the presence of such fabric in units 1 and 2 is a depositional, rather than pedogenic feature.

Clay illuviation features. Units 2 and 1 show abundant microscopic evidence for clay translocation processes. Overall, samples from these units are richer in clay than

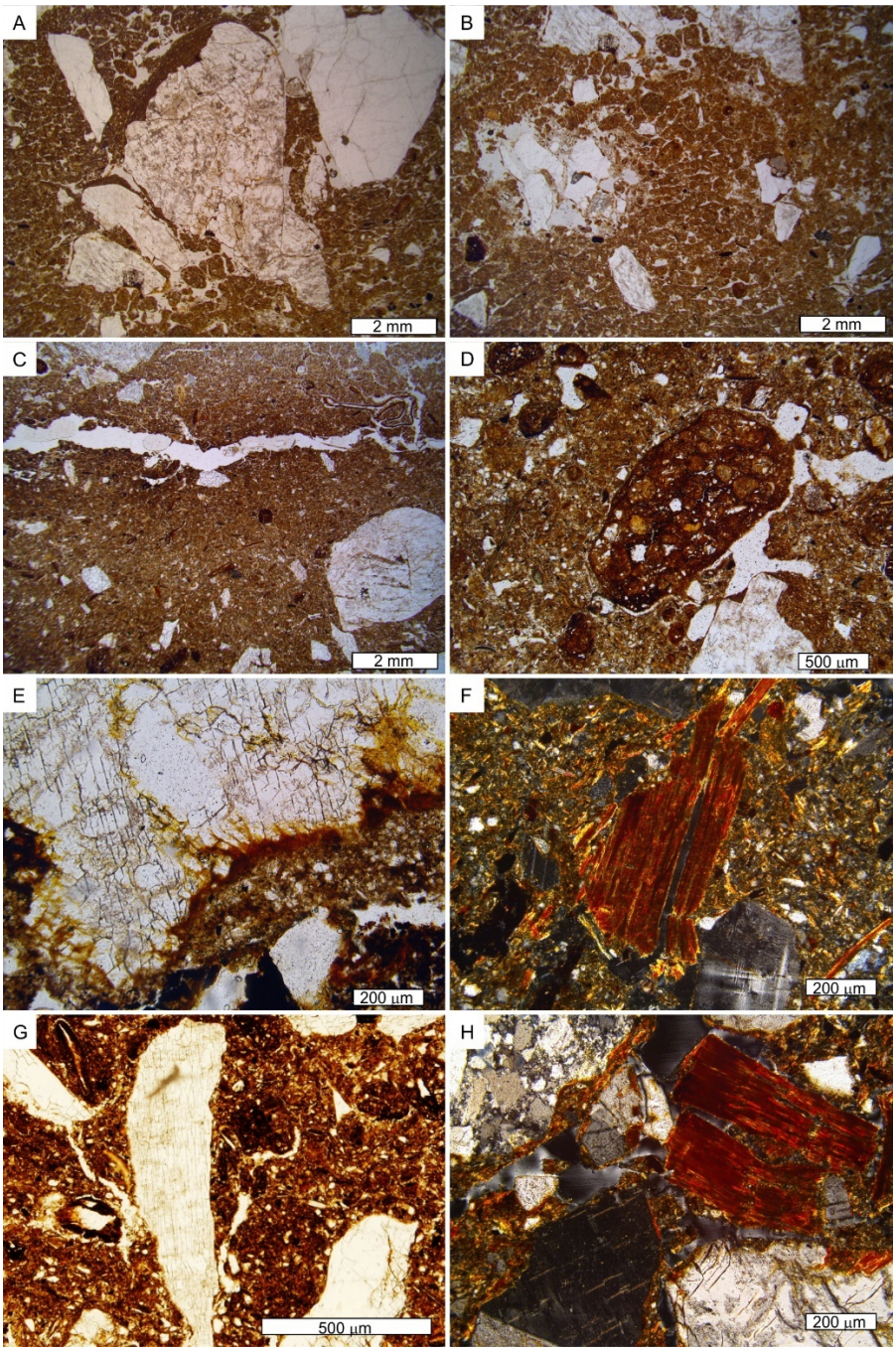

Figure 3.6. Cryogenic pedofeatures from thin sections S-03 and S-04 (unit 3). A) Silt-capped grain (PPL); B) platy and microgranular fabrics (PPL); C) Lenticular-shaped pore with Fe-oxide hypocoating (PPL); D) Microgranular aggregate (PPL); E) Frost-shattered potassium feldspar (PPL); F) Delaminated biotite (XPL); G) Vertically-oriented, frost-jacked elongated grain (PPL); H) Granostriated b-fabric in unit 2 (XPL).

those from unit 3 above (Fig. 3.7 A-C). In addition to the granostriated b-fabrics discussed above, units 1 and 2 have many meniscate clay coatings on larger soil pores (Fig. 3.7 D-F). These clay coatings are well-oriented and highly birefringent, indicating that these are not authigenic or stress-related features, but rather that the clays have been translocated as colloids in soil water from elsewhere in the soil profile (Kühn et al., 2010). The clay coatings are poorly-sorted, coarse, and dusty. Their occurrences within pore spaces distinguishes them from weathered phyllosilicates, such as biotite. In some instances, Fe-oxides have stained the upper layers of these clay coatings (Fig. 3.7 D, E).

Podzolization and redoximorphic features. Also present in units 2 and 1 are features indicative of Fe-redistribution within the soil. Redoximorphic features are present in all horizons, primarily in the form of Fe-oxides which have precipitated both in the soil matrix and along fractures and cleavage planes in coarse grains. Fe-oxides universally appear to have formed subsequent to any chemical weathering or clay formation along these fracture surfaces and also seem to post-date any of the clay illuviation features discussed in section 4.3.3.

In addition to redoximorphic features are dark reddish brown to black patches 2-4 mm in diameter, which are interpreted to represent an incipient placic horizon within the soil (Fig. 3.8). These nodules are significantly darker in color than the redoximorphic features in the soil, suggesting that they are organo-metallic in nature. Such horizons are commonly found in soils with porphyric c/f-related distributions that have coarse grains in groundmass (De Coninck et al., 1985; Hseu et al., 1999). The dark color suggests that both Fe- and Mn-oxides, in addition to organic matter, have infiltrated the soil matrix in these lowermost soil horizons.

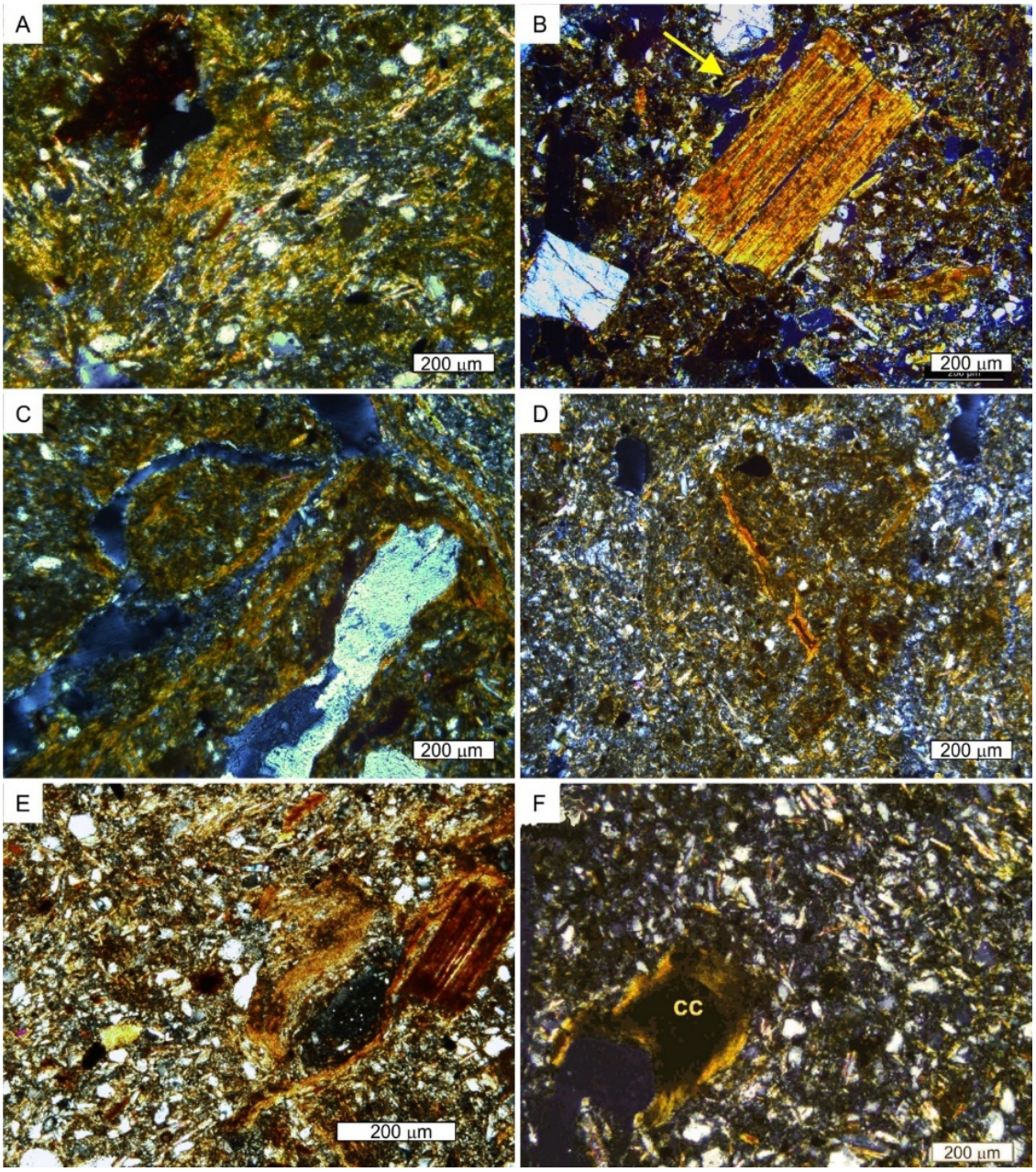

Figure 3.7. Clay illuviation features. A-C) Randomly striated b-fabrics and accumulations of clay in the soil matrix (A, XPL, S-01, unit 2;, B-XPL, S-02, unit 2, C-XPL, S-01, unit 2); D-F) Birefringent, meniscate-lined clay pore-coatings (XPL, S-02, unit 2).

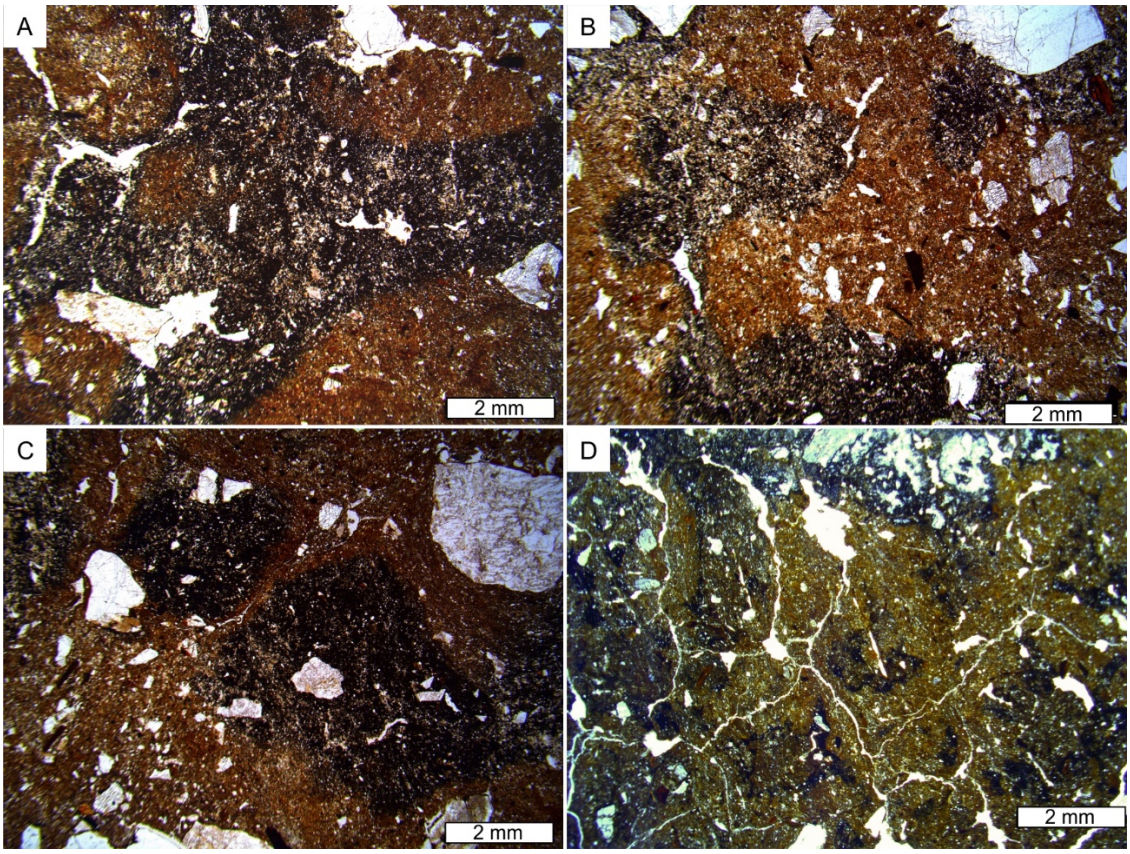

Figure 3.8. Podzolization features, including nodules suggesting incipient placic horizon formation (PPL, S-02 (A), S-01 (B,C), S-06 (D), units 2 and 1).

Anthropogenic features. Unit 2 is the most culturally-significant depositional unit at the site. Several accumulations of anthropogenic charcoal, identified as hearth features, have been found, and it is from this layer that all of the >2000 artifacts recovered from the site were excavated (Goebel et al., 2013). Although thin section samples were not collected from the hearth features themselves, microscopic evidence for human occupation of the site during the deposition of unit 2 is plentiful. Well-preserved charcoal fragments are abundant in unit 2, much more so than in units 3 and 1 (Fig 3.9 A-C). Also evident in thin section are several large grains that have been identified as microdebitage (Fig. 3.9 D-F). The lithology of these grains is variable, but most are composed of quartzite or chert, two of the most common raw materials found in the site's lithic

assemblage (Goebel et al., 2013). These grains may be distinguished from other naturally occurring coarse clasts by their extreme angularity, their lithology, and the presence of small, conchoidal-type fractures occurring along the grain boundaries, perhaps as a result of percussion during the knapping process (Angelucci, 2010).

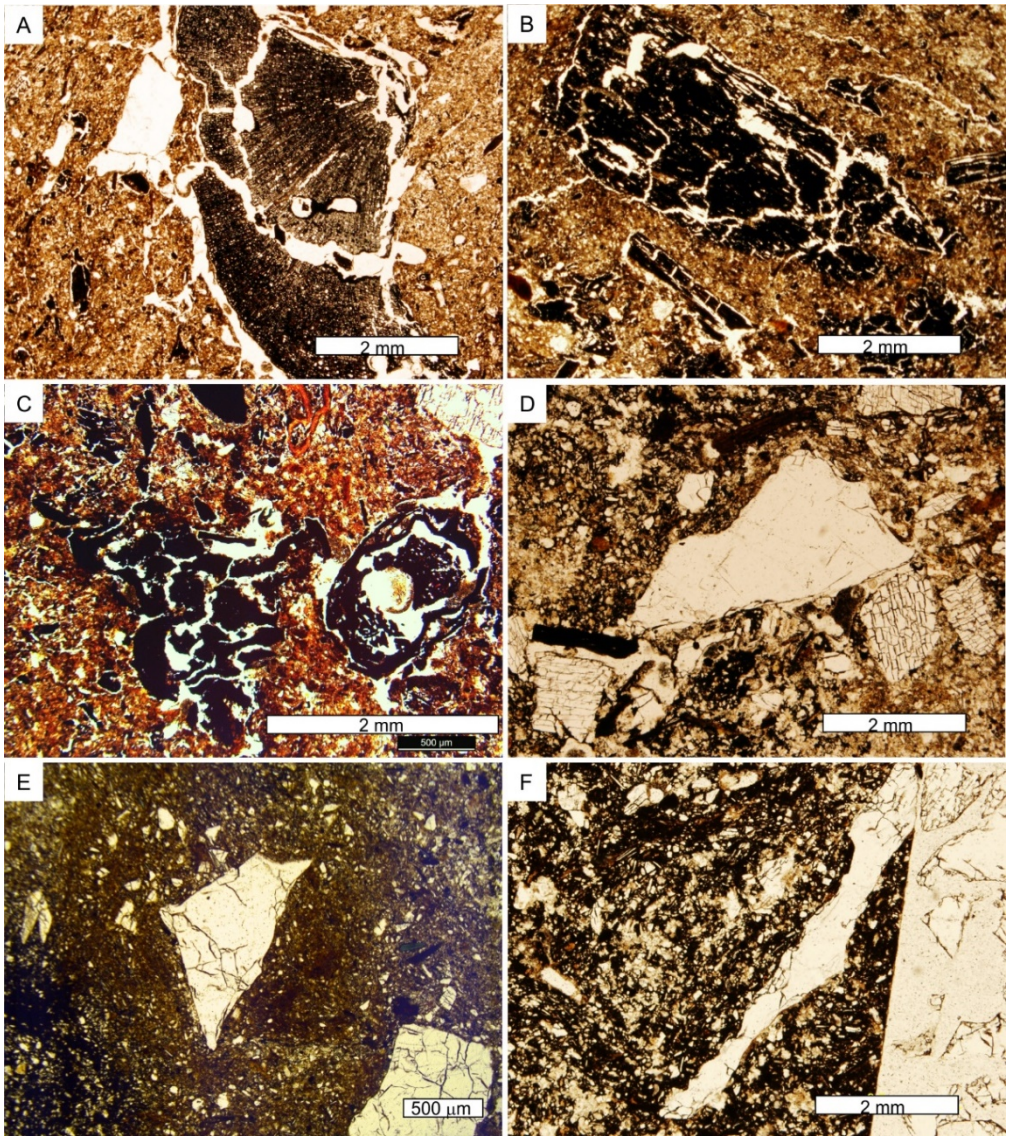

Figure 3.9. Anthropogenic features from unit 2 (PPL). A-C) well-preserved charcoal; D-F) lithic microdebitage.

Clay Mineralogy

The clay-sized (<2μm) fraction of the soil is composed of quartz, micas, potassium and plagioclase feldspars, and two clay minerals that exhibit distinct diffraction behaviors in response to the four pre-treatments (Fig. 3.10). The first of these clays has a primary peak at 7 Å when K-saturated and air dried. Saturation with Mg and solvation with glycerol produce no change in the d-spacing of this peak and heating to 550°C for an hour causes peak destruction. The second clay has a primary peak at 14 Å that is unchanged by Mg saturation, glycerol solvation, or heat treatment. These responses suggest that the clay minerals present in the soil are kaolinite and chlorite, respectively. Both are present in comparable amounts in all three depositional units, as well as in the gruss.

Particle Size Distributions

Despite the textural variations observed in the field, the particle-size distributions of units 1, 2, and 3 are broadly quite similar (Fig. 3.11). All three units and the underlying gruss are polymodal in nature, though there are differences in the sizes of these modes among the three depositional units and between the sediment package and the gruss.

From a sedimentological perspective, each grain size mode in a sedimentary unit is representative of a unique depositional process or source (Ashley, 1978; Bagnold and Barndorff-Nielsen, 1980). By identifying these modes and their sources, and comparing their abundances within a package of sediment, it is possible to assess the relative importance of various depositional mechanisms throughout the time period represented. Four readily identifiable grain-size modes are present in units 1-3 at Serpentine:

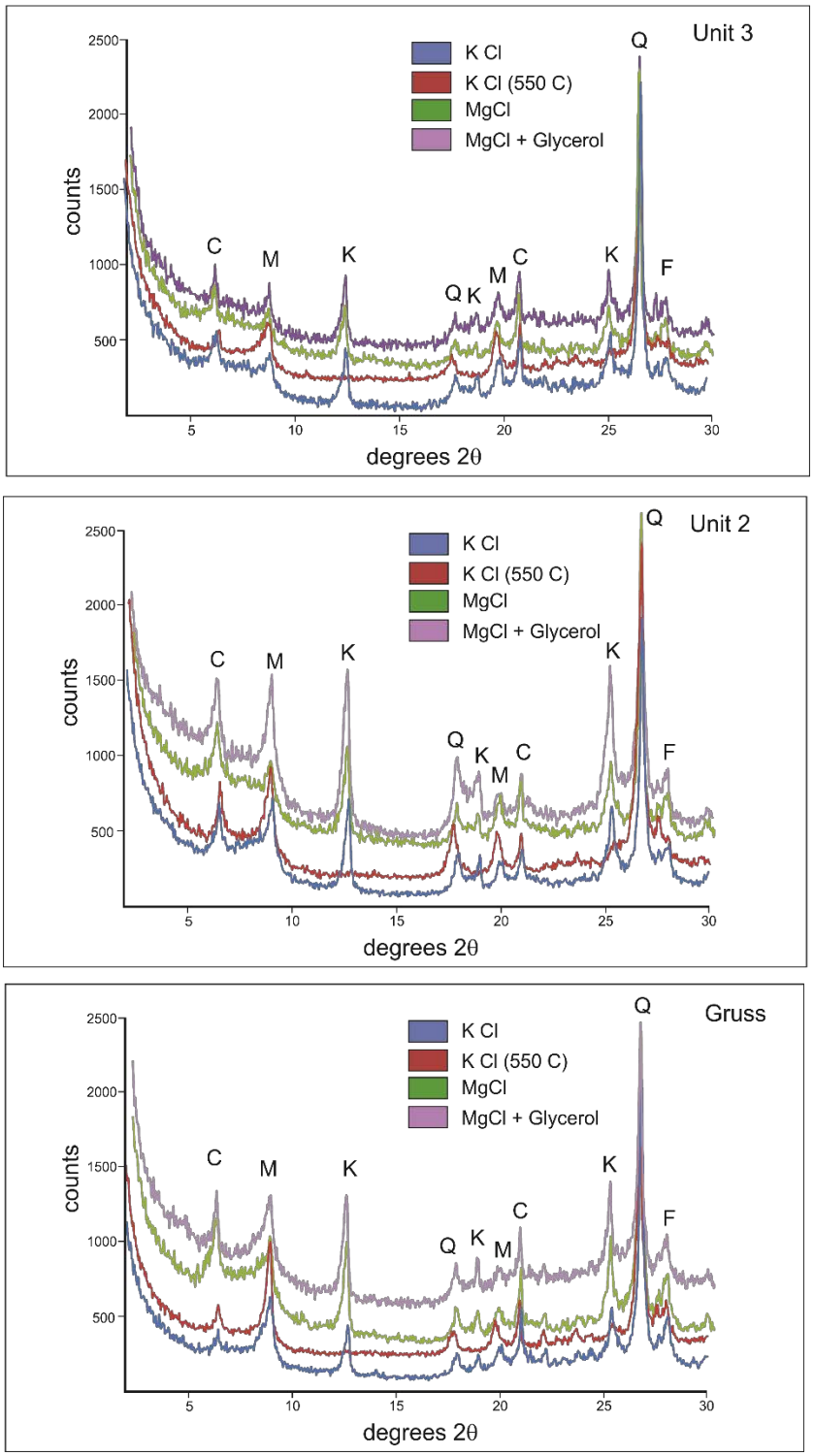

Figure 3.10. X-ray diffractograms of the less-than-two-micron fraction of the gruss, unit 2, and unit 3 at Serpentine Hot Springs. Data from all four treatments are displayed in the following order, from bottom to top KCl, heat-treated (550°C), MgCl, MgCl+glycerol. Minerals are labelled as follows: C-chlorite, M-mica, K-kaolinite, Q-quartz, F-feldspars.

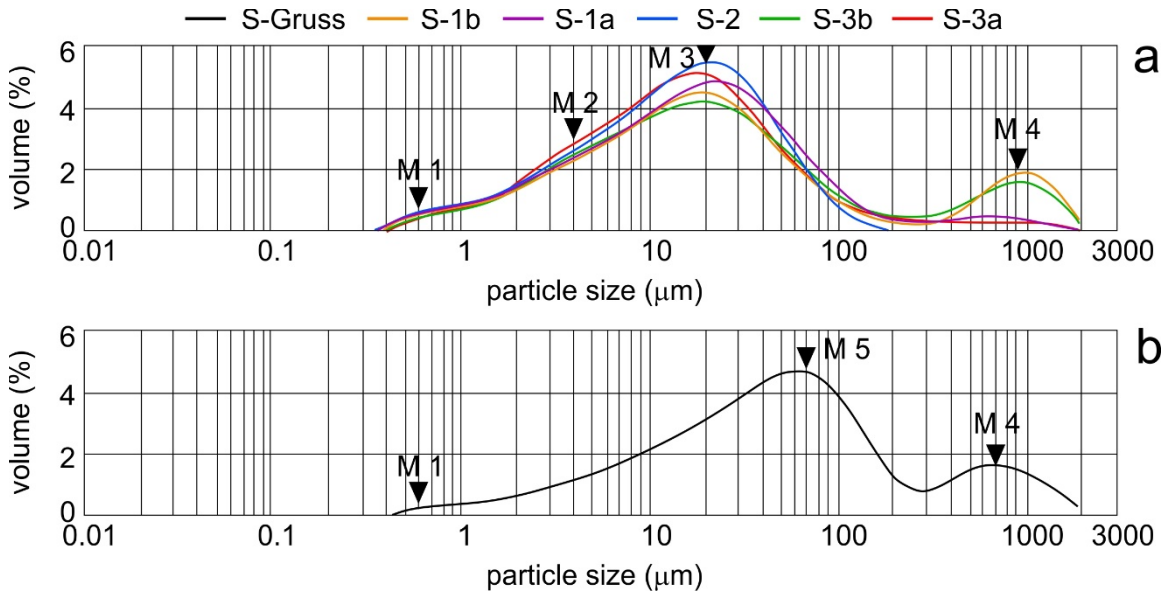

Figure 3.11. Particle-size distribution of samples from Serpentine Hot Springs geologic trench (a) and gruss (b). Particle-size distributions represent the less-than-two-millimeter fraction of the soil. Samples 1a and 1b come from unit 1, sample 2 from unit 2, and samples 3a and 3b from unit 3.

~0.6 μm (M1), ~4 μm (M2), ~20 μm (M3), and ~500-1000 μm (M4) (Fig. 3.11A). M1 is present in relatively constant abundances in all three units, although it is slightly more prevalent in units 1 and 2 than in unit 3. M2 and M3 are significantly more abundant in unit 2 and in the upper portion of unit 1 than in any other samples from the site, whereas M4 is generally coarser-grained and more abundant in the upper part of units 1 and 3 and virtually absent from unit 2. Of the four grain-size modes discussed above, two are also present in the gruss: M1 and M4 (Fig. 3.11B). Rather than the silt-sized M2 and M3, the gruss has a mode in the fine-sand category (~70 μm) designated as M5 that is not represented in the overlying sediment.

Bulk Geochemistry

The concentrations of major and select trace elements show very little variation throughout the soil profile (Fig. 3.12). Elements with the most variability in terms of concentration appear to be those associated with organic matter in the profile. Both C and N concentrations are high at the surface and drop sharply around the upper boundary of unit 2 ($3Bts_1$). Fe ranges between 3% and 5% by weight, with maximum concentrations occurring in unit 2 ($3Bts_1$) and the lower portion of unit 1 ($3Bts_2$), and the lowest concentrations in the gruss. The distributions of Al and Mg with depth are like the distribution of Fe. The concentration of P increases in association with buried soil horizons 2Ab and $3Bts_2$. Base cation (Ca, Na, K) concentrations are slightly lower in the soil material than in the underlying gruss, but the magnitude of this apparent loss is quite small (less than a weight percent in all cases), albeit consistent. The immobile element Ti, generally used as an indicator of parent material homogeneity in soils, is conserved throughout.

Discussion

Depositional History

Deposition of sediment at the Serpentine fluted-point site is the result of two concurrent processes. The poorly-sorted nature of the deposits suggests that colluviation is the primary mode of deposition at the site. Because the site sits at the edge of a gently-sloping bluff (Fig. 3.1), the most reasonable source for colluvium is the gruss upslope from the excavated area. This interpretation is supported by the mineralogical composition of

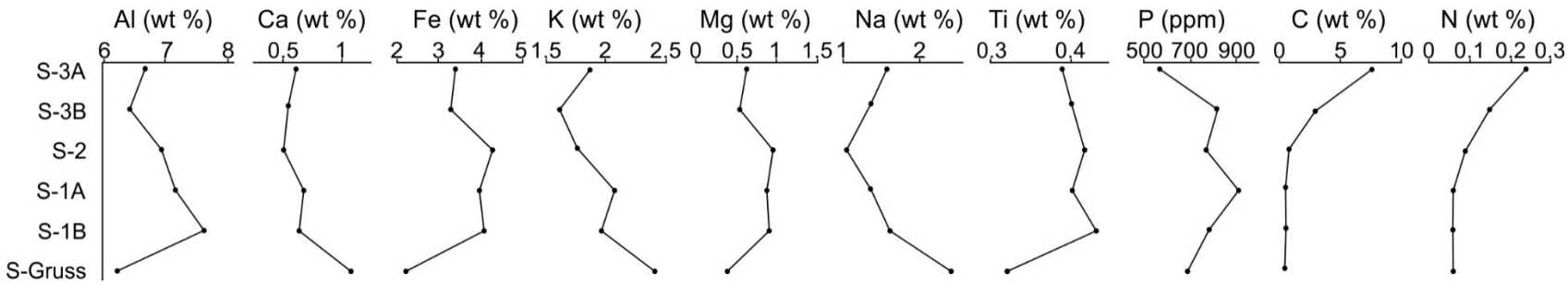

Figure 3.12. Major and trace element geochemistry. Note scale differences between each element.

the sediment, which is virtually indistinguishable from that of the gruss, and by its angularity. The presence of sericitized feldspars also strongly suggests that at least the coarse-grained fraction of the sediment has been reworked from a previously-weathered source, such as the local granite stock.

Since the gruss serves as the source of these colluvial deposits, the particle size distribution of the gruss sample collected from the site should be roughly representative of the particle size distribution of the rest of the sedimentary units at the time of deposition. However, the particle size distributions of units 1, 2, and 3 are not identical to that of the gruss (Fig. 3.11), suggesting either post-depositional modification, an additional sediment source, or a combination of the two. Although it is possible that this variation in texture originated during the deposition of the three lithostratigraphic units, the similarity of the particle size distributions of units 1, 2, and 3 makes this highly unlikely. Instead, it seems parsimonious to assume that the particle size distributions were approximately the same as the gruss during deposition and that the same post-depositional processes have acted on all three units, altering their size distributions in similar ways. The abundance of frost shattered grains observed in thin section as well as the presence of the silt size M3 at the expense of sandy M5 suggest that freeze-thaw processes have altered the particle size distribution in the frost-affected sediments relative to their source material. The near-complete removal of M5 from units 1, 2, and 3 indicates that this is the dominant process affecting the particle size distribution of the site's sediments.

There is, however, an additional silt-sized component, M2 whose abundance is not inversely proportional to M5 and which appears to form via a different process

altogether. If M2 was also derived from M5 as is M3, it seems unlikely that it would be as distinct from M3 as it is. This suggests that M2 has a different source than does M3. The size of M2 (2-10 μm in diameter) is quite small and falls well within the range of grain sizes transported in high suspension clouds by regional-scale winds (Vandenberghe, 2013). Thus, it seems likely that M2 represents aeolian input to the site. In addition to the particle size data, the clay mineralogy provides clear evidence that there is a sediment source other than the local granite. Although biotite and muscovite are both present in the Oonatut Granite, chlorite is not. Despite this, chlorite is present in varying amounts in all the sedimentary layers (Fig. 3.10). Its presence in the gruss suggests that at least some aeolian material is being deposited upslope from the excavation area and being reworked during colluviation, but the increased abundance of chlorite in units 2 and 3 indicates additional primary aeolian input directly into these deposits as well. Additionally, late Quaternary aeolian deposits are nearly ubiquitous across western Alaska (Black, 1951; Dijkmans and Koster, 1990; Muhs et al., 2003), so it seems prudent to assume that the site has at least some aeolian component. Local aeolian sources are plentiful in the Serpentine area. The site itself sits along the edge of a blowout feature, which could serve as an immediate source for silt-sized particles. Other potential sources are the braided streams which are present locally, from the small unnamed creek directly below the bluff upon which the site rests to the much larger Hot Springs Creek farther south (Fig. 3.1). These creeks flow seasonally and have silty beds which could readily serve as a source for aeolian sediment.

Because the gruss is the likely source of colluvial material at the site, the grain-size modes present in both the gruss and in the overlying sediment (M1 and M4) can be

considered colluvial in origin. M5, the fine-sand-sized mode present in the gruss, however, is entirely absent from the soil profile (Fig. 3.11). Whereas it is unlikely that material of this size would be selectively removed from the soil, the likely explanation is that M5 has been modified by post-depositional processes that have converted most of these sand grains into the siltier M3 in the soil. Based on the geomorphic location of the site, colluvial deposition at Serpentine is probably a relatively constant process. Aeolian deposition, however, is much more dependent upon variable conditions. Thus, there are likely to have been periods of time in the history of the soil profile where aeolian input was very important to the site versus other periods when it was not. With these grain-size interpretations in mind (an aeolian source for M2, a colluvial source for M1 and M4 and a colluvial source with post-depositional alteration for M3), it is possible to reconstruct the depositional history for each of the three units at the site.

The granite bedrock at Serpentine was shallowly emplaced during the Late Cretaceous (Hudson, 1979). Since that time, it has not been deeply buried and thus has become highly weathered, eroded, and saprolitized at the surface. It seems prudent to assume that sediment accumulated on the bedrock surface prior to the Quaternary, but none of these earlier sediments are preserved at the site. Instead, the oldest depositional unit preserved is unit 1, which dates to the late Pleistocene following the Last Glacial Maximum (LGM), around 15,000 years ago. Unit 1 appears to be almost entirely colluvial in origin. M2 is not present in either sample from this unit, and the thickness of the unit is primarily controlled by the topography of the underlying gruss. Unit 1 represents the initial phase of landscape stability following the LGM. In a few places, it has been eroded, leaving gruss overlain by unit 2. This is not surprising, given the

~1,500-year gap between the radiocarbon dates for units 1 and 2. Even though it is clearly an unconformity, the uppermost portion of unit 1 does not appear to exhibit an enhanced degree of pedogenesis compared to the rest of the unit. This, in combination with the irregular surface of unit 1 and the occasional superposition of unit 2 directly over gruss, suggests that the upper part of unit 1 has been eroded. Since the site is located on the edge of a tall bluff several meters above the modern-day stream channel, aeolian deflation seems a likely mechanism for such erosion, possibly in association with cold, very windy conditions during the Oldest Dryas.

Unit 2 represents a combination of aeolian and colluvial deposition, though the absence of M4, the abundance of M2, and the presence of more chlorite suggest that aeolian deposition played a larger role in its formation than the formation of the other units. Dates for unit 2 are widely spread, ranging from about 12,500-9,900 BP (Table 1). It is difficult to determine whether deposition occurred slowly over this entire interval or whether younger, natural charcoal was incorporated into the unit via cryoturbation or root burn. If the earliest radiocarbon dates from this unit correspond to the onset of deposition, it seems likely that unit 2 corresponds to sediment deposition during the Younger Dryas chronozone, when humans appear to have occupied the site. Aeolian silt deposition in high-latitude regions occurs more readily during cool, dry climatic intervals (Tsoar and Pye, 1987), so unit 2 may be taken as evidence for a cold, dry Younger Dryas in this part of the Seward Peninsula. Unit 2 is discontinuous across the excavation, indicating the presence of yet another hiatus in deposition and an erosive event sometime following its deposition.

Unit 3, the uppermost unit at the site, was deposited sometime after Unit 2. Although no charcoal suitable for dating was recovered above unit 2, bulk humate dates suggest that deposition of unit 3 has been somewhat episodic, likely spanning much of the Holocene. Like unit 1, unit 3 fines upwards slightly. Towards the top, sand and gravel become less abundant. Unlike unit 1, however, is the presence of M2 in the uppermost portions of unit 3, suggesting that aeolian deposition played an important role in deposition at the site within the last ~4000 years.

Pedogenic processes and soil evolution

The pedogenic history at Serpentine Hot Springs is one characterized by overprinting, not surprising given the relative thinness of the soil profile. Pedogenic processes indicative of three distinct soil temperature/moisture/pH regimes have acted to form the site's soil: cryogenic features are associated with cold, relatively dry, and seasonally frozen soil conditions; clay illuviation features associate with temperate, well-drained, mildly acidic conditions; and podzolization features suggest warm or cold, moist, acidic conditions. However, the degree of overprinting present at the site need reduce its significance for reconstructing soil conditions during the last ~15,000 years. To fully understand the record of soil development and landscape evolution preserved at the site, it is crucial to be able to place these three distinct regimes in a chronological context. This can be accomplished by integrating geochemical and particle size data with cross-cutting relationships and observations gleaned from careful microscopic analysis.

The earliest pedogenic process observed in the soil material is the intensive chemical weathering of unstable mineralogical grains, namely plagioclase and potassium feldspars. Nearly all feldspars within the soil profile show some evidence of hydrolysis

and clay formation, which occurs only along the randomly-oriented fracture network that cross-cuts many of these grains. EDS analysis suggests, and x-ray diffraction confirms that this clay is primarily kaolinite, or a kaolin-type 1:1 phyllosilicate clay (Fig. 3.10).

Pedogenic kaolinite is characteristic of highly weathered, well-drained soils with near-complete depletion of base cations, low pH, and high iron and aluminum content (Dixon, 1989), and it is generally associated with warm, humid environments (Chamley, 1989). Climatic data from the Seward Peninsula, however, suggest that conditions at Serpentine were never sufficiently warm and wet to form pedogenic kaolinite within the past 15,000 years. Close inspection of the boundaries between these weathered feldspars and the surrounding matrix reveals that the clay within the grains is entirely separate from the clays in the matrix (Fig. 3.13 A, B). Furthermore, the distinct, layered texture of the clays along fractures in the feldspars is quite different from the texture of clays in the matrix (Fig. 3.13 C, D). It seems likely, then, that these highly weathered feldspars were not altered *in situ*, but, rather, prior to transport. Conditions warm and wet enough to support an arctic rainforest and alligatorid species have been documented in northern Alaska and Canada during the Eocene (Estes and Howard Hutchison, 1980; Jahren and Sternberg, 2003), subsequent to the exhumation of the Oonatut Granite Complex (Hudson, 1977). It is probable that the kaolinite formed during this interval and has persisted on the landscape since that time, and therefore that it does not record a period of intense weathering during the Quaternary.

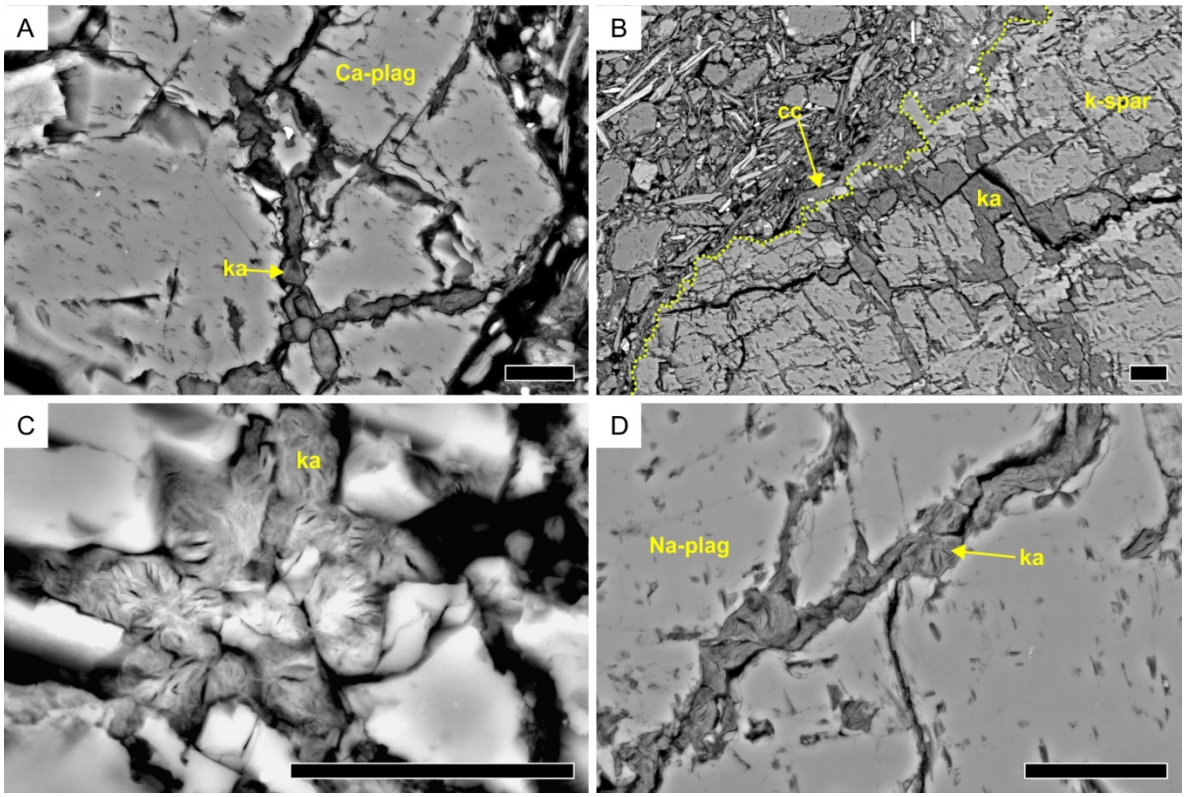

Figure 3.13. Scanning electron micrographs showing clay alteration products along randomly oriented fractures in plagioclase and potassium feldspar grains. Scale bars are 20 microns in size.

The lowermost portions of the sediment package at Serpentine have been affected by all three pedogenic processes present at the site, albeit to varying degrees. Of the three, the clay illuviation features appear to be the most prevalent and to have occurred deepest into the profile. Clay linings occur directly on pore surfaces (Fig. 3.7 D-F), suggesting that the clays were translocated prior to Fe-oxide precipitation. Accumulations of oriented, translocated clays are ubiquitous in the matrix of both the 3 Bts_1 and $4Bts_2$ horizons (Fig. 3.7 A-C), whereas organo-metallic accumulations are concentrated in nodules within this matrix (Fig. 3.8), suggesting that clay illuviation occurred prior to podzolization. Cryogenic features are limited to a few frost-shattered feldspars, and the exposed cleavage planes show no evidence of clay infiltration, Fe-oxide production, or

podzolization, suggesting that the cryogenic features postdate both illuvial processes (Fig. 3.5 D-F).

Because clay illuvial features are present in both units 2 and 1, illuviation occurred after the deposition of both units. Clay illuviation in soils requires three conditions: liquid water, free soil drainage, and a mildly acidic pH. There are a variety of surface environments which could produce a soil with these characteristics, and there is some variability in the range of conditions under which clay illuviation can occur. As such, clay illuviation, in general, is not a reliable indicator of any one particular set of environmental conditions. However, one may use the character of the clay coatings present in the soil to narrow the range of potential interpretations.

The clay coatings at Serpentine are meniscate, suggesting repeated cycles of illuviation occurring over time. This requires that the soil be relatively well-drained for a long period. Repeated freeze-thaw cycles in permafrosted areas typically lead to variably drained redoximorphic or mottled soils, rather than well-drained soils where clay illuviation can occur, so it is unlikely that there was significant permafrost in the area during this time. Illuviated clay coatings have been documented in association with seasonal thaws in frost-affected soils. Clay and fine silt can be carried downward in the profile along with meltwater, a rapid process that would likely produce the kind of poorly-sorted, dusty clay coatings observed here. That the mud cutans at Serpentine are preserved suggests the absence of deep frost penetration during the winter months. These features all point to warmer, more temperate soil temperatures during this interval, an interpretation that is further supported by the abrupt decrease in the C/N ratio at the upper boundary of unit 2 (Table 2), suggesting that the organic matter in the lower portions of

the soil is much more degraded than in unit 3. Clay illuviation is a subsurface process, suggesting that the erosional processes that removed the upper portions of unit 2 occurred after pedogenesis. It is possible that some amount of clay illuviation occurs at the surface at Serpentine today and that the active cryogenic processes in unit 3 have disrupted the resulting clay coatings. Illuviation features are best preserved at depth in soils that are well-drained, but even where these conditions are not met, fragmented clay coatings are commonly observed (Van Vliet-Lanoë, 2010). This does not appear to be the case in unit 3, suggesting that clay illuviation processes have largely ceased.

Chronosequence studies of modern soils developed on granitic materials in periglacial environments show that clay illuviation can begin in less than 1650 years after the onset of pedogenesis (Sauer et al., 2009). Assuming the range of radiocarbon dates collected from Unit 2 represents the entire interval of deposition, pedogenesis would have begun no earlier than 10,000 BP. Moist, mildly acidic soil conditions without permafrost or deep seasonal freezing, then, could have persisted at least until 8,200 BP. These dates coincide with the expression of the Holocene Thermal Maximum, a time-transgressive period of warm, moist conditions associated with an insolation maximum in the early- to middle Holocene, which dates between 8,000 and 11,000 BP in Alaska (Kaufman et al., 2004, 2016). The increase in clay illuviation features, lack of permafrost, and absence of cryogenic features in units 1 and 2 point to not only a warmer HTM, but also one with increased precipitation. This most likely took the form of increased snowfall, which would have insulated the underlying soil from temperature changes at the surface, inhibited the formation of cryogenic features and provided increased meltwater to translocated clays down-profile in the spring.

In addition to clay illuviation, units 1 and 2 are marked by podzolization features, which formed after the clay illuviation features, but prior to the development of cryogenic features. Podzolic or spodic soils are characterized by the translocation of chelated organic material, Fe, and Al in solution as the result of acidic soil pH. This part of the soil profile appears to represent incipient placic horizon development. Placic horizons occur in moist, variably-drained soils with low pH, where organo-metallic compounds are solubilized and translocated during periods when the soil is anoxic then re-precipitated when oxic conditions are restored (Buurman et al., 2005). Although changes in the redox state of a soil generally reflect periods when the soil is waterlogged (Vepraskas, 2001; Vepraskas et al., 2002), the redox changes responsible for the formation of placic nodules at Serpentine are likely the result of seasonal freezing, though the lack of cryogenic features in these spodic horizons suggests that the soil still lacked permafrost during this time. Placic horizons can be found in soils forming under a range of temperature regimes, but occur exclusively in udic or perudic soil moisture regimes (Hseu et al., 1999; Pinheiro et al., 2004; Wu and Chen, 2005), conditions that are wetter than the interior of the Seward Peninsula today.

Like argillic horizons, spodic horizons are illuvial in nature. This requires the presence of overlying eluvial horizons. Both the BE and A horizons associated with this incipient placic horizon are preserved in the lower part of unit 3. Organic matter from this buried A horizon dates between 6,400 and 6,500 BP, suggesting that podsolization persisted for no more than ~2000 years.

The co-occurrence of clay illuviation and podzolization features within the same soil are interpreted here as independent features, each representing pedogenesis at a

different time in the soil's history and likely corresponding to different vegetation cover, perhaps deciduous woodland (with species such as dwarf birch, poplar, or willow) during the HTM transitioning into moist, acidic tundra later in the Holocene. Previous studies have interpreted the existence of such woodlands in uplands of the Seward Peninsula during the HTM (Kaufmann et al., 2004; Hunt et al., 2013). Alternatively, the clay illuviation and podzolization features observed here could be the result of a single phase of pedogenesis under a boreal forest. In some silty soils in cold climates, podzolization can be initiated in the upper, more acidic portions of the soil profile and clay illuviation can occur at depth where pH is higher (Fèdoroff et al. 1981). The bulk humate dates collected from unit 3 suggest that deposition at the site has occurred gradually through time, at least in the upper portions, supporting the interpretation of two separate buried soils, rather than one, but it is impossible to be certain. Both interpretations require significant perturbation of annual temperature, precipitation, and surface vegetation relative to conditions at the site today.

Cryogenic features at Serpentine are best-developed and most abundant in the uppermost portion of unit 3, suggesting that freeze-thaw processes have played an important role in the development of the modern surface soil. Layered silt cappings of coarse grains, frost-jacked clasts, and wavy to platy microfabrics indicate that the uppermost horizons of the soil have undergone repeated cycles of freezing and thawing. These features are restricted to unit 3 because it is within the active layer of the soil. Units 2 and 1 are deeper and, therefore, have not undergone enough freeze-thaw cycles to develop cryogenic microfabrics in any significant way.

The radiocarbon chronology of the site indicates that the Bw horizon of the cryogenic surface soil dates between 4300 and 4100 BP. Although the dates from this horizon are bulk humate dates, rather than traditional radiocarbon dates on charcoal, and thus represent an average age of material incorporated during deposition and subsequent pedogenesis, they can be treated as an estimate of the minimum age of the deposition of this material. They suggest that freeze-thaw processes, and cold, permafrosted soil conditions, have been established for at least the past 4,000 years. A number of other climate records suggest that widespread cooling began in northern Alaska around 4,500 BP, leading to the glacial and sea ice expansion and permafrost aggradation. The cryogenic features observed in the upper part of the soil at Serpentine are likely associated with this late Holocene Neoglacial period.

Because cryogenic features are so well-developed in the most recent portions of the soil profile, the absence of cryogenic fabrics in unit 1, which dates to the late glacial period, is somewhat puzzling. Although cryogenic features are certainly associated with cold, generally dry conditions, there is good evidence that, even in the coldest of soils, there is a certain soil moisture threshold necessary to produce cryogenic features (Campbell and Claridge, 1987). It may be that, even though soil temperatures at Serpentine were likely cold enough to promote the formation of ice lensing-related features just after the LGM, there was not enough water in the soils to form ice and, by extension, cryogenic fabrics.

Stratigraphic Integrity

The stratigraphic integrity of archaeological sites in periglacial settings depends primarily on the degree of cryogenic disturbance a soil has undergone. Cryogenic disturbance in

frost-affected soils is the result of the volumetric increase that occurs during the transition from liquid water to ice when soil temperatures drop below freezing. The most concerning types of disturbances are those related to cryoturbation-churning of soil material from repeated freeze-thaw cycles, solifluction-slope creep of unconsolidated materials downslope across the permafrost table, and ice wedge formation. Fortunately, all three processes leave clear morphological and micromorphological traces.

Cryoturbation at its worst is easily recognized at outcrop-scale and is typically most severe in soils and sediments that exhibit textural variation (Van Vliet-Lanoë, 2004). It represents a broad class of soil processes involving soil movement caused by frost action and can range from small-scale features like irregular horizon boundaries and cryogenic microfabrics to large-scale soil involution of soil material (Bockheim, 2015). From both the soil profile and micromorphological analysis, it is clear that cryoturbation at Serpentine has been relatively small-scale. Horizon boundaries in the soil are irregular and occasionally broken, but these disturbances are easily traced in profile (Fig. 3.2). Nowhere in the soil profile is complete involution of soil material observed. These profile-scale observations hold true micromorphologically as well. Although cryogenic microfabrics are certainly present in the upper parts of the soil, they are only moderately developed at best. There is little evidence for grain rotation or vertical soil displacement at a scale larger than a few centimeters.

From analysis of the artifacts recovered from unit 2, however, there can be no question that at least some degree of vertical artifact displacement has occurred. Although the cultural assemblage at the site was found entirely within unit 2, artifact plunge data suggest that there has been slight re-orientation of grains within this interval.

Generally speaking, artifacts with plunges in excess of 45° are more likely to have moved in the soil profile than those with shallower plunges (Goebel et al., 2000; Graf et al., 2015; Johnson et al., 1977; Schweger, 1985; Wood and Johnson, 1978). The average artifact plunge at Serpentine is 45.1°, indicating that approximately half the artifacts at the site for which plunge was measured have been affected by some degree of frost heave (Fig. 3.3). The true degree of vertical displacement by frost heave is likely less than this, however. Artifact plunge was scored only on artifacts which were deemed sufficiently large, the population of artifacts that is also more susceptible to cryogenic disturbance (Johnson et al., 1977). Thus, the degree of cryoturbation as indicated by artifact plunge is likely a worst-case scenario. Instead, the narrow range of depths at which artifacts are found indicates that vertical displacement has not significantly affected the stratigraphic integrity of the site.

Of perhaps greater concern for the interpretability of the archaeological record at Serpentine is the degree to which the site has been affected by solifluction. Solifluction processes, particularly those occurring at sites where the primary mode of deposition is colluviation, have been shown to significantly distort living surface in Paleolithic archaeological sites in permafrosted or perennially frozen areas (Bertran, 1994; Bertran et al., 2010, 2015; Bertran and Texier, 1995; Vorob'eva and Mendvedev, 1984). Stretching of living floors as well as wholesale transport of artifacts and charcoal downslope have been documented (Bertran et al., 2015), so constraining the degree to which solifluction has disturbed the spatial distribution of artifacts at Serpentine is crucial to interpreting the site.

From a morphological perspective, evidence for solifluction may be seen at both profile and thin-section scale. In profile, solifluction features are broadly similar to other mass-wasting features, involving rotation and flow of soil down slope, a process which can often be initiated by gravity-driven debris flows and avalanching of coarse material down the slope (Bertran, 1994) or which can occur slowly as soil creeps down slope. In unvegetated settings, solifluction processes lead to graded bedding and clast-supported deposits (e.g. Benedict, 1976; Kinnard and Lewkowicz, 2006), but in vegetated areas, solifluction leads to poorly-stratified, matrix-supported deposits. Because all three units at Serpentine are unstratified, matrix-supported, and lack flow features, it is difficult to say whether solifluction has occurred simply by considering the character of the sedimentary structures. Granostriated b-fabrics are present, but these could be from stresses related to ice lensing just as easily as from solifluction processes, and they are hardly conclusive of solifluction as well. Silt-cappings in unit 3, the deposit at the site perhaps most susceptible to cryogenic disruption, show no signs of rotation. Slope creep features similarly are relatively minor and were only, observed at Serpentine in the excavation units nearest the bluff edge. In thin section, solifluction via slope creep converts platy microfabrics to granular fabrics as soil material rolls down slope (Van Vliet-Lanoë et al., 2004), however granular microfabrics are uncommon in the thin sections collected from Serpentine. Instead, platy microfabrics dominate the suite of cryogenic features, suggesting that the soil is relatively undisturbed across the sample locations.

Although the fabrics visible in the thin sections and profile sketches from the site strongly suggest that solifluction has not played a major role in site formation at

Serpentine, the spatial arrangement and orientation of the archaeological materials at the site are the ultimate authority on the matter. At sites where solifluction has reworked archaeological materials, artifacts are preferentially oriented with their long axes parallel to the slope angle (Bertran, 1994). Statistical analysis of the trend scores for artifacts from unit 2 indicates that a preferred orientation does not exist at the site; artifacts are randomly oriented (Fig. 3.3). Additionally, Goebel et al. (2013) provide a strong case for the primary association of the charcoal features and stone artifacts. Spatially, there is a strong association between the charcoal features interpreted as hearths and lithic artifacts, fluting flakes, and faunal remains together suggesting that both the features and associated archaeological materials have not been substantially removed from their primary context. In addition, more than 10% of the excavated artifacts displayed evidence of having been burnt (H. Smith, personal communication, October 2017), whereas artifacts collected from the surface blowouts at the north locus at the site, 25 m from the excavation, showed no evidence of burning. This suggests a direct relationship between the hearth features and thermal alteration of artifacts. Nothing in the archaeological data suggests that the remains are either randomly distributed or post-depositionally associated . If they were in a secondary context, one would expect significantly more randomness in their spatial distribution and techno-typological character, as well as a much smaller proportion of burnt lithic material associated with charcoal. These data, taken with the soil morphology, micromorphology, and overall shallow slope of the site strongly indicate that solifluction has not disturbed the cultural layer characterized by fluted points.

Conclusions

This study synthesized soil microscopy, particle-size analysis, clay mineralogy, and geochemistry to reconstruct the depositional and pedogenic history of the periglacial sediments and buried soils at the Serpentine Hot Springs archaeological site (Fig. 3.14). Deposition occurred over the past ~15,000 years because of colluvial and aeolian processes. Colluvial processes dominated early in the soil's history, as well as in the early to middle Holocene, whereas aeolian processes were more important during the Younger Dryas and late Holocene Neoglacial periods. Three classes of pedofeatures were observed in the two buried soils and surface soil. Pedogenesis did not begin in earnest until the early Holocene, when warmer temperatures likely led to the formation of a well-drained, slightly acidic soil that did not experience deep seasonal freezing, characterized by clay illuviation processes during the Holocene Thermal Maximum. This soil underwent a period of erosion, followed by deposition and the formation of a cool, variably-drained, acidic soil characterized by podsolization processes and the formation of an incipient placic horizon in the middle Holocene. Late Holocene Neoglacial cooling led to the formation of the modern surface soil, which is characterized by the presence of cryogenic features. Anthropogenic materials including charcoal and lithic microdebitage are observed in unit 2, the primary cultural layer at the site. These materials have been re-oriented and slightly reworked vertically, likely because of frost-heaving, but have not experienced major disturbance via solifluction. This paper serves as a model for the application of a suite of archaeological, geological, and pedological analytical techniques to complex soils. Although soils such as those at Serpentine which are relatively thin, overprinted, and form in complex environments are challenging to interpret, this study

shows that, with proper care and attention, their simultaneous contributions to our understanding of both landscape evolution and archaeological site formation processes can be significant.

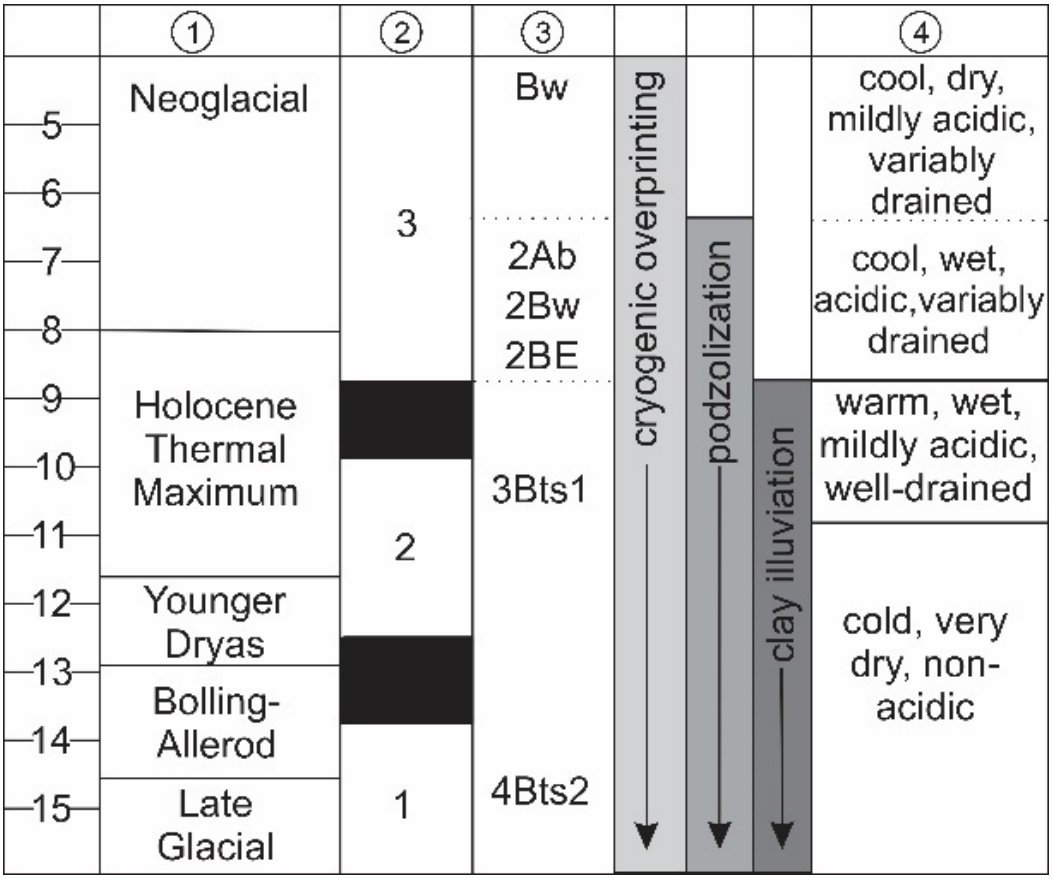

Figure 3.14. Summary of results. All ages are in thousands of calendar years BP. 1-Major late Quaternary climatic intervals; 2-Depositional units. Black boxes indicate periods of erosion. 3-Soil horizon development and dominant cryogenic processes; Interpreted soil temperature, moisture, and pH conditions.

References

Angelucci, D.E., 2010. The recognition and description of knapped lithic artifacts in thin section. Geoarchaeology 25, 220–232. doi:10.1002/gea.20303

Ashley, G.M., 1978. Interpretation of polymodal sediments. The Journal of Geology 411–421.

Bagnold, R.A., Barndorff-Nielsen, O., 1980. The pattern of natural size distributions. Sedimentology 27, 199–207.

Benedict J.B., 1976. Frost-creep and gelifluction features: a review. Quaternary Research 6, 55-76.

Bertran, P., 1994. Dégradation des niveaux d'occupation paléolithiques en contexte périglaciaire : exemples et implications archéologiques. Paléo 285–302. (translated from French)

Bertran, P., Beauval, C., Boulogne, S., Brenet, M., Costamagno, S., Feuillet, T., Laroulandie, V., Lenoble, A., Malaurent, P., Mallye, J.-B., 2015. Experimental archaeology in a mid-latitude periglacial context: insight into site formation and taphonomic processes. Journal of Archaeological Science 57, 283–301.

Bertran, P., Klaric, L., Lenoble, A., Masson, B., Vallin, L., 2010. The impact of periglacial processes on Palaeolithic sites: The case of sorted patterned grounds. Quaternary International, Geoarchaeology and Taphonomy 214, 17–29.

Bertran, P., Texier, J.-P., 1995. Fabric Analysis: Application to Paleolithic Sites. Journal of Archaeological Science 22, 521–535. doi:10.1006/jasc.1995.0050

Black, R.F., 1951. Eolian deposits of Alaska. Arctic 4, 89–111.

Bockheim, J.G., 2015. Cryogenic Soil Processes, in: Cryopedology. Springer, pp. 53–63.

Bronger, A., Bruhn-Lobin, N., Heinkele, T., 1993. Micromorphology of paleosols genetic and paleoenvironmental deductions: Case studies from central China, south India, NW Morocco and the Great Plains of the USA, in: Ringrose-Voase, A.J., Humphreys, G.S. (Eds.), Developments in Soil Science, Soil Micromorpohlogy: Studies in Management and Genesis. Elsevier, pp. 187–206.

Bunting, B.T., 1983. High Arctic Soils Through the Microscope: Prospect and Retrospect. Annals of the Association of American Geographers 73, 609–616.

Buurman, P., Van Bergen, P.F., Jongmans, A.G., Meijer, E.L., Duran, B., Van Lagen, B., 2005. Spatial and temporal variation in podzol organic matter studied by pyrolysis-gas chromatography/mass spectrometry and micromorphology. European journal of soil science 56, 253–270.

Calkin, P.E., 1988. Holocene glaciation of Alaska (and Adjoining YUKON Territory, Canada). Quaternary Science Reviews 7, 159–184.

Campbell, I.B., Claridge, G.G.C., 1987. Antarctica: soils, weathering processes and environment. Elsevier.

Chamley, H., 1989 Clay sedimentology, 1989. Springer, Berlin.

Courty, M.-A., 1991. Soil Micromorphology in Archaeology, in: Proceedings of the British Academy. Presented at the Joint Symposium of the Royal Society and the British Academy, pp. 39–59.

Davidson, E.A., Janssens, I.A., 2006. Temperature sensitivity of soil carbon decomposition and feedbacks to climate change. Nature 440, 165–173.
De Coninck, F., Keague, M., A, J., 1985. Micromorphology of Spodosols. Soil Micromorphology and Soil Classification: Soil Science Society of America Special Publication, 121–144.
Dijkmans, J.W., Koster, E.A., 1990. Morphological development of dunes in a subarctic environment, central Kobuk Valley, northwestern Alaska. Geografiska Annaler. Series A. Physical Geography 93–109.
Dixon, J.B., 1989. Kaolin and serpentine group minerals. Minerals in soil environments 2, 467–525.
Douglas, L.A., International Society of Soil Science, Sub-commission of Soil Micromorphology (Eds.), 1990. Soil micromorphology: a basic and applied science: 8th International working meeting: Papers. Elsevier, Amsterdam; New York.
Driese, S.G., Ashley, G.M., 2016. Paleoenvironmental reconstruction of a paleosol catena, the Zinj archeological level, Olduvai Gorge, Tanzania. Quaternary Research 85, 133–146.
Driese, S.G., Nordt, L.C., Waters, M.R., Keene, J.L., 2013. Analysis of Site Formation History and Potential Disturbance of Stratigraphic Context in Vertisols at the Debra L. Friedkin Archaeological Site in Central Texas, USA. Geoarchaeology 28, 221–248.
Dumanski, J., St. Arnaud, R.J., 1966. A micropedological study of eluvial soil horizons. Canadian Journal of Soil Science 46, 287–292.
Estes, R., Howard Hutchison, J., 1980. Eocene lower vertebrates from Ellesmere Island, Canadian Arctic Archipelago. Palaeogeography, Palaeoclimatology, Palaeoecology 30, 325–347.
Fèderoff, N., De Kimpe, C.R., Page, F., Borbeau, G., 1981. Essai d'interpretation des transferts sous forme figuree dans les podzols du Quebec meridional a partir de l'etude micromorphologique des profils. Geoderma 26, 25-45.
Flato, G.M., Boer, G.J., 2001. Warming asymmetry in climate change simulations. Geophysical Research Letters 28, 195–198.
Fox, C.A., 1983. Micromorphology of an orthic turbic cryosol--a permafrost soil. Soil micromorphology: soil genesis / edited by P. Bullock and C.P. Murphy.
Gilbert, P.J., 2011. Micromorphology, site spatial variation and patterning, and climate change at the Mead Site (XBD-071): A multi-component archaeological site in Interior Alaska (M.A.). University of Alaska Fairbanks, United States -- Alaska.
Goebel, T., Potter, B., 2016. First Traces, in: The Oxford Handbook of the Prehistoric Arctic. Oxford University Press, p. 223.
Goebel, T., Smith, H.L., DiPietro, L., Waters, M.R., Hockett, B., Graf, K.E., Gal, R., Slobodin, S.B., Speakman, R.J., Driese, S.G., 2013. Serpentine Hot Springs, Alaska: Results of excavations and implications for the age and significance of northern fluted points. Journal of Archaeological Science 40, 4222–4233.

Goebel, T., Waters, M.R., Meshcherin, M.N., 2000. Masterov Kliuch and the Early Upper Palaeolithic of the Transbaikal, Siberia. Asian Perspectives 39, 47–70.
Graf, K.E., DiPietro, L.M., Krasinski, K.E., Gore, A.K., Smith, H.L., Culleton, B.J., Kennett, D.J., Rhode, D., 2015. Dry Creek Revisited: New Excavations, Radiocarbon Dates, and Site Formation Inform on the Peopling of Eastern Beringia. American Antiquity 80, 671–694.
Hopkins, D.M., 1959. History of Imuruk Lake, Seward Peninsula, Alaska. Geological Society of America Bulletin 70, 1033–1046.
Hseu, Z.-Y., Chen, Z.-S., Wu, Z.-D., 1999. Characterization of Placic Horizons in Two Subalpine Forest Inceptisols. Soil Science Society of America Journal 63, 941 947.
Hudson, T., 1979. Igneous and metamorphic rocks of the Serpentine Hot Springs area, Seward Peninsula, Alaska. US Govt. Print. Off.
Hudson, T., 1977. Genesis of a zoned granite stock, Seward Peninsula, Alaska (USGS Numbered Series No. 77–35), Open-File Report. U.S. Geological Survey.
Hunt, S., Yu, Z., Jones, M., 2013. Lateglacial and Holocene climate, disturbance, and permafrost peatland dynamics on the Seward Peninsula, western Alaska. Quaternary Science Reviews 63, 42-58
Jahren, A.H., Sternberg, L.S.L., 2003. Humidity estimate for the middle Eocene Arctic rain forest. Geology 31, 463–466.
Johnson, D.L., Muhs, D.R., Barnhardt, M.L., 1977. The effects of frost heaving on objects in soils, II: Laboratory experiments. The Plains Anthropologist 133–147.
Kaplar, C.W., 1965. Stone Migration by Freezing of Soil. Science 149, 1520–1521.
Kaufman, D.S., Ager, T.A., Anderson, N.J., Anderson, P.M., Andrews, J.T., Bartlein, P.J., Brubaker, L.B., Coats, L.L., Cwynar, L.C., Duvall, M.L., 2004. Holocene thermal maximum in the western Arctic (0–180 W). Quaternary Science Reviews 23, 529–560.
Kaufman, D.S., Axford, Y.L., Henderson, A.C.G., McKay, N.P., Oswald, W.W., Saenger, C., Anderson, R.S., Bailey, H.L., Clegg, B., Gajewski, K., Hu, F.S., Jones, M.C., Massa, C., Routson, C.C., Werner, A., Wooller, M.J., Yu, Z., 2016. Holocene climate changes in eastern Beringia (NW North America) – A systematic review of multi-proxy evidence. Quaternary Science Reviews 147, 312-339.
Kaufman, D.S., Hopkins, D.M., 1986. Glacial history of the Seward Peninsula. Glaciation in Alaska—The Geologic Record, Hamilton TD, Reed KM, Thorson RM (eds). Alaska Geological Society: Anchorage, AK 51–78.
Kaufman, D.S., Manley, W.F., 2004. Pleistocene Maximum and Late Wisconsinan glacier extents across Alaska, U.S.A., in: Ehlers, J., Gibbard, P.L. (Eds.), Developments in Quaternary Sciences, Quaternary Glaciations-Extent and Chronology. Elsevier, pp. 9–27.
Kemp, R.A., 1999. Micromorphology of loess–paleosol sequences: a record of paleoenvironmental change. CATENA 35, 179–196.

Kemp, R.A., 1998. Role of micromorphology in paleopedological research. Quaternary International, Revisitation of Concepts in Paleopedology 51, 133–141.
Kinnard C., Lewkowicz A., 2006. Frontal advance of turf-banked solifluction lobes, Kluane Range, Yukon Territory, Canada. *Geomorphology* 73, 261-276.
Kubiëna, W.L., 1938. Micropedology. Collegiate Press, Ames, Ia.
Kühn, P., Aguilar, J., Miedema, R., 2010. Textural pedofeatures and related horizons. Interpretation of micromorphological features of soils and regoliths 217–250.
McCarthy, P.J., Martini, I.P., Leckie, D.A., 1998. Use of micromorphology for palaeoenvironmental interpretation of complex alluvial palaeosols: an example from the Mill Creek Formation (Albian), southwestern Alberta, Canada. Palaeogeography, Palaeoclimatology, Palaeoecology 143, 87–110.
McMillan, N.J., Mitchell, J., 1953. A microscopic study of platy and concretionary structures in certain Saskatchewan soils. Can. J. Agric. Sci 33, 178–183.
Miedema, R., 1987. Soil formation, microstructure and physical behaviour of Late Weichselian and Holocene Rhine deposits in the Netherlands. PhD thesis,
Moore, D.M., Reynolds Jr, R.C., 1989. X-ray Diffraction and the Identification and Analysis of Clay Minerals. Oxford University Press (OUP).
Muhs, D.R., Ager, T.A., Been, J., Bradbury, J.P., Dean, W.E., 2003. A late Quaternary record of eolian silt deposition in a maar lake, St. Michael Island, western Alaska. Quaternary Research 60, 110–122.
Pinheiro, J., Salguero, M.T., Rodriguez, A., 2004. Genesis of placic horizons in Andisols from Terceira Island Azores—Portugal. Catena 56, 85–94.
Ringrose-Voase, A.J., Humphreys, G.S., International Society of Soil Science, Sub commission of Soil Micromorphology, 1994. Soil micromorphology: studies in management and genesis : 9th International working meeting : Papers.
Rupp, T.S., Chapin, F.S., Starfield, A.M., 2000. Response of subarctic vegetation to transient climatic change on the Seward Peninsula in north-west Alaska. Global Change Biology 6, 541–555.
Rutherford, G.K. (Ed.), 1974. Soil microscopy proceedings of the fourth International Working-Meeting on Soil Micromorphology, Department of Geography, Queen's University, Kingston, Ontario, Canada, 27th-31st August, 1973. Limestone Press, Kingston, Ont.
Sauer, D., Schülli-Maurer, I., Sperstad, R., Sørensen, R., Stahr, K., 2009. Albeluvisol development with time in loamy marine sediments of southern Norway. Quaternary International 209, 31–43.
Schweger, C., 1985. Geoarchaeology of northern regions: Lessons from cryoturbation at Onion Portage, Alaska. Center for the Study of Early Man, Institute for Quaternary Studies, University of Maine at Orono.
Smith, H. L., and Goebel, T., (2018, in press) Origins and spread of fluted-point technology in the Canadian 'Ice-Free Corridor' and eastern Beringia. Proceedings of the National Academy of Sciences 10.1073/pnas.1800312115.

Smith, H.L., Rasic, J.T., Goebel, T., Graf, K.E., Ketron, C.V., Waters, M.R., 2013. Biface traditions of northern Alaska and their role in the peopling of the Americas. Paleoamerican odyssey 105–123.

Solecki, R.S., 1950. A preliminary report of an archaeological reconnaissance of the Kukpowruk and Kokolik rivers in Northwest Alaska. American Antiquity 16, 66 69.

Stoops, G., 2003. Guidelines for analysis and description of soil and regolith thin sections. Soil Science Society of America Inc….

Tarnocai, C., Smith, C.A.S., 1989. Micromorphology and development of some central Yukon paleosols, Canada. Geoderma 45, 145–162.

Todisco, D., Bhiry, N., 2008. Micromorphology of periglacial sediments from the Tayara site, Qikirtaq Island, Nunavik (Canada). CATENA 76, 1–21.

Tsoar, H., Pye, K., 1987. Dust transport and the question of desert loess formation. Sedimentology 34, 139–153.

Van Vliet-Lanoë, B., 2010. Frost action. Interpretation of micromorphological features of soils and regoliths 81–108.

Van Vliet-Lanoë, B., 2004. Properties and processes of Cryosols: Introduction. Cryosols: Permafrost-affected Soils, Springer-Verlag, Berlin, Heidelberg, New York 341 346.

Van Vliet-Lanoë, B., 1985. Frost effects in soils. Soils and quaternary landscape evolution / edited by John Boardman; sponsored by the Quaternary Research Association.

Van Vliet-Lanoë, B., Fox, C.A., Gubin, S.V., 2004. Micromorphology of cryosols, in: Cryosols. Springer, pp. 365–390.

Vandenberghe, J., 2013. Grain size of fine-grained windblown sediment: A powerful proxy for process identification. Earth-Science Reviews 121, 18–30.

Vepraskas, M.J., 2001. Morphological features of seasonally reduced soils. Wetland soils: Genesis, hydrology, landscapes, and classification 163–182.

Vepraskas, M.J., Craft, C.B., Richardson, J.L., 2002. Wetland soils: genesis, hydrology, landscapes, and classification. CRC Press.

Vorob'eva, G.A., and Mendvedev, G.I., 1984. Pleistotsen-Golotsenovye Otlozheniia i Pochvy Arkheologicheskikh Pamiatnikov Iuga Srednei Sibiri [Pleistocene Holocene Deposits and Soils of Archaeological Monuments of South Central Siberia]. Irkutskii Gosudarstvennyi Universitet, Irkutsk

Wood, W.R., Johnson, D.L., 1978. A survey of disturbance processes in archaeological site formation. Advances in archaeological method and theory 1, 315–381.

Wu, S.-P., Chen, Z.-S., 2005. Characteristics and genesis of Inceptisols with placic horizons in the subalpine forest soils of Taiwan. Geoderma 125, 331–341.

CHAPTER FOUR

Microstratigraphy of Owl Ridge: A Small-Scale Approach to Site Formation and Paleoenvironment at a Pleistocene-Holocene Boundary Site in Central Alaska

Abstract

The Owl Ridge archaeological site is a classic Pleistocene-Holocene boundary site in central Alaska and, as such, plays a key role in understanding the ways in which early human populations adapted to rapid environmental and climatic shifts during the late glacial period in Beringia. Although the lithic assemblage at the site has been studied, very little geoarchaeological work has been published to test some of the hypotheses put forth to link human behavior to paleoenvironment. This study utilizes high-resolution micromorphological, particle size, and bulk and organic geochemical analysis to reconstruct the depositional, pedogenic, and climatic history of the site. The Pleistocene record at the site is aeolian, indicating overall cool/dry conditions punctuated by warm/wet intervals during which time the site was inhabited. These warmer, wetter intervals are indicated by the presence of paleosols dating to the Allerød and the latter half of the Younger Dryas chronozone. A rapidly deposited, colluvial sand layer indicates very wet conditions at the Pleistocene-Holocene boundary. The Holocene record at the site is marked by alternating cool/dry and warm/wet conditions, indicated by alternating aeolian deposition and pedogenesis. Holocene buried soils are spodic in nature, indicating the presence of spruce forests at Owl Ridge. The site records a shift in climatic and environmental conditions across the Pleistocene-Holocene boundary, which may have been a significant obstacle for human occupants of eastern Beringia during this period.

Introduction

The late Quaternary was marked by rapid, dramatic shifts in global climate (Begét and Hawkins, 1989; Dansgaard et al., 1993; Taylor et al., 1993; Petit et al., 1999). The Pleistocene-Holocene transition, in particular, had profound effects on floral (Ager, 1983; 2003; Mann and Hamilton, 1995; Zimov et al., 1995; Erlandson and Moss, 1996), faunal (Guthrie, 2003; 2006; Stuart et al., 2004), and human (Powers and Hoffecker, 1989; Straus et al., 1996; West, 1996; Graf and Bigelow, 2011; Goebel and Buvit, 2011) populations as they struggled to adapt to these shifting environments. In few places has this transition and its impact on Paleolithic peoples been more hotly debated than in eastern Beringia, where researchers have hypothesized that this time interval represents a major shift in lithic technology.

Humans first appeared in the Alaskan archaeological record just prior to the Allerød, an insolation-driven warm period beginning around 14 ka, in the Tanana River Valley using an artifact assemblage characterized by microblade technology (Potter et al., 2013). During the Allerød, human populations likely expanded across central Alaska, leaving traces in both the Tanana and Nenana River Valleys (Potter, 2008; Graf and Bigelow, 2011; Graf and Buvit, 2017). Rather than using microblade technology, however, many of these early Alaskans generally utilized thinly-worked, bifacial teardrop-shaped or triangular-shaped projectile points and unifacial tools (Powers and Hoffecker, 1989; Goebel et al., 1991; Hoffecker et al., 1993; Yesner, 2001; Graf and Goebel, 2009; Graf and Bigelow, 2011; Graf et al., 2015; Gore and Graf, 2018). Following the Allerød, during the Younger Dryas (YD) chronozone, central Alaska experienced a climate reversal as well as a resurgence in microblade technology,

accompanied by lanceolate and concave-based points and burins (chisel-like tools). It should be noted that this pattern holds true broadly, particularly in the Nenana River Valley, but that it is far from universal because Allerød-age sites in the Tanana Valley often lack diagnostic artifacts, retain triangular-shaped points into the early Holocene, or, in the case of the Healy Lake Village site, may have both the small bifacial points (both teardrop and triangular) and microblades in the same cultural horizons, though direct association of these two technologies at the site remain questionable (Erlandson et al., 1991; Hamilton and Goebel, 1999; Younie and Gillispie, 2016).

The origin of this technological variability has been one of the fundamental points of contention in Alaskan archaeology. Researchers have ascribed the variability to everything from differences in site usage or seasonality, faunal populations, or regional paleoenvironment between sites, to raw material availability, climate-driven shifts in paleoenvironment, and population turnover with no consensus in sight (Holmes, 2001; Gal, 2002; Potter, 2005; Wygal, 2009; Graf and Bigelow, 2011; Wygal and Goebel, 2011; Gore and Graf, 2018). To begin testing these hypotheses, integrated and innovative research strategies that employ a variety of analytical techniques are necessary.

This study attempts to take a step in that direction by assessing the role that site formation processes and climatic shifts played at the Owl Ridge site in the Teklanika River Valley in central Alaska. The site is a well-stratified, multi-component Pleistocene-Holocene boundary site with distinct cultural horizons representing both a triangular-shaped, bifacial point-bearing assemblage and two microblade-bearing assemblages with lanceolate points. Additionally, several paleosol horizons have been described within the sediment package, indicating that the site may have utility as a paleoenvironmental

record as well as an archaeological one. Although a large area of Owl Ridge has been excavated and significant work has been done on the lithic artifacts at the site, little geoarchaeological work has been reported and very few results of any kind have been published yet. This work is part of a larger effort to remedy that situation and to conduct a holistic analysis of the site.

The goal of this study is threefold: first, to construct a depositional and pedogenic history for Owl Ridge using particle-size analysis, soil micromorphology, and organic and inorganic geochemistry to identify depositional processes and climatic transitions represented by the sediment package; second, to ascertain what implications this history may have for the interpretation of paleoenvironment and lithic technology at the site during the latest Pleistocene and early Holocene; and third, to place these findings in the context of central Alaskan paleoecology during the late Quaternary.

The Owl Ridge Site

Geographic Setting

The Owl Ridge site sits on a south-facing glacial outwash terrace approximately 61 m above the confluence of First Creek and the Teklanika River, 2 km north of the boundary of Denali National Park (Fig. 4.1). To the south and east of the site are the northern foothills of the Alaska Range, consisting of metasedimentary and metavolcanic rocks. To the north and northeast are terraced, loess-covered uplands overlying thick gravel deposits. The terrace upon which the site rests is bounded by incised stream valleys created by First Creek to the south, Second Creek to the north, and a deeper valley formed by the Teklanika River, a braided stream complex flowing north out of the

Alaska Range, to the west. The site occupies the southwestern-most corner of the terrace, which itself is composed of fluvial and glaciofluvial sands and gravels.

Modern vegetation cover near Owl Ridge is highly dependent upon topography and water availability (Phippen, 1988). The site itself, located along the top of the terrace near the treeline, is covered by a combination of trees (spruce-*Picea glauca*, alder-*Alnus crispa*, and birch-*Betula papyfira*), shrubs (cranberry-*Vitas idea*, crowberry-*Empetrium negrum*, and various *Ericaceae*), mosses, lichens, and grasses. Aspen (*Populus tremuloides*) dominate the gentler slopes in the area and dense spruce forests cover the lower-lying areas. Willow (*Salix sp.*) grows along stream margins. Above treeline, shrub tundra spotted with krummholz spruce, dwarf birch, and alder trees is common.

Climatologically, Owl Ridge is generally comparable to many other locations in central Alaska, with cold, dry winters (avg: -14.5°C, 53 mm precipitation) and mild, wetter summers (avg: 11.7°C, 205 mm precipitation). Mean annual precipitation (MAP) is approximately 380 mm/yr and mean annual temperature is -2.3°C, with a range from -20.5°C to 18.3°C (NPS, 2018). Annual snowfall averages nearly 2 meters, but snow accumulation is often dependent upon wind conditions (Phippen, 1988). Mean annual potential evapotranspiration is less than 15 inches/year (USGS, 1990). The site's proximity to the Alaska Range means that strong winds are common. Research suggests that katabatic-type winds had major influences during the late glacial period, even more so in the Teklanika River Valley than in the nearby Nenana Valley (Thorson and Bender, 1985), and that similar high-velocity, density-driven winds may have played a role even into the Holocene (DiPietro et al., 2017).

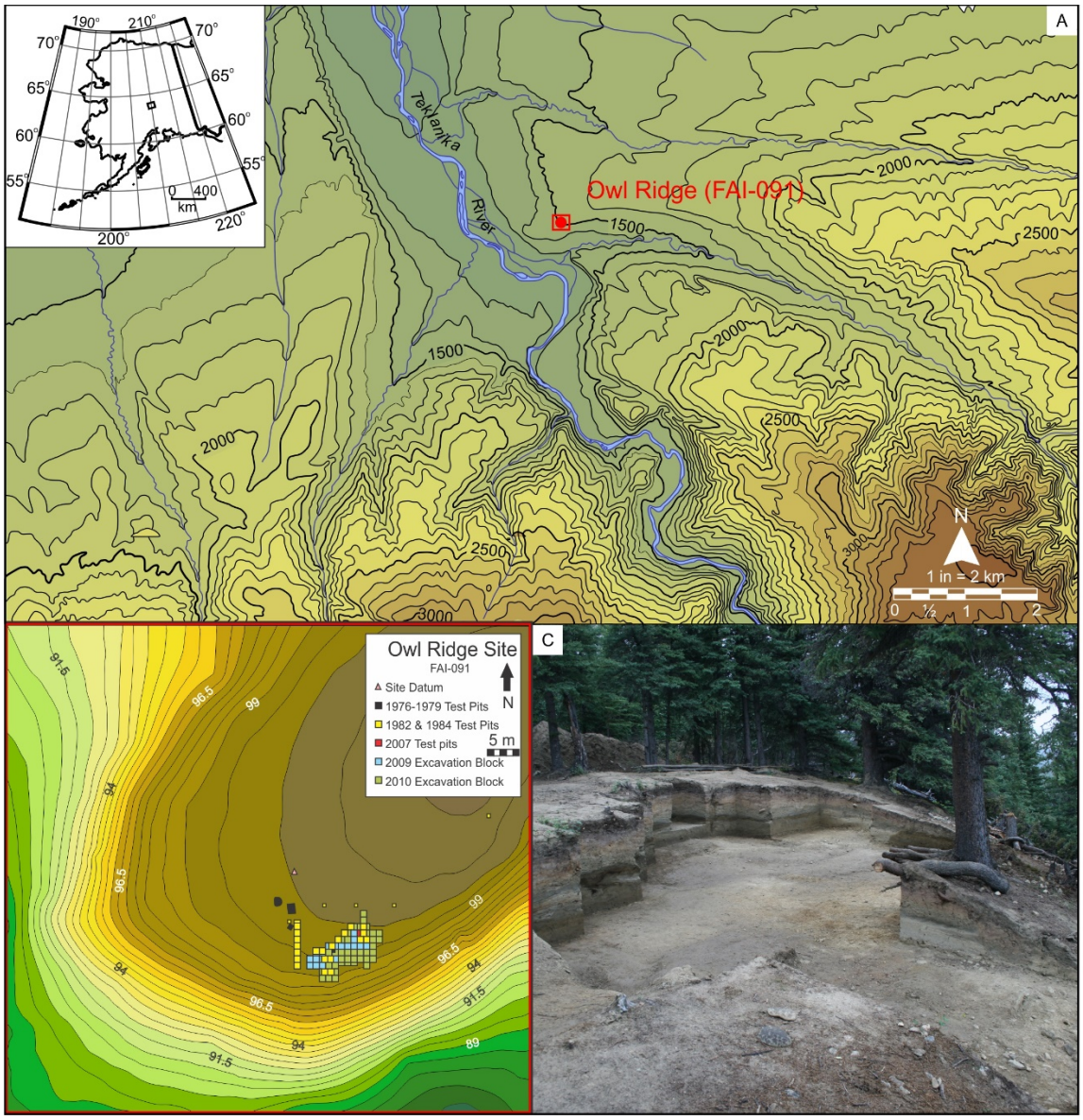

Figure 4.1: Location of the Owl Ridge archaeological site overlooking the confluence of First Creek and the Teklanika River. A) Topographic map showing the Teklanika River Valley and situation of the Owl Ridge site on a glacial outwash terrace; B) Topographic profile of the upper part of the bluff on which the site rests, showing locations and dates of excavation units and test pits; C) Photograph of the Owl Ridge site.

Previous Geoarchaeological Work

The Owl Ridge site was initially discovered in 1976 as part of a reconnaissance survey of the Teklanika River conducted by a group of archaeologists from University of

Alaska at Fairbanks (Plaskett, 1976). This early testing initiative resulted in the first geoarchaeological analysis of the site, conducted by Robert Thorson and recorded in an unpublished manuscript. This manuscript documented the stratigraphy of the site and proposed a site history model which remains the basic framework for interpreting the site today.

Though this survey uncovered a promising accumulation of deeply-buried cobbles that were interpreted as anthropogenic in origin and a limited number of lithic artifacts, excavation did not begin in earnest until the mid-1980s when Peter Phippen began his masters work at the site. Phippen completed the testing initiative begun in 1976 and excavated an additional 26 m^2, identifying three archaeological components, documenting the site's stratigraphy, and collecting samples for several radiocarbon dates. Phippen's (1988) thesis, which, in addition to documenting the archaeology at the site, summarizes and expands upon Thorson's geoarchaeological work, remains the seminal publication on Owl Ridge today. Following this work, the site remained untouched until additional excavations by Texas A&M archaeologists in 2007-2010. Graf and the Texas A&M team conducted a full-scale excavation at Owl Ridge, opening an additional 58 m^2 over the course of three field seasons and collecting a new suite of samples for radiocarbon dating and geoarchaeological work, including the materials used in this study.

Three archaeological components are present at Owl Ridge. Although Phippen (1988) identified and dated all three components, recent work (Graf et al., 2010; Gore and Graf, 2018) suggests that his dates for components 2 and 3 are anomalously young and that all three occupations of the site occurred between the latest Pleistocene and

earliest Holocene. It is this revised age model for the site that is utilized here. Component 1, assigned to the Nenana complex, is characterized by triangular-shaped projectile points and dates to between 13.3 and 13 ka (calendar years ago, based on previously reported radiocarbon dates from Graf et al. 2010), during the Allerød. Component 2 is a microblade-bearing assemblage dating to between 12.5 and 11.3 ka, within the Younger Dryas chronozone. Component 3 also contains microblades but is younger than component 2, dating between 11,390 and 11,170 cal BP, just prior to the Holocene Thermal Maximum. Both microblade-bearing components have been assigned to the Denali complex. All three components are well-separated stratigraphically and represent time periods associated with different climatic events, providing an excellent opportunity to better understand the relationship between rapidly-shifting environmental conditions and human behavior.

Site Stratigraphy

The terminal Pleistocene stratigraphy at Owl Ridge consists of a series of interbedded glacial, aeolian, and colluvial silts and sands. Phippen (1988) identified eight depositional units at the site, whereas recent work combines Phippen's three uppermost units into a single stratum and subdivides another to arrive at seven strata, described below.

At its most fundamental, the site is composed of three sandy loam units separated by two sands all resting atop poorly-sorted outwash (Fig. 4.2, 4.3, 4.4). These outwash deposits, designated as stratum 1, date at least to the early Wisconsin glaciation, locally known as the Healy, Riley Creek, and Carlo Creek glacial advances, but may be significantly older (Péwé et al., 1966; Phippen, 1988). The first silt unit, stratum 2, overlies the outwash. Graf et al. (2010) subdivide stratum 2 into stratum 2a, a more

poorly-sorted, greyish brown silt which was frozen when encountered during excavation, and stratum 2b, a well-sorted, yellowish mottled silt with a weak paleosol developed at the uppermost surface. Component 1 occurs within the uppermost portion of stratum 2b, largely in close association with this weakly-developed paleosol. Stratum 3 is the lowermost of the two sand units at Owl Ridge. It is poorly sorted, medium-to-coarse-grained, and thin, yet thickens slightly toward the bluff edge. Stratum 4, the middle of the three silt units, is an olive to greyish brown silt with sand intermixed, particularly in the lower portions. Stratum 4 is noteworthy for the apparent buried soils it contains. Phippen noted the presence of several dark, organic bands within the unit, and Graf et al. (2010) noted a strong buried A horizon in the unit. These organic-rich bands have been distorted and folded. Component 2 occurs within stratum 4, possibly in association with the observed paleosol horizon(s). Stratum 5 is the second sand unit at the site, although it is quite different in nature from stratum 3. It consists of yellowish-brown to olive unweathered sand which is medium to fine at its upper and lower contacts but contains lenses or beds of coarse to very coarse sand in the center of the stratum. Phippen describes stratum 5 as thinning upslope from the site, but more recent excavation suggests that the unit in fact thickens away from the bluff edge, sometimes manifested by as many as seven beds of sand furthest from the terrace edge. Isolated gravel lenses and lags are present within the sand. Near the base, small channelized gravel and coarse sand deposits have incised into the underlying stratum 4 silt. Stratum 6 is the uppermost silt unit and is the thickest, comprising nearly a third of the total thickness of the profile. It is a sandy silt with linear, reddish-orange and light-gray mottling. Towards the top of stratum 6 is a light grey band (Phippen's stratum 7) and thick root mat (Phippen's stratum

8), which likely represent the E and O horizons of the modern surface soil, respectively.

Component 3 occurs at the boundary between strata 5 and 6.

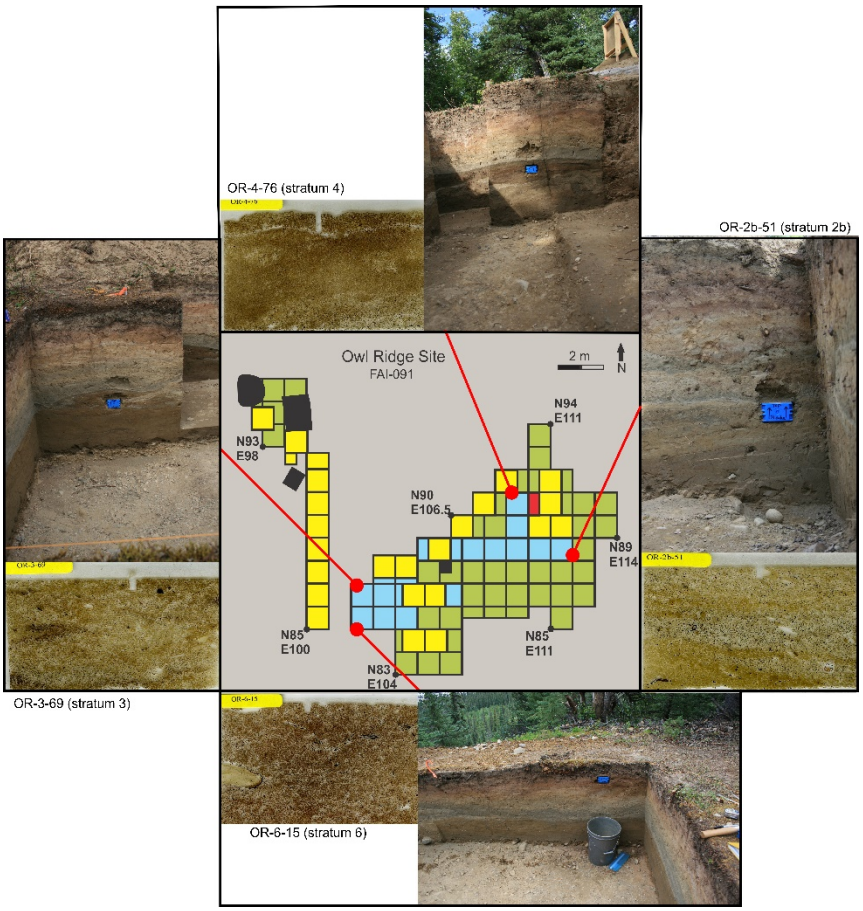

Figure 4.2: Photographs and thin section scans from the 2009 suite of samples, showing source location within the excavation block.

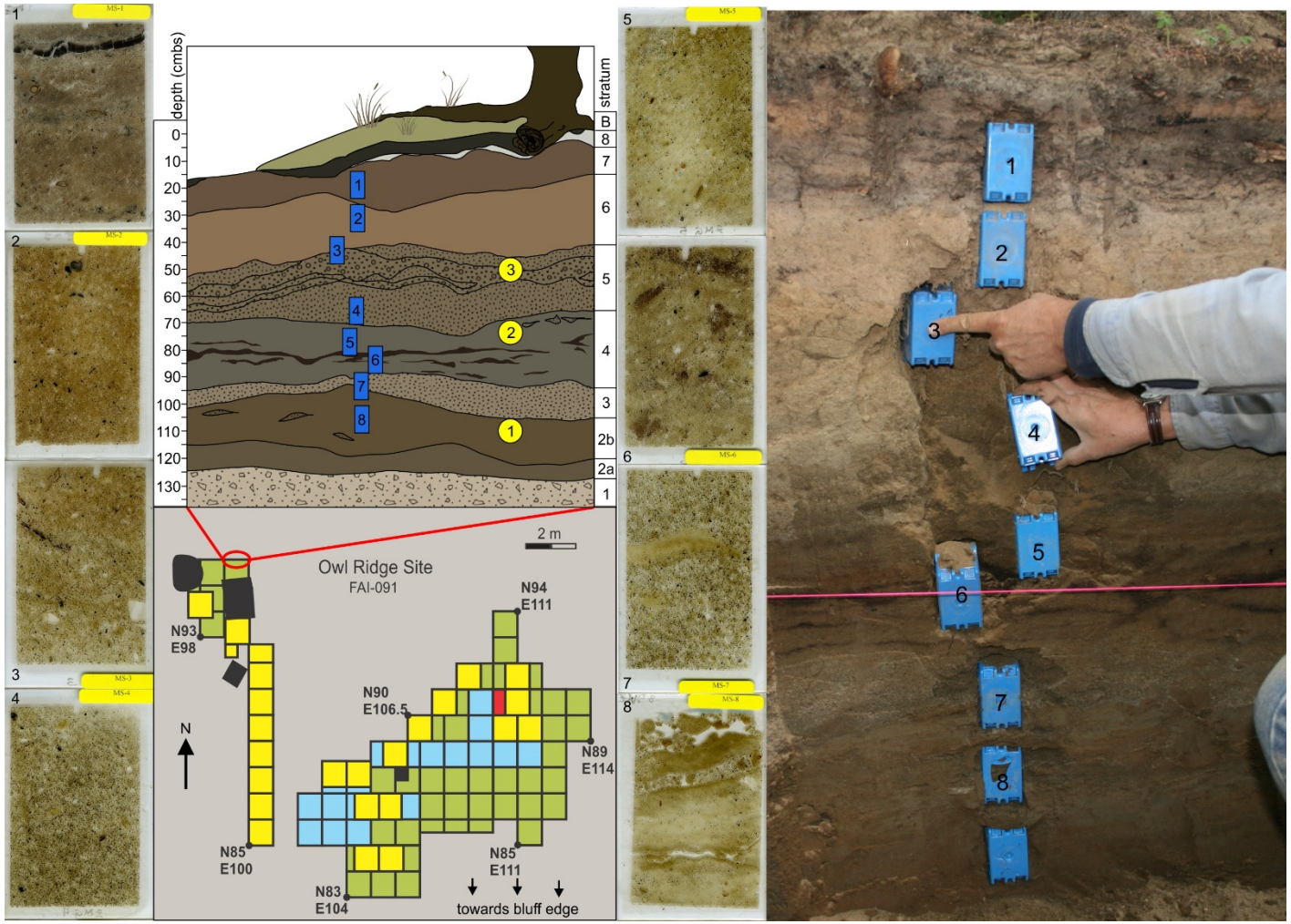

Figure 4.3: Photograph and soil profile showing locations of the eight thin sections collected from an E/W trending wall, as well as scans of the thin sections.

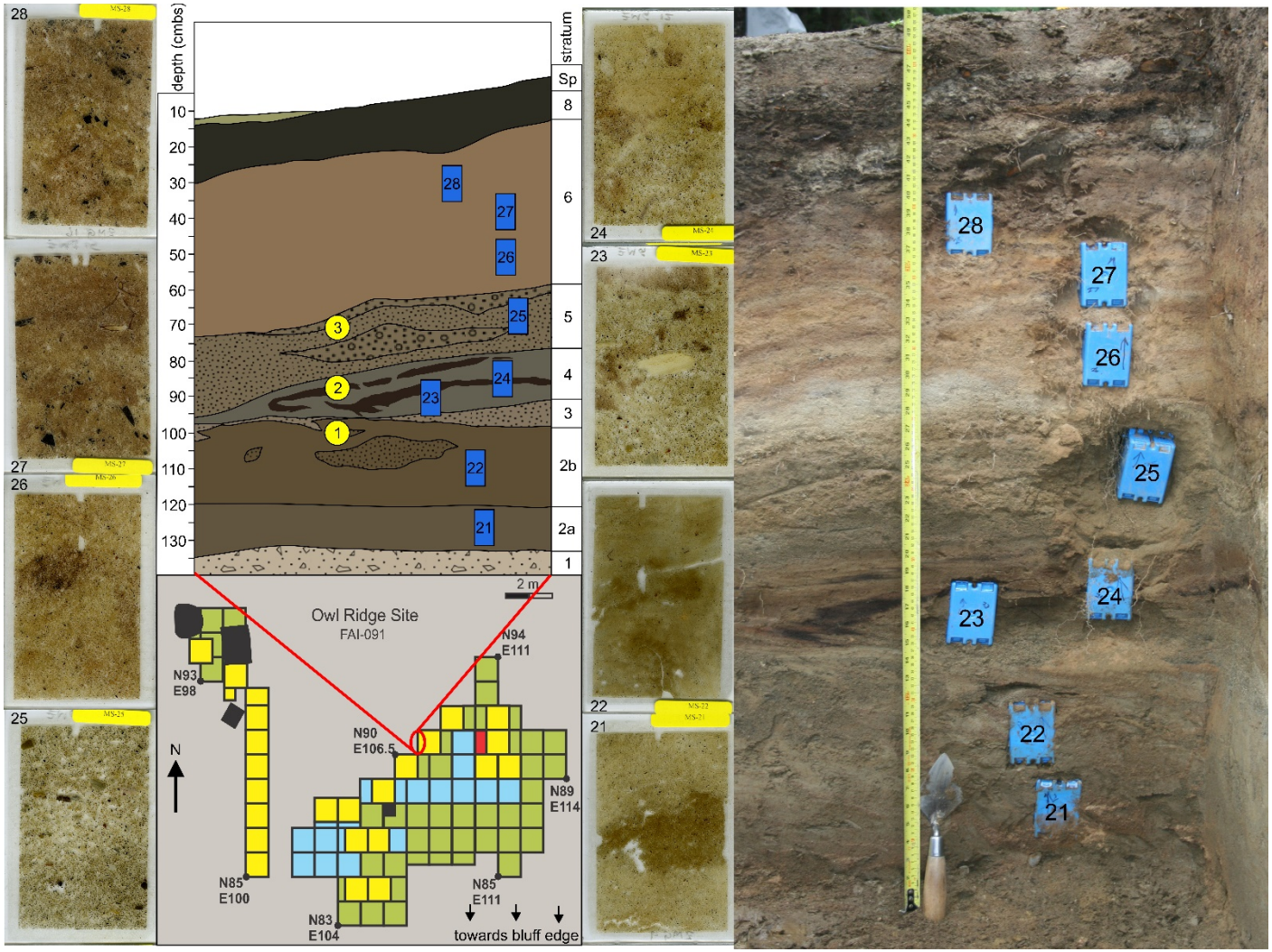

Figure 4.4: Photograph and soil profile showing locations of the eight thin sections collected from a N/S trending wall, as well as scans of the thin sections.

Material and Methods

Field description and sampling

Excavation for this study took place over the course of three seasons of field work in 2007, 2009, and 2010, expanding the area originally excavated by Phippen in 1982-1984 to include an additional 58 m^2 (Fig. 4.2, 4.3, 4.4) and including six geological test extending about 1 km up the ridge behind the site. Once excavation was complete, profile walls were described, sketched, and photographed by Kelly Graf and Michael Waters (Texas A&M University). 27 100-g bulk sediment samples were collected every five centimeters for geochemical and particle size analysis. In the summer of 2009, four oriented samples were collected by driving plastic conduit boxes into the walls at areas of interest for preliminary micromorphological analysis (Fig. 4.2). A larger micromorphology sampling initiative took place during 2010, when a suite of sixteen additional oriented samples spanning the entire soil profile were taken, eight from an east-west trending wall (Fig. 4.3) and eight from a north-south trending wall (Fig. 4.4).

Laboratory and analytical methods

Oriented samples collected for soil micromorphology were air-dried, surface impregnated with Hillquist thin-section epoxy, and sent to Spectrum Petrographics Inc. for vacuum impregnation and thin-section preparation. Prepared slides were 5x7 cm (Fig. 4.2, 4.3, 4.4). Microscopy was performed using an Olympus® BX51 binocular polarizing microscope, and photomicrographs were taken using a 12.5 MPx Leica® digital camera attachment and Leica image-processing software. Thin sections were described using the terminology set forth by Stoops (2003).

Samples for particle-size analysis were sieved to remove grains larger than 2 mm in diameter. Once sieved, the remaining material was pre-treated with 30% H_2O_2 until reaction ceased to remove particulate organic matter. X-ray and micromorphological analyses indicated that carbonates were absent, so HCl pre-treatment was unnecessary. Samples were then suspended in 1L of de-ionized water, dispersed with 10 mL of 10% $(NaPO_3)_6$ and sonicated for 3 minutes to ensure complete disaggregation. Particle-size analysis was performed using a Malvern MasterSizer® 2000 with a Hydro MU dispersion unit. Data were collected in quarter-phi increments and were converted to grain sizes using the Mie Theory. Duplicate analyses were performed periodically to ensure accuracy. Weight percent gravel was determined at Texas A&M Soil, Water, and Forage Testing Laboratory after samples were sieved.

Aliquots of each sample were powdered and sent to ALS Chemex (Reno, NV) to determine bulk elemental chemistry. Samples were put into solution using a four-acid, near-total digestion process and analyzed for the concentrations of 33 major and trace elements via ICP-MS. Bulk soil organic matter from each crushed sample was analyzed for weight percent carbon and nitrogen, as well as the carbon isotopic composition. HCl pre-treatment was not performed because the samples were not calcareous. Organic carbon and nitrogen abundance were quantified by dry combustion on a Costech elemental analyzer. The CO_2 evolved by combustion was then conveyed to a Thermo Delta V Advantage® stable isotope-ratio mass spectrometer for carbon isotopic analysis. Precision for carbon isotopic analysis is ±0.03‰ and for concentration analysis analytical precision is ±0.08 wt% for C and ±0.01 wt% for N. All $\delta^{13}C$ values are presented relative to the Vienna Pee Dee Bee (V-PDB) standard.

Results

Soil Micromorphology

Texture and c/f Related Distribution The coarse-fine (c/f)-related distribution of the strata at Owl Ridge varies considerably with depth (Fig. 4.5), generally in conjunction with field-designated textural changes. Most units are either porphyric, chitonic, or enaulic, although considerable variability exists, sometimes even within the same thin section, and distributions ranging from monic to massive are observed.

In general, the silt units (strata 2, 4, and 6) have a porphyric distribution, ranging from open porphyric in stratum 2 (Fig. 4.5a) to close porphyric in stratum 6 (Fig. 4.5b), where the overall sand content is much higher. Chitonic and enaulic zones are present in stratum 4 (Fig. 4.5c, d) which are not observed in the other silts, except for the uppermost portion of stratum 6, which is enaulic in places. Stratum 3, the lowermost sand unit at the Owl Ridge, has an enaulic c/f distribution (Fig. 4.5e) and appears quite similar in nature to the enaulic zones present within stratum 4. It also includes some areas richer in silt that have a close porphyric distribution (Fig. 4.5e), similar to the majority of stratum 4. Stratum 5 is the only unit at the site to have a monic c/f distribution, although some isolated chitonic regions are present (Fig. 4.5f).

Cryogenic Features The character and development of cryogenic features at Owl Ridge vary across the site (Fig. 4.6). Each field-assigned depositional unit exhibits a slightly different assemblage of cryogenic features. Stratum 2a has relatively few cryogenic features, but moderately-developed cryogenic fabrics. Small lenticular and vesicular pores are present in what is otherwise a massive unit, except for a small, isolated portion of the soil which appears to have weakly-developed banded fabric (Fig. 4.6a). Stratum

2b, conversely, exhibits some of the best-developed cryogenic fabrics present in the site. Well-developed banded fabric where lenses of coarse and fine material have formed is present (Fig 4.3 and 4.4-thin section scans 7, 8, 22, Fig. 4.6b). Within the siltier portions of this banded fabric a second, less-well-developed, smaller-scale stage of banded fabric has formed (Fig. 4.2, 4.3-thin section scans 7, 8, 22). In some areas, this banded fabric has been disturbed by what appear to be traces of mud boils (Fig. 4.6b). Both lenticular and vesicular porosity are observed. Some very large lenticular pores have been infilled with sand and large soil aggregates (Fig. 4.6c). Stratum 3 generally lacks cryogenic features or fabrics. In the field, however, small-scale involutions were present along the lower boundary of stratum 3, perhaps suggesting solifluction processes. It may be that the coarser nature of the sand and scarcity of elongated grains has prevented any cryogenic alteration from being apparent at a micro-scale. Stratum 4 does not exhibit banded microfabrics, except for that which occurs in the dark bands identified as paleosols in the field. More common in this stratum are silt capped grains (Fig. 4.6d), many of which have been rotated (Fig. 4.6e), and vertically- or subvertically-oriented, elongated coarse grains (Fig. 4.6f). Cryogenic features are also limited in stratum 5, where silt-capped grains are commonly observed, but little else. Stratum 6 exhibits perhaps the most diverse suite of cryogenic features in the profile. Silt-capped and vertically-oriented elongated coarse grains are also present here (Fig. 4.6g), in addition to microgranular and banded fabrics (Fig. 4.6h) near the surface. Lenticular aggregates with incipient silt cappings are observed, as well as large, fragmented pieces of plant material and charcoal.

In addition to stratigraphic controls on the nature of cryogenic features, there also appear to be spatial controls, because some of the original suite of samples collected from

the site, which came from nearer the bluff edge, exhibit a better-developed and more variable suite of cryogenic features than do the remainder of thin sections. Microfabrics featuring granular aggregates are present in this portion of the site and are more common at the base of the profile, but present to varying degrees throughout (Fig. 4.7 a-c). Silt cappings, many of which are rotated, are nearly ubiquitous on sand grains, which are generally oriented parallel to the slope on which the deposits rest. Although rare, microgranular aggregates consisting of many small particles welded together by silt are observed in this near-edge portion of the site (Fig. 4.7d).

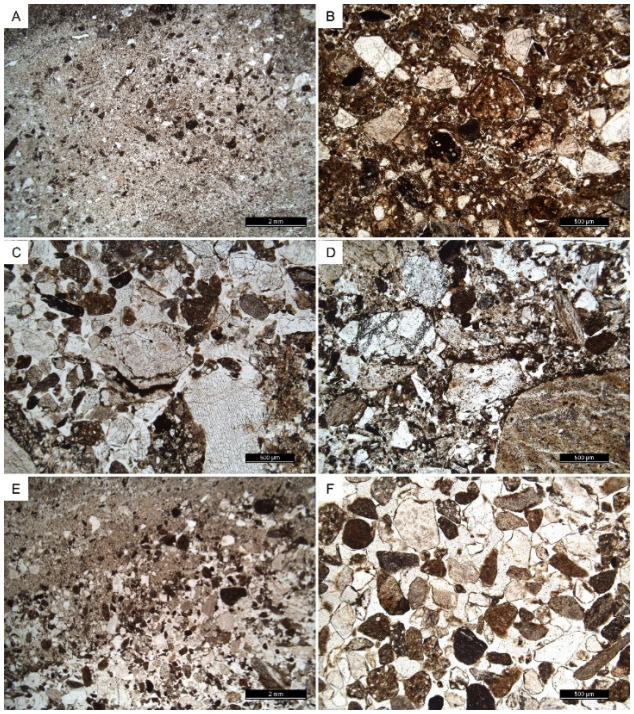

Figure 4.5: Photomicrographs showing the coarse/fine (c/f) distribution of samples from Owl Ridge. A) open porphyric c/f distribution in stratum 2b (MS-8, 1.25x PPL); B) close porphyric c/f distribution in stratum 6 (MS-2, 4x PPL); C) enaulic c/f distribution in stratum 4 (MS-5, 4x PPL); D) chitonic c/f distribution in stratum 4 (MS-6 4x PPL); E) close porphyric and enaulic c/f distribution in stratum 3 (MS-7 1.25x PPL); F) monic c/f distribution in stratum 5 (MS-25, 4x PPL).

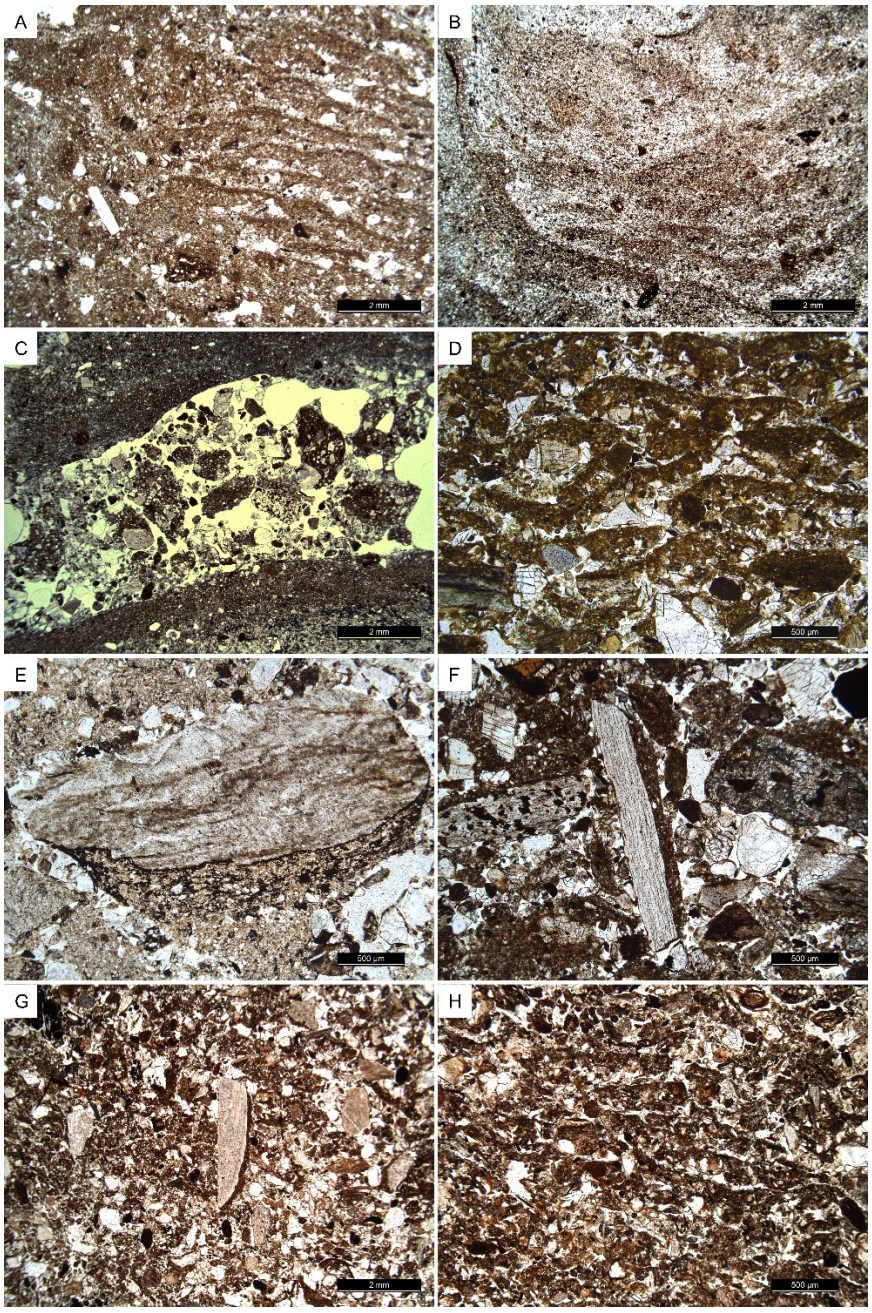

Figure 4.6: Cryogenic fabrics and pedofeatures in thin sections from the 2010 excavations. A) weakly-developed banded fabric in stratum 2a (MS-21, 1.25x PPL); B) banded fabric in stratum 2b disrupted by a mud boil (MS-22, 1.25x PPL); C) large lenticular pore in stratum 2b infilled by sand, silt, and soil aggregates (MS-8, 1.25x PPL); D) banded fabric in the field-interpreted A horizon in stratum 4 (MS-6, 4x PPL); E) silt capped grain in stratum 4 with alternating layers of silt and monomorphic spodic material (MS-5, 4x PPL); F) elongated, silt capped grain which has been frost-jacked into a vertical orientation in stratum 4 (MS-6 4x PPL); G) silt capped, vertically oriented elongated grain in stratum 6 (MS-4, 1;25x PPL); H) banded fabric in stratum 6 (MS-1, 4x PPL)

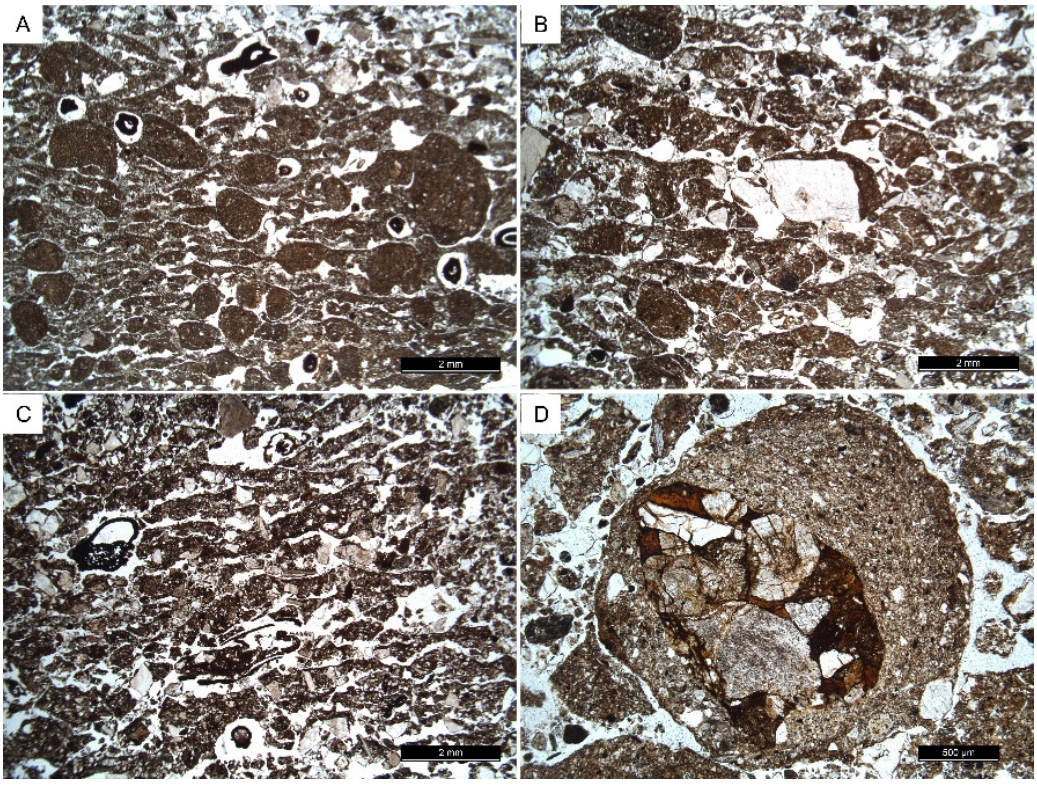

Figure 4.7: Cryogenic fabrics in the 2009 thin sections. A) microgranular fabric in stratum 2b (OR-2b-51, 1.25x PPL); B) microgranular fabric and silt capped grains in stratum 3 (OR-3-69, 1.25x PPL); C) microgranular and banded fabric in stratum 6 (OR-6-15, 1.25x PPL); D) microgranular aggregate in stratum 2b (OR-2b-51, 4x PPL).

Podzolization and Redox Features Pedofeatures related to the translocation of Fe-oxides, both alone and in conjunction with organic matter, are the dominant non-cryogenic features in the soil profile. Redox features are common in the lowermost and uppermost portions of the site. Fe-oxide nodules and grain coatings are present in the upper parts of stratum 6. Nodules are also observed, albeit uncommonly, in stratum 2a (Fig. 4.8a). Many ped boundaries in stratum 2b show Fe-oxide hypocoatings (Fig. 4.8b). Matrix accumulations of Fe-oxides are present in portions of stratum 6, in the field-identified A horizons in stratum 4 and 2b, as well as in the portion of stratum 2a that has banded microfabric.

Far more abundant within the profile is evidence for podzolization. Both monomorphic and polymorphic materials are present, though monomorphic is more common, particularly at depth. Reddish-brown grain coatings are present in portions of stratum 5, resulting in the chitonic c/f distribution noted in section 4.1.1 (Fig. 4.8c). Similar material is present as coatings on pore surfaces (Fig. 4.8d) and the upper surfaces of grains (Fig. 4.8e) in stratum 4, though here it is black in color. In places, this monomorphic spodic material is present within silt cappings on large grains, often in alternating layers with the silt, suggesting several stages of cheluviation interspersed with silt translocation. These horizons of illuviated monomorphic spodic material are often associated with Fe-oxides and banded microfabric in the field-identified paleosol portions of stratum 4. Monomorphic spodic material is present to a lesser degree in both the silty portions of stratum 3 (Fig. 4.8f) and in stratum 2b (Fig. 4.8g) but is lacking in stratum 2a. Although illuviated monomorphic spodic material is not present in stratum 6, there is evidence for increased weathering caused by organic acids, as evidenced by pitted quartz grains (Fig. 4.8h).

Slope Processes Microfabrics indicative of slope processes are also present at Owl Ridge, though in a somewhat limited fashion. The most striking slope-related feature at the site is the abundance of elongated coarse grains oriented parallel to the slope of the ground surface in strata 4, 5, and 6 (Fig. 4.9). Most clearly seen in stratum 5, likely due to the overall coarser nature of the unit, these grains are silt-capped and inclined at an angle of roughly 10-20°. This orientation is most evident further away from the bluff edge.

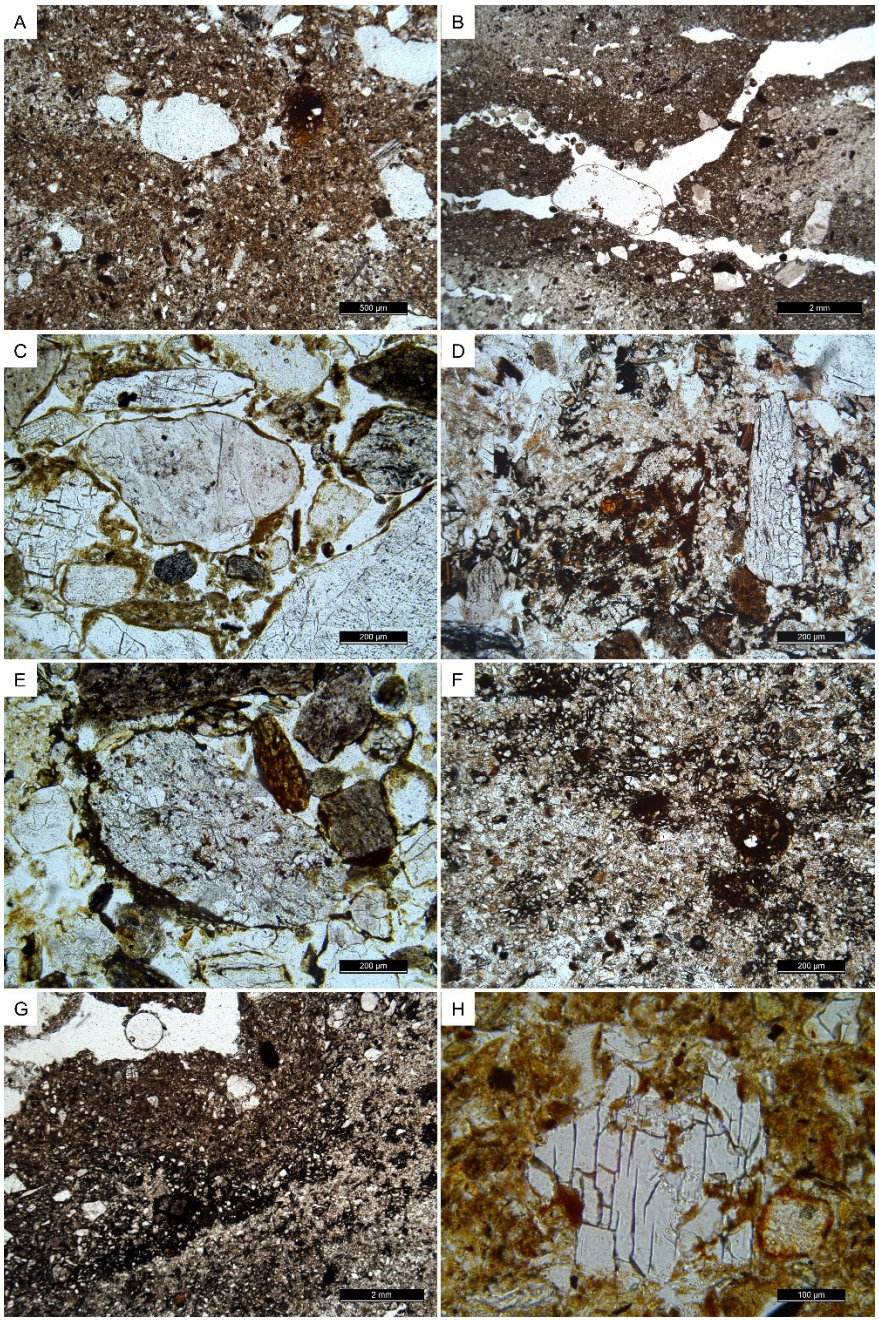

Figure 8: Redoximorphic and podzolization features at Owl Ridge. A) Fe-oxide nodule in stratum 2a paleosol (MS-21, 4x PPL); B) Fe-oxide hypocoatings on ped surfaces in stratum 2b (MS-8, 1.25x PPL); C) monomorphic spodic material coating sand grains in stratum 5 (MS-3, 10x PPL); D) monomorphic spodic material coating pore surfaces in stratum 4 (MS-5, 10x PPL); E) monomorphic spodic material coating sand grains in stratum 4 (MS-5, 10x PPL); F) monomorphic spodic material accumulation in stratum 3 matrix (MS-7, 10x PPL); G) monomorphic spodic material in stratum 2b matrix, pre-dating Fe-oxide hypocoating (MS-8, 1.25x PPL); H) pitted quartz grain in the upper part of stratum 6 (MS-1, 20x PPL).

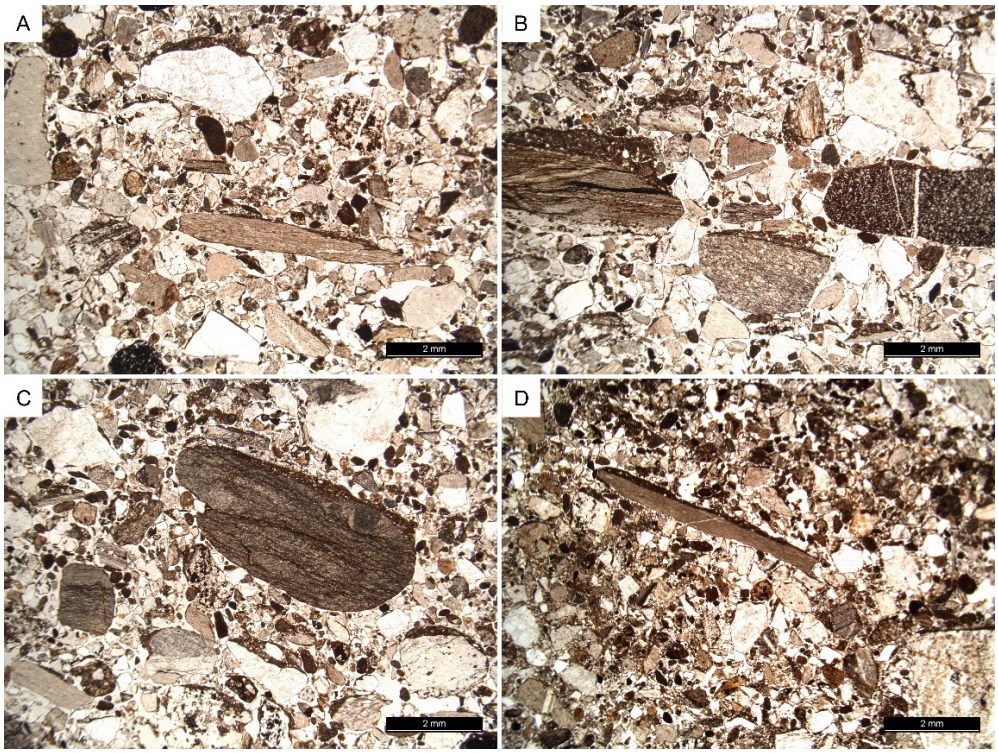

Figure 4.9: Elongated, silt-capped grains oriented parallel to the sloping ground surface in stratum 5 (A-C: MS-25, 1.25x PPL) and at stratum 5/6 interface (D: MS-3, 1.25x PPL).

Particle Size Analysis

There is considerable variability among the particle size distributions from Owl Ridge (Fig. 4.10). Broadly, the data confirm the separation of strata based upon field textural attributes; samples from within each stratum are generally more like one another than they are samples from other strata, with a few notable exceptions. Nearly all samples are polymodal in nature, exhibiting grain size components with modal sizes around 0.6 μm (mode 1, M1), 20-50 μm (mode 2, M2), and 300-500 μm (mode 3, M3). M2 is the most abundant component in all samples, save the lower sample from stratum 1 and stratum 5. The character of M2 varies considerably throughout the profile, ranging from a well-sorted, slightly fine-skewed distribution to a poorly-sorted distribution, where it almost appears to be composed of sediment falling into two size classes: one ranging

from 2-10 μm (hereafter referred to as M2a) and one ranging from 20-100 μm (hereafter referred to as M2b). In general, where they are both present, the abundances of M2a and M2b are inversely related. M3 is most variable throughout the profile, virtually absent in some samples and comprising a clear majority of others. M1 is the most consistent component: its abundance remains essentially unchanged throughout the profile.

Although variations in the particle size distribution between strata are important for designating depositional units and understanding major shifts in the mode of deposition at Owl Ridge, variations within each depositional unit are also helpful for understanding gradual changes in deposition over time. Stratum 1, the basal unit, is very poorly sorted, with approximately equal abundances of sediment in M2a and M2b and slightly more M3 (Fig. 4.10). In addition to the material analyzed with the Mastersizer, the lowermost sample contained an abundance (nearly 50 weight percent) of gravel. Stratum 1 rapidly fines upward, however, losing much of the gravel and coarse sand in favor of silt only 5 cm above the base of the excavation. Stratum 2a shows both M2 and M3 at the base, though the amount of M3 decreases rapidly up-profile (Fig. 4.10). Stratum 2b is by far the best sorted unit at the site, consisting almost exclusively of M2 until near its upper boundary where M3 appears. Stratum 3 and stratum 4 are quite similar in nature. Both have strong M2 and M3 components. Stratum 5 is unlike any other depositional units at the site, with M3 comprising almost the entirety of the samples from this unit. The remainder of volume in these samples consists mainly of M2. Stratum 6, the uppermost unit, exhibits the most textural variability over its thickness and is the only unit, except for the basal outwash, which consistently contains all three grain size modes, including M2a and M2b. M3 is prominent at the base of stratum 6 but decreases

in abundance and ultimately disappears near the surface. M2a and M2b are present in all samples but vary in relative abundance with depth. M2b is always the more abundant of the two, but M2a is present in almost equal abundance near the base of stratum 6. At approximately 20 cm below the surface, M2b becomes much more abundant than M2a, but M2a becomes prevalent again near the top of the profile.

Bulk Geochemistry

Inorganic Geochemistry The concentrations of major elements with depth at Owl Ridge are broadly similar, showing slight variation near the top of the profile and a significant accumulation around 100 cm depth (Fig. 4.11). Al, Fe, and Ti are distributed virtually identically, with moderate variation in stratum 6, a marked increase beginning at the top of stratum 4, accumulation at the boundary between stratum 2a and 2b, and a decrease below. Ca, Mg, and Na are similar, but do not increase as drastically in abundance in stratum 4. K shows very little variation at all in the profile, with concentrations ranging between 1.2 and 1.6 weight percent, whereas Mn decreases gradually from around 900 ppm at the base of section to 200 ppm near the surface.

Trace element concentrations generally follow one of the trends described above and are of limited interpretive value here, save for the concentrations of Sc and Cr, which have been shown to be useful in assessing changes in the provenance of central Alaskan loess samples (Muhs and Budahn, 2006). A ratio of Cr/Sc plots very closely along a linear trendline (Fig. 4.12).

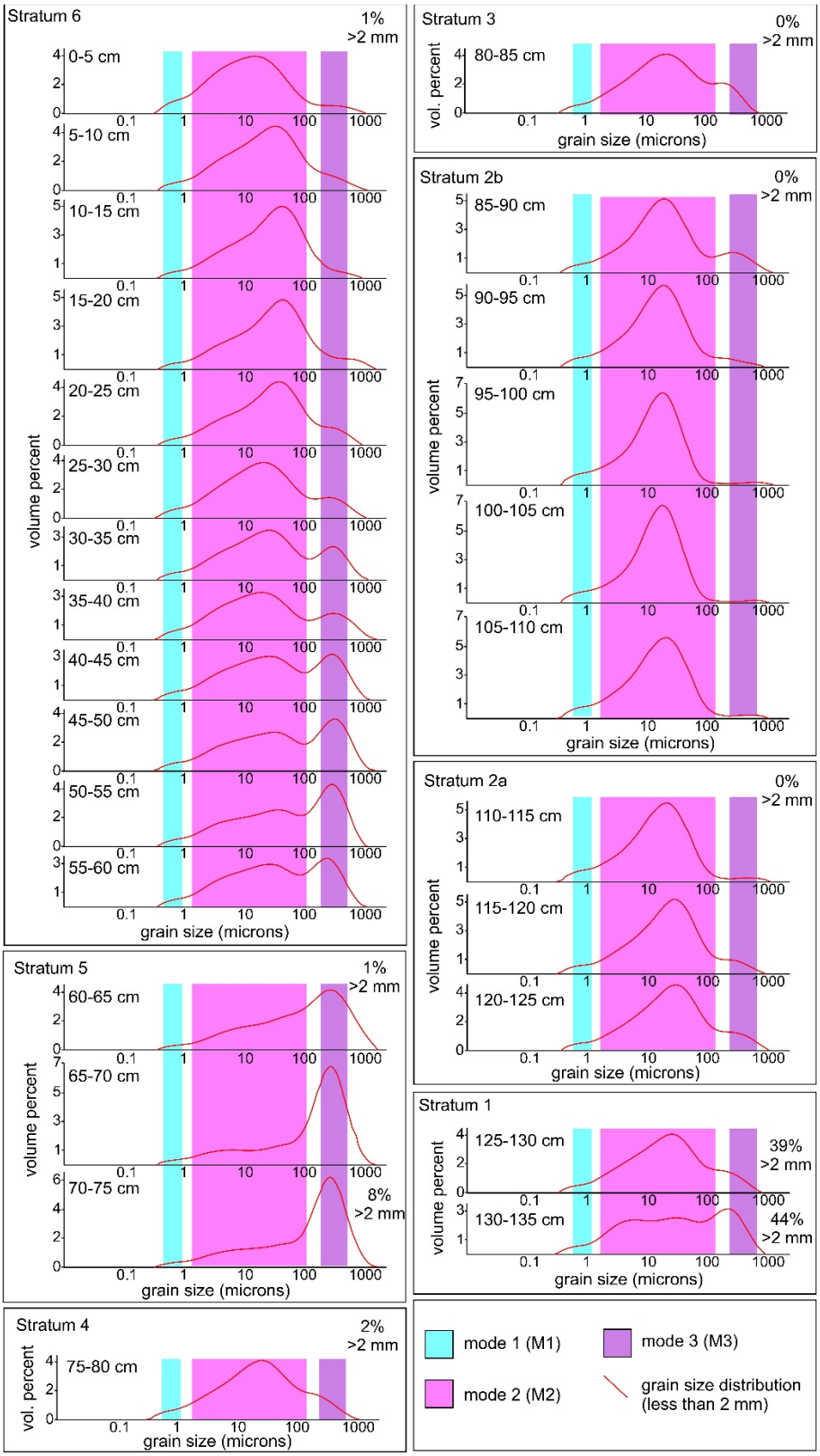

Figure 4.10: Particle size distribution of samples from Owl Ridge.

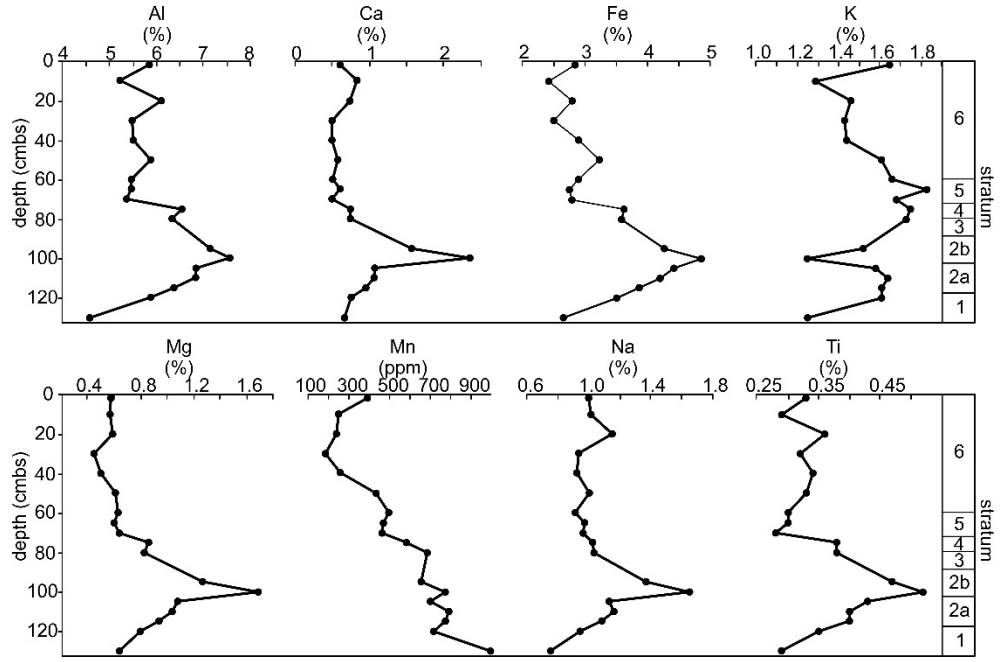

Figure 4.11: Major element concentrations in weight percent from Owl Ridge samples, plotted vs. depth.

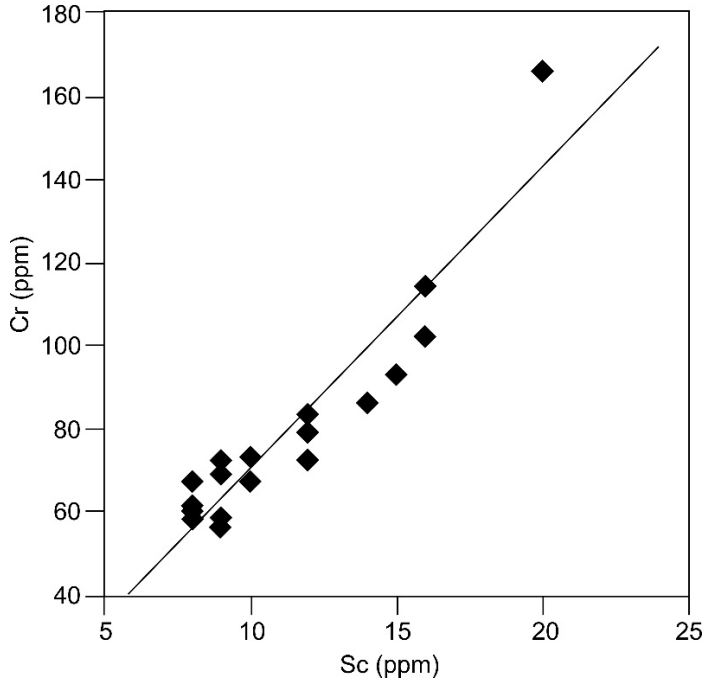

Figure 4.12: Ratio of Cr to Sc in Owl Ridge samples.

Organic Geochemistry Depth trends of organic carbon and nitrogen concentrations are generally consistent with modern soil profiles, with higher values near the top and lower near the bottom. The average abundance of organic carbon is 1.72%, with a range between 0.07% at the base and 7.99% in the O-horizon, and nitrogen averages 0.09%, with a range between 0.01% and 0.35% (Fig. 4.13). The mean carbon/nitrogen (C/N) ratio is 16.10 but can be as low as 7 or as high as 32.86. Generally, C/N is high at the top of the profile, decreasing abruptly by an order of magnitude around 60 cm depth (at the stratum 5/6 boundary) and remaining low for the bottom half of the profile (Fig. 4.14). The carbon isotopic ratio of organic matter in the soil varies by 3‰, decreasing from -23.39‰ at the base to -26.38‰ at the top (Fig. 4.13).

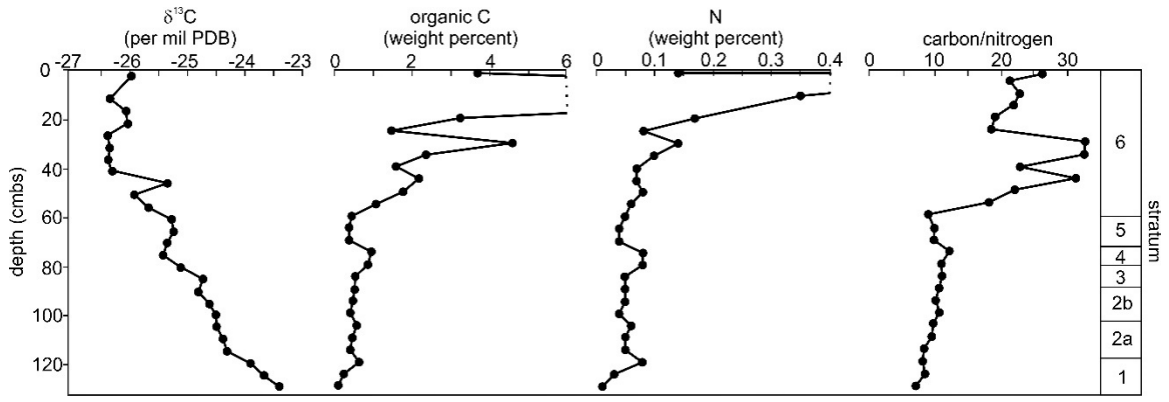

Figure 4.13: Organic geochemistry of Owl Ridge samples.

Discussion

Depositional History

The classic interpretation of the strata at Owl Ridge suggests that the entire sediment package is the result of aeolian deposition that began sometime during the late glacial period and which has extended to recent times, with a significant unconformity or

"overland erosion event" occurring early in the Holocene (Phippen, 1988: 101) leading to partial erosion of sediment from strata 3 and 4 and subsequent bluff-edge dunal accumulation of stratum 5. However, renewed research at the site suggests that the processes delivering sediment to the site were more nuanced than previously thought and that deposition at Owl Ridge is the result of both colluvial and aeolian processes. Grain-size distributions, as well as field- and thin section-scale depositional fabrics support this assertion.

Samples with polymodal grain size distributions, such as those from Owl Ridge, are the result of the mixing of sediment from different depositional mechanisms, or end members. Different depositional processes produce unique modal grain size distributions in the sediment they deposit (Harding, 1949; Folk and Ward, 1957; Middleton, 1976; Ashley, 1978; Bagnold and Barndorff-Nielsen, 1980). In some cases, such as in aeolian depositional settings, these end members are unimodal, but in others, such as fluvial systems where multiple sediment sources are coming together and fluid dynamics are more complex, polymodal end members may exist (Weltje and Prins, 2003).

To properly interpret the grain size distribution of the samples from Owl Ridge, it is important first to identify and then to determine the depositional process associated with each of the end members contributing to the sediment package. As discussed above, the Owl Ridge samples contain sediment-concentration peaks with three distinct grain size components which are present to varying degrees throughout the profile (Fig. 4.10). M1, the finest component, varies little with regard to either its modal size or its relative contribution to the profile, suggesting that it represents a single, unimodal end member. M1 is well-sorted and very fine-grained, likely representing aeolian transport over

extremely long distances, and probably indicating global dust input to the site carried from Asia by high-level westerlies (Pye and Zhou, 1989; Pye, 1995; Vandenberghe, 2013). Given the predominance of aeolian deposition in this part of Alaska (e.g. Thorson and Hamilton, 1977; Muhs and Bettis, 2003; Muhs et al., 2003; 2008; Muhs and Budahn, 2006; Graf et al., 2015; DiPietro et al. 2017), it is likely that M2, a generally well-sorted mode in the silt-to-very-fine-sand-size range, represents a regional loess signal. Indeed, the modal grain size of M2b ranges from 20-50 μm in diameter, indicating a transport as low-suspension clouds (Tsoar and Pye, 1987) travelling tens of meters from their source to the site (Vandenberghe, 2013). The modal size of M2a falls within a range very uncommon in global Quaternary loess deposits (Vandenberghe, 2013), but more common in Alaskan loess, where it has been interpreted as representing the waning stages of loess deposition, or decreasing wind velocities (Muhs et al. 2003). We suggest that M2b represents loess deposition by strong regional winds and that M2a represents loess deposition by weak regional winds. The sampling interval in this study (5 cm) is quite coarse, relative to the amount of time represented by the profile in total, so each sample is time averaged, recording conditions at the site over a period of time, rather than at a particular instant. Because of this, both strong and weak winds are often recorded in the same sample. Where M2a and M2b are quite distinct from one another, such as in the lower two samples from stratum 6, there was a greater difference between velocities of strong and weak winds likely with a more abrupt change from one size class or sub-mode to the other, whereas in samples where M2a and M2b are closer in size, wind velocities were more similar throughout the interval of deposition, or changed more gradually. M3, where present without significant quantities of silt and with high abundances of gravel,

such as in stratum 5, is likely colluvial in origin, whereas when present with M2, M3 is perhaps aeolian in origin (e.g., several samples from strata 2, 3, 4, 6), representing even stronger episodic wind storms capable of entraining and depositing sand originating from the exposed south-facing terrace riser immediately below the site. Episodic aeolian sand deposition has been well-documented in central Alaska (Thorson and Bender, 1985; Bigelow et al., 1990; DiPietro et al., 2017; Graf et al. 2017).

In addition to understanding the depositional mechanism associated with each grain size mode (or set of modes) at Owl Ridge, it is important to consider the source of each mode as well to fully understand how the sediment package was deposited. The Cr/Sc ratio of each of the samples plots along a linear trendline (Fig. 4.12), indicating that all samples are part of the same compositional mode, suggesting they may have a similar source area. However, textural data and sedimentary structures observed in the field and in thin section indicate that the sediments at the site are almost certainly of both colluvial and aeolian origin. The consistency in the Cr/Sc ratio of these sediments despite this difference in depositional mechanism suggests that the colluvium and loess are both derived from the same ultimate source, likely from the regionally extensive Healy glacial outwash and Nenana Gravels alluvial deposits forming the base units through which First and Second Creeks and the Teklanika River have incised (Péwé et al., 1966).

Once the depositional mechanisms associated with each of the grain size modes has been established, reconstructing the depositional history of the sediment profile is less complicated. The lowermost sample from stratum 1 is a sample of the glacio-fluvial outwash which forms the terrace upon which the site rests. The upper stratum 1 sample is primarily composed of M2, indicating the onset of aeolian deposition at the site, likely

characterized by relatively high wind velocities (Fig. 4.10). Stratum 2a is a continuation of this aeolian deposition, characterized by strong regional winds and very strong episodic high-velocity windstorm events, which were more prevalent early in the deposition of this stratum than later. The lower portions of stratum 2b are similar in nature to the upper part of stratum 2a, characterized by steady loess deposition with little interruption. Wind storms become more prevalent near the top of the unit, carrying into stratum 3. The grain size distribution of the single sample from stratum 3 seems to indicate a combination of loess deposition and the deposition of aeolian sand. However, field observations indicate that stratum 3 is a very distinct sandy unit with very little silt. This disparity indicates that the sample taken from stratum 3 probably contains stratum 3 sand as well as silty material from either stratum 2b, stratum 4, or both. Stratum 3 itself probably represents aeolian deposition by very high velocity winds, perhaps representing the local manifestation of the YD climate event. Stratum 4 denotes a return to more stable conditions, marked by loess deposition and decreased wind velocities relative to stratum 3.

Stratum 5 appears to be composed almost entirely of colluvium with varying proportions of fine silt and sand throughout. Microfabrics also suggest a colluvial origin for stratum 5 (Fig. 4.9) and monic to enaulic c/f related distribution is more indicative of an overland flow deposit (Bertran and Texier, 1999); however, the orientation of elongated coarse grains parallel to the slope of the site within this unit, as well as the silt cappings atop these grains, suggest periglacial solifluction played a role in the formation of this stratum. Gravel lenses and lags observed in the field, including several small channelized bodies of sand incised into the underlying stratum, as well as the presence of

at least three distinct sand layers within stratum 5 at the toe of slope support this latter interpretation. Additionally, there is also evidence for periglacial solifluction at work in strata 4 and 6, suggesting that the sub-horizontal grains in stratum 5 may be a post-depositional feature and that the unit itself is an overland flow deposit. The radiocarbon dates for archaeological component 2, directly underlying stratum 5, and those for component 3 in the upper 5 cm of stratum 5, overlap at 2-sigma standard deviation, indicating that deposition of this colluvium was extremely rapid. Particle size distributions for the upper 5 cm of stratum 5 change slightly to reflect an increase in finer sediment at the expense of sand when compared with the rest of stratum 5.

Sediment particle size data from stratum 6 support field observations of a gradual boundary with underlying stratum 5. Samples from the lower 30 cm of stratum 6 contain bimodal distributions with peaks in sand as well as the loess fraction with a continued decrease in sand through time as we approach the top of the sediment column so that particle size distributions for the upper 30 cm of stratum 6 mirror those from stratum 2 and stratum 4. Although the presence of M3 in these lower stratum 6 samples would seem to indicate continued colluvial input to the site during the early Holocene, the field features which supported a colluvial origin for the sand and gravel in stratum 5 are absent from these lower stratum 6 sediments. Also noteworthy in these samples is the distinctness of M2a and M2b, both of which are present and easily distinguished from one another near the base of stratum 6, rather than forming one continuous M2 distribution near the top of the stratum. Together, these observations suggest that stratum 6 is entirely aeolian in origin. The lower 30 cm or so of stratum 6 represent a period during which wind velocities varied considerably, sometimes carrying fine silt, other

times fine sand, and other times medium-to-coarse sand. The distinctiveness of sub-modes 2a and 2b indicate that wind velocities shifted rapidly during this interval. This portion of the profile may correspond to the HTM, which has been identified at the nearby Dry Creek site in the Nenana Valley as a period of highly variable wind velocities (DiPietro et al., 2017), perhaps correlating to variable temperatures in the region throughout the HTM (Kaufman et al., 2016). Coming out of this variable interval, very strong winds carrying medium-to-coarse sand diminish in frequency. Fine sand deposition, indicating moderate velocity regional winds, dominates during the deposition of the middle portion of stratum 6, and a shift towards silt deposition towards the surface indicates weakening wind velocities in recent times.

Soil Development and Disturbance

As the presence of at least three field-identified buried soil horizons in just under 1.5 m of sediment suggests, pedogenesis at Owl Ridge was a complex process. The micromorphological data, as well as the geochemical analyses performed as part of this study provide new insights into the pedogenic processes which have contributed to the formation of these buried soils.

The oldest buried soil horizon at Owl Ridge occurs at the stratum 2a/2b interface. This is the only buried soil at the site that was not identified in field, likely because it has a very weakly-developed A horizon. It is characterized by humification, as evidenced by a slight increase in the weight percent organic carbon at this horizon (Fig. 4.13) and as observed in thin section (Fig. 4.3, 4.4, 4.8a). In contrast to this weakly developed paleosol, a second paleosol in the uppermost portions of stratum 2b is much more easily distinguished both in the field and from the data collected for this paper. The stratum 2b

paleosol is somewhat similar in nature to the 2a paleosol, but better-developed. Robust banded microfabric is present (Fig. 4.3, 4.4), as are well-developed Fe-oxide nodules and concentrations (Fig. 4.8b). Neither stratum 2 paleosol appears to be significantly overprinted, save for in the most distal portions of the site, where a second generation of cryogenic activity appears to have occurred at some point later in the development of the soil profile (discussed above, Fig. 4.2).

The next stratigraphic interval that has clear evidence of pedogenic processes is stratum 4, where Phippen (1988) described a series of thin, dark organic bands and Gore and Graf (2018) described a buried A/B horizon. Both organic carbon and nitrogen increase in abundance in this interval (Fig. 4.13), supporting the interpretation that these dark bands are organic in nature. Micromorphological data collected for this study can help reconcile the disparity between the thin organic layers described by Phippen and the more prominent paleosol described during the 2007-2010 excavations. Rather than being the result of a single interval of pedogenesis, the stratum 4 ‘paleosol’ represents a buried A horizon dating to the time during which stratum 4 itself formed, and the thinner, darker organic bands, clearly evident in thin section but to a lesser degree in outcrop, represent spodic overprinting from above. Fe-oxide nodules are present in the buried A horizon, as well as moderately developed banded fabric. This horizon likely represents a stable surface that formed during the deposition of stratum 4, an assertion supported by the preponderance of both component 2 lithics and anthropogenic charcoal found in association with the paleosol during excavation (Graf et al., 2010; Gore and Graf, 2018).

The final soil complex at Owl Ridge is found in stratum 6. Several paired reddish-brown over light grey intervals are noted within stratum 6. Phippen (1988) interprets

these as distinct horizons, but they are often discontinuous and individual couplets cannot be traced for long distances across the site. Though they may not be distinct spodic horizons, these zones do indicate spodic processes acting on the soil as stratum 6 material was deposited during the late Holocene. The spodic material found coating grains in stratum 4 and, to a lesser degree, 5 and 3 results from this part of the profile. Monomorphic spodic material eluviated from the upper part of stratum 6 has been translocated downwards in the profile (Fig. 4.8) and accumulated at depth, predominantly in the buried A horizon in stratum 4. Spodic material may have accumulated at this depth as a result of small textural changes associated with the buried A horizon, a process documented in other spodosols (Schaefer et al., 2002). Spodic processes and cryogenic processes have alternated within this stratum 6 buried soil complex over time. Many of the silt cappings observed in stratum 4 alternate with layers of monomorphic spodic material (Fig. 4.6e), and these interlayered cappings have themselves been rotated in many instances (Fig. 6e, 8e).

Three of the four soils identified in this study were identifiable in the field and the fourth was identified from geochemical and micromorphological data. Even a cursory look at these paleosols within the profile in person or in photograph makes it equally evident that the profile at Owl Ridge has undergone significant alterations since it formed, particularly near the bluff edge. Broken, irregular, and folded contacts between units are common (Fig. 4.3, 4.4), particularly in the portions of the profile dating to the latest Pleistocene and earliest Holocene, and nearest to the bluff edge. These features, coupled with micromorphological evidence presented above (elongated clasts oriented parallel to slope, granular microfabrics, rotated grains, and extensive silt cappings)

suggest that solifluction has played a significant role in the formation of the profile (Van Vliet-Lanoe, 1985; Bertran, 1993; Bertran and Texier, 1995; 1999). Across the top of the bluff, the lowermost strata appear to show little evidence for solifluction. The contact between strata 2a and 2b is relatively flat, and the lower silts retain approximately the same thickness across the area of excavation. Strata 3, 4, 5, and the lower portions of stratum 6, however, have wavy to irregular contacts and occasionally fold over themselves as they approach the edge of the bluff, clearly indicating that solifluction affected the profile beginning sometime during the middle to late Holocene. It is worth noting, however, that solifluction processes appear to have affected all depositional units nearest the bluff edge. As described above, periglacial solifluction features and fabrics are significantly better developed towards the edge of the bluff and are present at all depths (Fig. 4.7). This is likely a result of the fact that the bluff itself is triangular (Fig. 4.1), providing three separate directions in which down-slope stresses may be released and allowing the sediment nearest to the edge of the bluff to creep at a faster rate than further up-slope, towards the center of the site. The degree of deformation here at the bluff edge is thus not indicative of the degree to which the rest of the site has been deformed.

The presence of cryogenic and periglacial solifluction features in soils containing archaeological materials can be cause for concern when it comes to interpreting the spatial and stratigraphic distribution of artifacts. To understand the degree to which the position of artifacts in the profile during excavation can be trusted, it is crucial to assess the extent to which solifluction and cryoturbation have disturbed the soil. Although there are well-developed cryogenic features at Owl Ridge, they are not features which indicate

extensive vertical translocation of artifacts within the profile. Wholesale involutions of soil material are absent from the site, as is evidence for frost cracks, such as silt-, sand-, or ice wedge casts. Horizontal ice lensing or frost jacking may have re-oriented artifacts to some degree, but these micro-processes have not caused mixing between the archaeological components. It is also worth noting that the illuviation processes responsible for translocating spodic materials down profile are incapable of moving material the size of lithic artifacts or anything else larger than a few microns in size. The monomorphic spodic material is transported colloidally in soil water and in no way indicates a threat to the stratigraphic integrity of the archaeological materials at the site. All three components are well-separated, and artifacts are likely within a few vertical centimeters of their original location.

Paleoclimate Reconstruction and the Archaeological Record

The presence of multiple paleosols and co-occurrence of two dominant modes of deposition make the sediment profile at Owl Ridge a rich record of paleoclimate and paleoenvironmental data for the late Quaternary. However, the relative thinness of the profile coupled with the rapid climatic shifts that likely occurred during the time the site formed mean that compound pedogenesis has taken place; soil forming features corresponding to different pedogenic processes occurring at different times and under different climatic conditions have become superimposed on one another, particularly in the deeper portions of the soil profile. It is necessary, therefore, to determine which features and fabrics occurred contemporaneously with deposition, formed post-depositionally because of subaerial exposure, and resulted from overprinting by later pedogenic processes following burial. Sedimentary structures, such as the gravel lenses

and lags in stratum 5, are depositional features. Many of the fabrics observed in the paleosols, including cryogenic banded fabrics, are primary pedogenic features, occurring when the paleosol was at the surface. Fe-oxide nodules are also primary pedofeatures, as are the formation of A and E horizons and accompanying features, such as the accumulation of soil organic matter and etching and pitting of mineral grains by organic acids. Some cryogenic features (e.g. silt cappings and frost-jacked grains) and redox features (e.g. matrix accumulations and hypocoatings) may fall into this category, but can also form post-burial, so care must be taken when interpreting the climatic significance of such features. Finally, illuvial features like podzolization and the translocation of spodic material downwards in the profile are post-burial features, present in some strata but associated with soil horizons forming long after those strata were buried. In many instances, the cross-cutting relationships observed between pedofeatures and fabrics can be used to create a relative chronology of climatic changes throughout the development of the soil profile.

Broadly speaking, we suggest that the alternation between cryogenic and spodic features represents alternation between cooler and warmer climatic conditions, and the alternation between aeolian and colluvial deposition represents alternation between times of decreased and increased effective precipitation, respectively. The earliest post-glacial record at Owl Ridge is contained within the lowermost loess units at the site (stratum 2). These units certainly postdate the Healy glaciation, which formed the underlying outwash sediment, but likely began accumulating sometime during the late glacial, probably during the Bølling-Allerød interval (14.7-12.7 ka). Archaeological component 1 in the paleosol at the top of stratum 2b dates to 13.3-13 ka (Graf et al. 2010b; Gore and Graf

2018), indicating the deposition of stratum 2b certainly occurred within the Allerød chronozone in the latest Pleistocene. The paleosol is characterized by well-developed banded fabric, indicating that ice-lensing took place during its formation. Ice lensing certainly indicates below-freezing temperatures during the winter months but does not necessitate the presence of permafrost during this interval. In fact, the absence of other cryogenic features, such as frost-jacking or silt cappings, suggests that winter conditions during this time may not have been as cold at Owl Ridge as they may have been at other times since the LGM. Ice lensing cannot occur without sufficient pore water (Van Vliet-Lanoë, 2010), meaning that effective moisture was perhaps higher during the formation of the stratum 2b paleosol than it was during the deposition of stratum 2. The presence of Fe-oxide nodules in the paleosol also suggests there were ice-free periods when the soil became well-drained during its formation. Well-drained, ice-free periods would have alternated seasonally with poorly-drained, frozen periods, resulting in the formation of a complex pattern of banded cryo-fabrics and Fe-oxide nodules over time (Vepraskas, 2001). Rising temperatures at Owl Ridge during this time would have created conditions ripe for establishment of a shrubby, non-acidic vegetative community, stable ground surface, and suitable place for humans to camp. Although there are few published radiocarbon dates to confirm this, it is possible that the stratum 2a and 2b paleosol couplet does represent the Bølling (13.9-13.6 ka) and Allerød (13.6-13 ka) warm intervals, respectively (Wygal and Heidenreich, 2014; Wygal, 2018). If this were the case, the increased development seen in the stratum 2b paleosol compared to the 2a paleosol would suggest that Allerød conditions were warmer and likely wetter than those during the Bølling; however, the couplet may simply represent early and late Allerød

with milder conditions during the latter half of the Allerød interval at this location in central Alaska. Without dates on stratum 2a we cannot be certain which scenario fits best. This may explain why humans initially use Owl Ridge site several hundred years after they initially spread into the region (Graf et al. 2015, 2017). Though this environment would have been harsh, it would also have been reasonably productive, as the prevalence of hunting tools in component 1 (Gore and Graf, 2018) suggest animal populations were present in the area. Although the two paleosols indicate two intervals of climate amelioration during the late glacial period, the dominance of aeolian deposition here signals conditions still relatively cool and dry between these periods of stability, allowing for the accumulation of loess in stratum 2.

Radiocarbon chronology suggests that stratum 3, the first post-glacial sand unit at Owl Ridge, and stratum 4 were deposited during the YD chronozone (Phippen, 1988; Graf et al., 2010; Gore and Graf, 2018). The character of the YD climate reversal in central Alaska has long been debated (Kokorowski et al., 2008). Although there are clear records of cooling and aridity in the Northern Pacific and southern Alaska, central Alaskan records tend to be more variable and more ambiguous, some showing moderate cooling, others warming, and still others little change in climatic conditions at all within the time interval between about 12.8-11.7 ka (Kokorowski et al., 2008). The presence of two texturally and pedogenically distinct units within this time at Owl Ridge highlights the heterogeneity of how the YD is expressed in central Alaska. In section 5.1, we interpret the stratum 3 sand as aeolian in origin, rather than colluvial. The presence of relatively coarse aeolian sand atop the bluff indicates a time interval of stronger than average, or at least stronger than modern, winds early in the YD chronozone. The contact

between stratum 3 and stratum 4 is gradual, suggesting that these strong winds gradually weakened and loess deposition resumed by about 12.5 ka. Pockets of sand within the stratum 4 loess may indicate episodic recurrences of high-velocity winds. The decrease in the abundance of M3 into stratum 4 indicates overall weaker winds late in the YD chronozone. This pattern of weaker winds culminates in the stratum 4 paleosol, which can be dated between 12.5 and 11.3 ka based upon the presence of archaeological component 2 and lots of *Salix* wood charcoal, representing yet another period of landscape stability, warmer temperatures, and increased moisture availability relative to stratum 3 conditions. The thickness of the stratum 4 paleosol indicates that conditions during its formation were perhaps warmer and more moderate than during any other time up until this point. The stratum 4 paleosol may also represent a landscape that was more stable for a longer period than the stratum 2 paleosols, perhaps playing a role in the more intensive use of the site by the component 2 occupants (Gore and Graf, 2018). Banded fabric is present in the paleosol, however, suggesting that at least seasonal ice lensing occurred during the YD and that winter temperatures were still cold enough to allow for seasonal freeze-thaw cycles.

Stratum 5 represents the only major colluvial input at Owl Ridge and, therefore, a marked shift in deposition at the site. It is also likely the first unit at the site deposited during the Holocene, probably around 11.3-11.1 ka, just prior to the earliest stages of the Holocene Thermal Maximum (HTM) (Kaufman et al., 2004; 2016) as it is expressed in central Alaska (Gore and Graf, 2018). Since stratum 5 was deposited via overland flow, two immediate assertions may be made: first, that the sediment upslope of the site which served as the source material for stratum 5 was ice-free and able to be easily eroded, and

second that there was sufficient precipitation during this time to produce a 15-20 cm thick deposit virtually instantaneously. These assertions suggest significantly wetter, possibly warmer conditions than occurred previously at the site.

It is perhaps these warmer, wetter conditions that are responsible for the decrease in the sediment accumulation rate during the transition between strata 5 and 6. Loess in central Alaska is often sourced from the numerous braided river complexes flowing out of the Alaska Range, particularly during the late summer when there is less meltwater flowing in the rivers and large areas of the braid plain are exposed (Muhs et al., 2003). Warmer spring and summer temperatures early in the Holocene would have led to more meltwater that may have persisted later in the year, decreasing the amount of sediment available for aeolian deflation and subsequent deposition as loess. This transitional period is characterized by winds of variable strength. Modelling studies suggest that there can be a lag of as much as a few hundred years in the response of vegetation to rapid warming (Rupp et al., 2000), meaning that, despite the warmer temperatures, shrub tundra vegetation could have persisted at the surface for a time. During this time the underlying sediments would have been exposed to warmer temperatures with little protection from surface vegetation, leading to degradation of soil organic matter, C/N ratio of which decreased by an order of magnitude below the stratum 5/6 interface as decomposition occurred (Fig. 4.13).

Eventually, however, warmer spring and summer temperatures also would have brought with them the first post-glacial forests in the region, initially deciduous hardwood trees like cottonwoods (Anderson and Brubaker, 1994; Anderson et al., 1994; Abbott et al., 2000; Bigelow and Edwards, 2001; Bigelow and Powers, 2001; Lloyd et al.,

2006), which could have tolerated the cooler-than-modern winters which some climate models indicate during this time (Viau et al., 2008) and later, once HTM warming had reached a maximum around 9-10 ka, spruce forests. Spruce is a highly effective loess trap (Muhs et al., 2003). This tree cover, coupled with eventual post-HTM cooling, led to enhanced aeolian deposition at Owl Ridge as stratum 6 began to accumulate more rapidly.

Relatively modern conditions in terms of vegetation, climate, and depositional processes were established by approximately 3-6 ka. Stratum 6 is marked by the alternation of spodic and cryogenic processes throughout its deposition, as indicated by alternating cycles of podzolization and aeolian deposition. Episodes of loess deposition probably indicate cooler, drier periods and correspond to silt capping and cryogenic features in stratum 6. Episodes of podzolization represent warmer, wetter periods during which pedogenesis acted upon the newly-deposited loess and monomorphic spodic material accumulated at depth in strata 4 and 3. The accumulation of Fe, Al, Ca, Na, Ti, and Mg at the stratum 2a/2b interface where the modern permafrost table exists suggests that this is a likely process. This is noteworthy, especially the co-variance of Fe and Ti, suggesting that, under these cool, acidic soil conditions, Ti may not be an immobile element (Land and Öhlander, 2000). Absence of spodic material in stratum 2a coupled with the presence of Fe-oxide hypocoatings on ped boundaries post-dating spodic material in stratum 2b (Fig. 4.8g) and indicate redox changes associated with annual active zone freeze-thaw processes. These conditions coupled with the absence of spodic material in lower stratum 2a suggest the permafrost table did not drop to its modern location until quite recently, perhaps because of increased global temperatures in the past

few decades. The rotation of grains in stratum 4 which have both silt cappings and monomorphic spodic coatings (Fig. 4.6e) indicates that the solifluction affecting the lower strata is also relatively recent feature.

The Pleistocene-Holocene Transition

The record of the transition from the latest Pleistocene to Holocene at Owl Ridge is a robust one, showing profound changes in sediment deposition and pedogenesis probably related to rapidly shifting central Alaskan paleoclimatic conditions across this boundary. The latest Pleistocene deposits at Owl Ridge are characterized by aeolian deposition and cryogenic paleosols, indicating relatively cool, dry conditions, albeit with short periods of landscape stability during which the site was occupied by humans. Paleosols are weakly developed and lack distinguishing features, save for banded fabrics which indicate that the primary pedogenic mechanism was ice lensing, indicating seasonal freeze-thaw processes, and Fe-oxide nodules, indicating the seasonal presence of freely draining liquid water. Conditions do appear to have warmed gradually over the course of the latest Pleistocene, as paleosol development increases up-profile, reaching a maximum (for non-spodic paleosols) in stratum 4, near the end of the YD chronozone, following a period of quiescence after intense winds of the early YD. This gradual warming was also likely accompanied by a shift away from herb/shrub tundra vegetation, which probably existed following the Last Glacial Maximum, towards open parkland vegetation which would have more intensively weathered the loess and helped to create a thicker, more robust paleosol. The gradual shift of the $\delta^{13}C_{SOM}$ towards more negative values up profile (Fig. 13) reflects this progressive transition to a more closed vegetation

system, though this trend may simply indicate increased soil organic matter decomposition with depth.

Whereas the Pleistocene at Owl Ridge is marked by gradual climate amelioration, the Holocene is a dynamic record of rapidly shifting climate. The early Holocene is heralded at Owl Ridge by a thick package of rapidly-deposited colluvium, signaling a major, though short-lived shift in the style of deposition at the site resulting from a rapid increase in effective precipitation as well as the end of open tundra conditions that made the site so attractive to its late Pleistocene human visitors. Early Holocene deposits at Owl Ridge are compressed, marked by a transition from colluvial back to loess deposition and decreased sedimentation rates, again perhaps related to increased moisture availability. Trees (first deciduous hardwoods and later spruce) colonized the site beginning during the HTM, perhaps the warmest time period in evidence at the site. Following this warm period, cooler temperatures brought with them renewed loess deposition which continues at the site until today. The middle to late Holocene deposits indicate a climate that alternates between cool/dry and warm/moist conditions, bringing with it a slight increase in sedimentation and subsequent podzolization under moist, acidic spruce forests. Owl Ridge thus tells the story of a climatic shift at the Pleistocene-Holocene boundary, which would have necessitated that all species, human and otherwise, inhabiting the area adapt rapidly or migrate to survive.

CHAPTER FIVE

Conclusions

The work recorded in this dissertation demonstrated the utility of employing high-resolution and multi-proxy approaches to terrestrial paleoclimate problems, especially in settings where pedogenesis is limited. Many Alaskan soil profiles are similar to those documented in this work: relatively thin and dominated by overprinting. Despite the complexity of these soil profiles, this study has shown that gathering paleoclimate data from these settings is still possible with careful, detailed work. In settings, such as at the Dry Creek site, where pedogenesis is severely limited and pedofeatures are lacking, high-resolution sedimentological studies may provide new insights into climatic processes instead.

The late glacial period in eastern Beringia was a time marked by cold temperatures, and low mean annual precipitation. In the Nenana River Valley, katabatic winds played an important role in sediment deposition and across central Alaska, low effective moisture inhibited both soil development and the formation of cryogenic features related to ice lensing. On the Seward Peninsula, however, where full glacial conditions may have been colder and loess deposition was less prevalent, deglaciation led to an instability in sediment along slopes, resulting in colluvial deposition. Owl Ridge records periods of climate stability and slightly warmer temperatures within this interval, perhaps corresponding to the Bolling-Allerød, but these conditions were short-lived and still relatively dry. The Younger Dryas, often considered to be cold and dry, appears to

Table 5.1: Summary of climatic, paleoenvironment, and pedogenic conditions at the three study localitites during the latest Quaternary

Climate Event	Nenana River Valley	Teklanika River Valley	Seward Peninsula
Late Glacial	Cold, dry, strong northerly winds, frequent and intense katabatic-type winds	Cool, moderately dry, aeolian deposition dominates	Cold, dry, little deposition, high permafrost table
Allerod	Low regional wind intensities, warm, dry	Warmer intervals resulting in paleosol development, human occupation	Slight warming, onset of colluvial deposition
Younger Dryas	Intermittent katabatic winds with decreasing northerly wind velocities culminating in weak paleosol formation	Strong winds at onset, decreasing in intensity and culminating in paleosol development	Cool, dry, dominated by loess deposition
Holocene Thermal Maximum	Variable wind intensities and intermittent weak paleosol development	Very wet at onset of chronozone, intermittent periods of intense winds	Warm, wet, freely drained soils, migration of deciduous hardwood trees northward
Neoglacials	Episodically strong northerly winds, intermittent katabatic-type winds alternating with weak paleosol development t	Alternating cool/dry and warm/wet conditions and resulting cryogenic and spodic soil development	Cool, wet, replacement of trees by moist acidic tundra, formation of spodic paleosols
Recent	Increase in depositional rate and wind velocity	Recent warming, permafrost degradation	Cool, dry, cryogenic features dominate soils

have been neither in significant measures, at least in central Alaska. Though katabatic-type winds may have occurred in the Nenana Valley during this time, regional wind intensities were relatively low. Owl Ridge also records strong winds in the early part of the YD chronozone, but warm, relatively mesic conditions later on. On the Seward Peninsula, the YD was marked by an increase in aeolian deposition, suggesting cool, dry conditions, though cryogenic features are generally absent from this time as well. The Holocene Thermal Maximum was a time of variability and vegetation change in both regions. Warm temperatures allowed for the northward migration of forests (initially deciduous, then coniferous) in both central Alaska and on the Seward Peninsula, and the first appearance of spruce and acidic spodosols. The Holocene is marked by relatively warm, moist conditions punctuated by short-term glacial readvances, evidenced by cryogenic features in the soil at Serpentine Hot Springs, intermittent katabatic-type winds in the Nenana Valley, and alternating spodic and cryogenic processes at Owl Ridge in the Teklanika Valley. Relatively modern conditions appear to have been established by the middle to late Holocene in both regions.

APPENDICES

APPENDIX A

Particle size distributions of samples from the Dry Creek site

Sam #	Depth	Age (BP)	12 f	11.75f	11.5f	11.25f	11f	10.75f	10.5f
57	22	418	0	0	0	0	0.1	0.12	0.13
56	24.5	1023	0	0	0	0	0.1	0.12	0.14
55	27	1607	0	0	0	0	0.02	0.18	0.2
54	29.5	2168	0	0	0	0	0.02	0.18	0.2
53	32	2709	0	0	0	0	0.02	0.15	0.18
52	34.5	3229	0	0	0	0	0.09	0.19	0.2
51	37	3728	0	0	0	0	0.1	0.22	0.24
50	39.5	4208	0	0	0	0	0.09	0.19	0.21
49	42	4669	0	0	0	0	0.02	0.17	0.19
48	44.5	5112	0	0	0	0	0.09	0.18	0.2
47	47	5536	0	0	0	0	0.02	0.16	0.18
46	49.5	5943	0	0	0	0	0.01	0.14	0.16
45	52	6333	0	0	0	0	0.01	0.14	0.16
44	54.5	6707	0	0	0	0	0.02	0.16	0.18
43	57	7065	0	0	0	0	0.02	0.15	0.18
42	59.5	7407	0	0	0	0	0.02	0.17	0.19
41	62	7735	0	0	0	0	0.02	0.16	0.18
40	64.5	8049	0	0	0	0	0.02	0.15	0.18
39	67	8349	0	0	0	0	0.01	0.13	0.16
38	69.5	8635	0	0	0	0	0.02	0.15	0.17
37	72	8910	0	0	0	0	0.02	0.16	0.18
36	74.5	9172	0	0	0	0	0.01	0.13	0.16
35	77	9422	0	0	0	0	0.02	0.17	0.19
34	79.5	9662	0	0	0	0	0.02	0.16	0.18
33	82	9891	0	0	0	0	0.02	0.16	0.18
32	84.5	10110	0	0	0	0	0.02	0.15	0.18
31	87	10319	0	0	0	0	0.01	0.12	0.15
30	89.5	10520	0	0	0	0	0.02	0.16	0.19
29	92	10712	0	0	0	0	0.1	0.2	0.22
28	94.5	10897	0	0	0	0	0.02	0.15	0.18

Particle size distributions of samples from the Dry Creek site (cont.)

Sam #	Depth	Age (BP)	10.25f	10f	9.75f	9.5f	9.25f	9f	8.75f
57	22	418	0.13	0.23	0.2	0.18	0.18	0.38	0.3
56	24.5	1023	0.13	0.23	0.2	0.18	0.18	0.39	0.32
55	27	1607	0.2	0.35	0.3	0.28	0.28	0.59	0.48
54	29.5	2168	0.19	0.35	0.3	0.28	0.28	0.59	0.47
53	32	2709	0.17	0.31	0.27	0.25	0.25	0.54	0.44
52	34.5	3229	0.2	0.35	0.3	0.28	0.27	0.57	0.45
51	37	3728	0.23	0.41	0.35	0.33	0.33	0.7	0.57
50	39.5	4208	0.2	0.35	0.3	0.28	0.28	0.6	0.48
49	42	4669	0.18	0.32	0.27	0.25	0.25	0.52	0.41
48	44.5	5112	0.19	0.34	0.29	0.26	0.26	0.55	0.44
47	47	5536	0.17	0.3	0.25	0.24	0.23	0.49	0.39
46	49.5	5943	0.15	0.27	0.23	0.21	0.21	0.43	0.34
45	52	6333	0.15	0.27	0.22	0.2	0.2	0.43	0.34
44	54.5	6707	0.17	0.3	0.25	0.23	0.23	0.48	0.39
43	57	7065	0.17	0.3	0.25	0.23	0.23	0.48	0.39
42	59.5	7407	0.18	0.31	0.26	0.23	0.23	0.49	0.39
41	62	7735	0.17	0.3	0.25	0.23	0.23	0.49	0.4
40	64.5	8049	0.17	0.3	0.26	0.24	0.23	0.5	0.4
39	67	8349	0.15	0.27	0.23	0.21	0.21	0.45	0.38
38	69.5	8635	0.17	0.29	0.25	0.23	0.23	0.48	0.4
37	72	8910	0.18	0.3	0.25	0.23	0.23	0.49	0.4
36	74.5	9172	0.15	0.27	0.23	0.21	0.21	0.44	0.36
35	77	9422	0.18	0.32	0.27	0.25	0.25	0.54	0.44
34	79.5	9662	0.17	0.3	0.26	0.24	0.24	0.51	0.41
33	82	9891	0.17	0.3	0.25	0.23	0.23	0.49	0.4
32	84.5	10110	0.17	0.3	0.26	0.24	0.24	0.51	0.42
31	87	10319	0.14	0.25	0.21	0.2	0.2	0.43	0.35
30	89.5	10520	0.18	0.31	0.26	0.24	0.24	0.52	0.42
29	92	10712	0.21	0.36	0.3	0.28	0.27	0.57	0.45
28	94.5	10897	0.17	0.3	0.26	0.24	0.23	0.49	0.39

Particle size distributions of samples from the Dry Creek site (cont.)

Sam #	Depth	Age (BP)	8.5□	8.25□	8□	7.75□	7.5□	7.25□	7□
57	22	418	0.53	0.56	0.7	0.83	1.09	1.33	1.43
56	24.5	1023	0.56	0.6	0.76	0.92	1.22	1.52	1.67
55	27	1607	0.86	0.9	1.13	1.35	1.77	2.16	2.32
54	29.5	2168	0.84	0.88	1.09	1.31	1.71	2.1	2.25
53	32	2709	0.77	0.82	1.03	1.24	1.64	2.03	2.2
52	34.5	3229	0.79	0.82	1.01	1.2	1.57	1.91	2.05
51	37	3728	1	1.04	1.29	1.53	1.97	2.39	2.54
50	39.5	4208	0.84	0.87	1.07	1.27	1.65	2.01	2.16
49	42	4669	0.73	0.76	0.94	1.12	1.46	1.8	1.96
48	44.5	5112	0.76	0.79	0.97	1.16	1.51	1.84	1.98
47	47	5536	0.67	0.7	0.87	1.04	1.36	1.68	1.82
46	49.5	5943	0.6	0.63	0.79	0.96	1.27	1.59	1.73
45	52	6333	0.6	0.64	0.8	0.96	1.28	1.59	1.74
44	54.5	6707	0.69	0.73	0.91	1.1	1.45	1.82	1.98
43	57	7065	0.69	0.74	0.93	1.13	1.5	1.87	2.04
42	59.5	7407	0.7	0.74	0.93	1.13	1.51	1.88	2.06
41	62	7735	0.72	0.77	0.98	1.19	1.59	2	2.19
40	64.5	8049	0.72	0.77	0.98	1.19	1.6	2	2.19
39	67	8349	0.69	0.75	0.97	1.2	1.62	2.04	2.25
38	69.5	8635	0.71	0.77	0.96	1.2	1.6	2.01	2.21
37	72	8910	0.73	0.78	0.99	1.22	1.63	2.05	2.27
36	74.5	9172	0.65	0.7	0.9	1.11	1.49	1.88	2.07
35	77	9422	0.79	0.85	1.08	1.31	1.75	2.18	2.39
34	79.5	9662	0.73	0.78	0.96	1.2	1.59	1.99	2.18
33	82	9891	0.71	0.76	0.96	1.18	1.58	1.97	2.16
32	84.5	10110	0.75	0.8	1.01	1.23	1.64	2.06	2.25
31	87	10319	0.63	0.68	0.87	1.07	1.43	1.8	1.99
30	89.5	10520	0.75	0.81	1.03	1.26	1.68	2.1	2.3
29	92	10712	0.79	0.83	1.04	1.25	1.65	2.05	2.23
28	94.5	10897	0.69	0.73	0.92	1.12	1.49	1.85	2.01

Particle size distributions of samples from the Dry Creek site (cont.)

Sam #	Depth	Age (BP)	6.75□	6.5□	6.25□	6□	5.75□	5.5□	5.25□
57	22	418	1.71	1.82	2.06	2.21	2.37	2.5	2.77
56	24.5	1023	2.05	2.25	2.65	2.96	3.31	3.6	4.04
55	27	1607	2.82	3.05	3.55	3.94	4.37	4.7	5.18
54	29.5	2168	2.75	2.97	3.44	3.78	4.16	4.43	4.88
53	32	2709	2.68	2.89	3.33	3.64	3.96	4.18	4.57
52	34.5	3229	2.48	2.66	3.06	3.34	3.65	3.9	4.34
51	37	3728	3.03	3.23	3.67	3.95	4.23	4.39	4.68
50	39.5	4208	2.62	2.82	3.25	3.57	3.89	4.12	4.49
49	42	4669	2.38	2.59	3.03	3.37	3.76	4.1	4.63
48	44.5	5112	2.4	2.6	3.01	3.31	3.64	3.91	4.35
47	47	5536	2.21	2.39	2.76	3.02	3.32	3.57	4.01
46	49.5	5943	2.12	2.31	2.69	2.99	3.33	3.65	4.2
45	52	6333	2.14	2.34	2.74	3.04	3.4	3.72	4.25
44	54.5	6707	2.42	2.64	3.08	3.43	3.84	4.2	4.75
43	57	7065	2.51	2.75	3.22	3.59	4.01	4.35	4.9
42	59.5	7407	2.53	2.76	3.24	3.61	4.04	4.42	5.01
41	62	7735	2.7	2.95	3.45	3.83	4.25	4.58	5.09
40	64.5	8049	2.7	2.95	3.45	3.83	4.25	4.63	5.19
39	67	8349	2.79	3.07	3.63	4.07	4.57	4.99	5.59
38	69.5	8635	2.74	3.03	3.61	4.09	4.63	5.1	5.74
37	72	8910	2.82	3.13	3.73	4.22	4.75	5.18	5.76
36	74.5	9172	2.57	2.85	3.39	3.83	4.35	4.79	5.44
35	77	9422	2.94	3.23	3.81	4.25	4.73	5.08	5.57
34	79.5	9662	2.67	2.89	3.34	3.65	3.97	4.21	4.63
33	82	9891	2.65	2.89	3.38	3.76	4.19	4.56	5.14
32	84.5	10110	2.78	3.05	3.58	3.98	4.41	4.71	5.17
31	87	10319	2.46	2.71	3.21	3.62	4.09	4.5	5.11
30	89.5	10520	2.83	3.1	3.63	4.05	4.52	4.9	5.45
29	92	10712	2.73	2.99	3.52	3.95	4.42	4.8	5.35
28	94.5	10897	2.47	2.7	3.18	3.59	4.09	4.55	5.23

Particle size distributions of samples from the Dry Creek site (cont.)

Sam #	Depth	Age (BP)	5□	4.75□	4.5□	4.25□	4□	3.75□	3.5□
57	22	418	2.95	3.75	4.09	4.67	5.05	5.29	5.26
56	24.5	1023	4.25	5.27	5.53	6.05	6.28	6.32	6.05
55	27	1607	5.3	6.31	6.29	6.48	6.32	5.95	5.3
54	29.5	2168	5.04	6.11	6.25	6.67	6.73	6.56	6.06
53	32	2709	4.69	5.69	5.85	6.3	6.44	6.37	5.98
52	34.5	3229	4.55	5.63	5.91	6.44	6.66	6.64	6.27
51	37	3728	4.7	5.55	5.58	5.85	5.88	5.71	5.29
50	39.5	4208	4.61	5.58	5.74	6.19	6.37	6.36	6.04
49	42	4669	4.92	6.15	6.5	7.11	7.34	7.29	6.82
48	44.5	5112	4.56	5.64	5.93	6.48	6.71	6.72	6.38
47	47	5536	4.28	5.44	5.9	6.66	7.12	7.34	7.15
46	49.5	5943	4.58	5.92	6.47	7.3	7.75	7.88	7.53
45	52	6333	4.59	5.87	6.35	7.12	7.54	7.68	7.38
44	54.5	6707	5.06	6.31	6.61	7.16	7.31	7.19	6.68
43	57	7065	5.15	6.36	6.61	7.11	7.22	7.06	6.52
42	59.5	7407	5.31	6.61	6.9	7.42	7.49	7.24	6.56
41	62	7735	5.3	6.45	6.62	7.04	7.07	6.83	6.22
40	64.5	8049	5.46	6.72	6.93	7.36	7.35	7	6.25
39	67	8349	5.83	7.06	7.13	7.4	7.21	6.71	5.86
38	69.5	8635	5.99	7.23	7.24	7.44	7.16	6.57	5.66
37	72	8910	5.93	7.07	7.03	7.2	6.94	6.42	5.59
36	74.5	9172	5.74	7.04	7.21	7.58	7.47	7.04	6.21
35	77	9422	5.66	6.67	6.57	6.69	6.43	5.95	5.21
34	79.5	9662	4.81	5.92	6.2	6.78	7.04	7.03	6.64
33	82	9891	5.42	6.68	6.9	7.35	7.36	7.05	6.35
32	84.5	10110	5.29	6.32	6.39	6.72	6.73	6.53	6.02
31	87	10319	5.4	6.67	6.91	7.38	7.43	7.19	6.56
30	89.5	10520	5.65	6.82	6.88	7.17	7.02	6.6	5.84
29	92	10712	5.53	6.65	6.67	6.91	6.72	6.28	5.52
28	94.5	10897	5.6	6.98	7.24	7.69	7.63	7.23	6.41

Particle size distributions of samples from the Dry Creek site (cont.)

Sam #	Depth	Age (BP)	3.25□	3□	2.75□	2.5□	2.25□	2□	1.75□
57	22	418	4.9	4.35	3.69	3.01	2.47	2.12	1.95
56	24.5	1023	5.41	4.58	3.62	2.67	1.88	1.29	0.91
55	27	1607	4.4	3.41	2.44	1.58	0.92	0.48	0.23
54	29.5	2168	5.2	4.18	3.09	2.09	1.29	0.71	0.36
53	32	2709	5.23	4.3	3.28	2.31	1.52	0.95	0.58
52	34.5	3229	5.51	4.56	3.49	2.46	1.61	0.96	0.54
51	37	3728	4.57	3.73	2.83	1.98	1.29	0.77	0.42
50	39.5	4208	5.37	4.5	3.51	2.53	1.68	1.02	0.57
49	42	4669	5.91	4.76	3.51	2.32	1.34	0.66	0.16
48	44.5	5112	5.64	4.68	3.59	2.52	1.64	0.98	0.56
47	47	5536	6.46	5.46	4.24	2.99	1.9	1.07	0.51
46	49.5	5943	6.64	5.43	4.05	2.71	1.59	0.79	0.27
45	52	6333	6.56	5.44	4.13	2.83	1.74	0.92	0.37
44	54.5	6707	5.76	4.64	3.43	2.27	1.32	0.64	0.15
43	57	7065	5.59	4.46	3.26	2.13	1.22	0.57	0.13
42	59.5	7407	5.47	4.2	2.9	1.74	0.87	0.26	0
41	62	7735	5.25	4.12	2.94	1.87	1.03	0.43	0.1
40	64.5	8049	5.13	3.86	2.61	1.52	0.72	0.19	0
39	67	8349	4.69	3.45	2.27	1.27	0.55	0.13	0
38	69.5	8635	4.48	3.28	2.16	1.24	0.59	0.17	0
37	72	8910	4.49	3.33	2.22	1.29	0.62	0.18	0
36	74.5	9172	5.03	3.74	2.49	1.42	0.67	0.18	0
35	77	9422	4.23	3.21	2.23	1.41	0.8	0.42	0.2
34	79.5	9662	5.8	4.7	3.47	2.28	1.3	0.6	0.13
33	82	9891	5.25	4	2.74	1.62	0.78	0.2	0
32	84.5	10110	5.17	4.15	3.05	1.99	1.13	0.48	0.11
31	87	10319	5.53	4.32	3.05	1.9	0.99	0.36	0.06
30	89.5	10520	4.76	3.58	2.42	1.43	0.69	0.19	0
29	92	10712	4.47	3.33	2.23	1.29	0.6	0.15	0
28	94.5	10897	5.22	3.91	2.62	1.52	0.72	0.18	0

Particle size distributions of samples from the Dry Creek site (cont.)

Sam #	Depth	Age (BP)	1.5□	1.25□	1□	0.75□	0.5□	0.25□	0□
57	22	418	1.92	1.99	2.1	2.24	2.38	2.51	2.57
56	24.5	1023	0.72	0.67	0.73	0.86	1.02	1.16	1.25
55	27	1607	0.14	0.15	0.22	0.31	0.4	0.47	0.5
54	29.5	2168	0.16	0.04	0	0	0	0	0
53	32	2709	0.38	0.28	0.25	0.24	0.26	0.29	0.32
52	34.5	3229	0.3	0.2	0.19	0.22	0.28	0.35	0.39
51	37	3728	0.22	0.13	0.12	0.17	0.27	0.38	0.48
50	39.5	4208	0.3	0.16	0.11	0.12	0.16	0.22	0.27
49	42	4669	0	0	0	0	0	0	0
48	44.5	5112	0.35	0.26	0.26	0.27	0.3	0.32	0.32
47	47	5536	0.21	0.09	0.08	0.12	0.16	0.19	0.21
46	49.5	5943	0.05	0	0	0	0	0	0
45	52	6333	0.09	0	0	0	0	0	0
44	54.5	6707	0	0	0	0	0	0	0
43	57	7065	0	0	0	0	0	0	0
42	59.5	7407	0	0	0	0	0	0	0
41	62	7735	0	0	0	0	0	0	0
40	64.5	8049	0	0	0	0	0	0	0
39	67	8349	0	0	0	0	0	0	0
38	69.5	8635	0	0	0	0	0	0	0
37	72	8910	0	0	0	0	0	0	0
36	74.5	9172	0	0	0	0	0	0	0
35	77	9422	0.11	0.09	0.11	0.14	0.17	0.2	0.23
34	79.5	9662	0	0	0	0	0	0	0
33	82	9891	0	0	0	0	0	0	0
32	84.5	10110	0	0	0	0	0	0	0
31	87	10319	0	0	0	0	0	0	0
30	89.5	10520	0	0	0	0	0	0	0
29	92	10712	0	0	0.09	0.24	0.35	0.44	0.49
28	94.5	10897	0	0	0	0	0	0	0

Particle size distributions of samples from the Dry Creek site (cont.)

Sam #	Depth	Age (BP)	-0.25□	-0.5□	-0.75□	-1□	-1.25□	Mean	Mode
57	22	418	2.47	2.13	1.57	0.8	0	75.34	72.083
56	24.5	1023	1.23	1.07	0.78	0.4	0	50.97	63.413
55	27	1607	0.49	0.43	0.32	0.16	0	34.57	49.158
54	29.5	2168	0	0	0	0	0	36.55	56.732
53	32	2709	0.33	0.3	0.23	0.11	0	39.60	59.71
52	34.5	3229	0.4	0.36	0.27	0.13	0	42.07	61.53
51	37	3728	0.53	0.5	0.4	0.21	0	34.11	55.45
50	39.5	4208	0.3	0.28	0.23	0.12	0	39.75	61.73
49	42	4669	0	0	0	0	0	41.14	60.77
48	44.5	5112	0.3	0.25	0.19	0.09	0	42.76	62.43
47	47	5536	0.2	0.18	0.13	0.07	0	47.31	68.14
46	49.5	5943	0	0	0	0	0	46.43	65.10
45	52	6333	0	0	0	0	0	46.28	65.60
44	54.5	6707	0	0	0	0	0	40.47	58.63
43	57	7065	0	0	0	0	0	39.11	57.60
42	59.5	7407	0	0	0	0	0	38.24	56.06
41	62	7735	0	0	0	0	0	36.71	55.32
40	64.5	8049	0	0	0	0	0	36.17	53.91
39	67	8349	0	0	0	0	0	43.20	49.52
38	69.5	8635	0	0	0	0	0	33.68	47.48
37	72	8910	0	0	0	0	0	33.00	47.38
36	74.5	9172	0	0	0	0	0	36.31	51.81
35	77	9422	0.23	0.21	0.16	0.08	0	32.57	46.43
34	79.5	9662	0	0	0	0	0	39.38	62.18
33	82	9891	0	0	0	0	0	36.81	54.56
32	84.5	10110	0	0	0	0	0	35.63	55.12
31	87	10319	0	0	0	0	0	38.84	55.76
30	89.5	10520	0	0	0	0	0	34.00	50.52
29	92	10712	0.5	0.44	0.33	0.17	0	34.53	49.27
28	94.5	10897	0	0	0	0	0	37.54	53.09

Particle size distributions of samples from the Dry Creek site (cont.)

Sam #	Depth	Age (BP)	Median	% C1	Std Error % C1	% C2	Std Error C2	Mode C1 phi	Mode C1 microns
57	22	418	89.52	0.84	0.007	0.158	0.007	3.999	62.530
56	24.5	1023	60.47	0.92	0.003	0.081	0.003	4.366	48.485
55	27	1607	41.15	0.97	0.002	0.032	0.002	4.832	35.101
54	29.5	2168	43.44	1.00	NA		NA	4.706	38.326
53	32	2709	47.00	0.98	0.002	0.019	0.002	4.621	40.651
52	34.5	3229	49.90	0.98	0.002	0.022	0.002	4.581	41.781
51	37	3728	40.65	0.97	0.002	0.027	0.002	4.874	34.098
50	39.5	4208	47.19	0.99	0.001	0.015	0.001	4.632	40.334
49	42	4669	48.80	1.00	NA		NA	4.556	42.516
48	44.5	5112	50.78	0.98	0.002	0.018	0.002	4.541	42.954
47	47	5536	56.14	0.99	0.001	0.011	0.001	4.393	47.589
46	49.5	5943	55.12	1.00	NA		NA	4.382	47.956
45	52	6333	54.93	1.00	NA		NA	4.379	48.077
44	54.5	6707	48.02	1.00	NA		NA	4.561	42.357
43	57	7065	46.41	1.00	NA		NA	4.602	41.170
42	59.5	7407	45.38	1.00	NA		NA	4.647	39.910
41	62	7735	43.63	1.00	NA		NA	4.683	38.924
40	64.5	8049	42.98	1.00	NA		NA	4.716	38.056
39	67	8349	40.73	1.00	NA		NA	4.766	36.759
38	69.5	8635	40.14	1.00	NA		NA	4.788	36.190
37	72	8910	39.39	1.00	NA		NA	4.809	35.673
36	74.5	9172	43.16	1.00	NA		NA	4.687	38.812
35	77	9422	38.89	0.99	0.001	0.015	0.001	4.852	34.620
34	79.5	9662	46.71	1.00	NA		NA	4.612	40.904
33	82	9891	43.73	1.00	NA		NA	4.692	38.691
32	84.5	10110	42.38	1.00	NA		NA	4.710	38.212
31	87	10319	46.11	1.00	NA		NA	4.593	41.446
30	89.5	10520	40.52	1.00	NA		NA	4.786	36.237
29	92	10712	41.13	0.97	0.002	0.030	0.002	4.843	34.853
28	94.5	10897	44.59	1.00	NA		NA	4.665	39.414

Particle size distributions of samples from the Dry Creek site (cont.)

Sam #	Depth	Age (BP)	Mode C2 phi	Mode C2 microns	Med C1 phi	Std Err Med C1 phi	Median C2 phi	Std Error Med C2 phi	Mean C1 phi
57	22	418	-0.049	1034.800	4.232	0.001	0.131	0.006	4.326
56	24.5	1023	-0.081	1058.104	4.608	0.001	0.091	0.012	4.711
55	27	1607	-0.111	1080.066	5.058	0.001	0.054	0.024	5.154
54	29.5	2168			4.937	0.001	NA	NA	5.036
53	32	2709	-0.198	1146.946	4.851	0.001	-0.044	0.048	4.948
52	34.5	3229	-0.228	1171.240	4.813	0.001	-0.083	0.048	4.912
51	37	3728	-0.299	1230.423	5.087	0.001	-0.162	0.048	5.175
50	39.5	4208	-0.332	1258.751	4.860	0.001	-0.201	0.048	4.957
49	42	4669			4.796	0.001	NA	NA	4.901
48	44.5	5112	-0.141	1102.603	4.775	0.001	0.017	0.048	4.875
47	47	5536	-0.246	1185.561	4.637	0.001	-0.105	0.048	4.744
46	49.5	5943			4.628	0.001	NA	NA	4.738
45	52	6333			4.624	0.001	NA	NA	4.734
44	54.5	6707			4.801	0.001	NA	NA	4.907
43	57	7065			4.841	0.001	NA	NA	4.946
42	59.5	7407			4.885	0.001	NA	NA	4.990
41	62	7735			4.919	0.001	NA	NA	5.022
40	64.5	8049			4.951	0.001	NA	NA	5.055
39	67	8349			5.000	0.001	NA	NA	5.104
38	69.5	8635			5.021	0.001	NA	NA	5.125
37	72	8910			5.041	0.001	NA	NA	5.144
36	74.5	9172			4.924	0.001	NA	NA	5.030
35	77	9422	-0.147	1107.595	5.080	0.001	0.015	0.048	5.178
34	79.5	9662			4.849	0.001	NA	NA	4.953
33	82	9891			4.928	0.001	NA	NA	5.033
32	84.5	10110			4.944	0.001	NA	NA	5.046
31	87	10319			4.832	0.001	NA	NA	4.939
30	89.5	10520			5.019	0.001	NA	NA	5.121
29	92	10712	-0.180	1132.873	5.072	0.001	-0.028	0.024	5.172
28	94.5	10897			4.902	0.001	NA	NA	5.008

Particle size distributions of samples from the Dry Creek site (cont.)

Sam #	Depth	Age (BP)	Std Error Mean C1 phi	Mean C2 phi	Std Error Mean C2 phi	Std Dev C1 phi	Std Error Std Dev C1 phi	Std Dev C2 phi	Std Error Std Dev C2 phi
57	22	418	0.031	0.228	0.033	1.938	0.023	0.689	0.023
56	24.5	1023	0.018	0.185	0.033	1.639	0.015	0.658	0.024
55	27	1607	0.016	0.143	0.041	1.576	0.012	0.624	0.031
54	29.5	2168	0.016	NA	NA	1.569	0.011	NA	NA
53	32	2709	0.017	0.039	0.058	1.645	0.012	0.576	0.042
52	34.5	3229	0.017	-0.003	0.046	1.642	0.012	0.542	0.034
51	37	3728	0.017	-0.087	0.036	1.699	0.013	0.509	0.027
50	39.5	4208	0.017	-0.129	0.049	1.660	0.012	0.485	0.037
49	42	4669	0.015	NA	NA	1.497	0.010	NA	NA
48	44.5	5112	0.017	0.103	0.060	1.640	0.013	0.595	0.043
47	47	5536	0.016	-0.028	0.061	1.558	0.011	0.524	0.045
46	49.5	5943	0.014	NA	NA	1.450	0.010	NA	NA
45	52	6333	0.015	NA	NA	1.468	0.010	NA	NA
44	54.5	6707	0.015	NA	NA	1.484	0.010	NA	NA
43	57	7065	0.015	NA	NA	1.484	0.010	NA	NA
42	59.5	7407	0.014	NA	NA	1.451	0.010	NA	NA
41	62	7735	0.015	NA	NA	1.487	0.010	NA	NA
40	64.5	8049	0.014	NA	NA	1.450	0.010	NA	NA
39	67	8349	0.014	NA	NA	1.421	0.010	NA	NA
38	69.5	8635	0.014	NA	NA	1.426	0.010	NA	NA
37	72	8910	0.014	NA	NA	1.443	0.010	NA	NA
36	74.5	9172	0.014	NA	NA	1.410	0.010	NA	NA
35	77	9422	0.015	0.102	0.061	1.529	0.011	0.611	0.046
34	79.5	9662	0.015	NA	NA	1.516	0.010	NA	NA
33	82	9891	0.014	NA	NA	1.451	0.010	NA	NA
32	84.5	10110	0.015	NA	NA	1.510	0.010	NA	NA
31	87	10319	0.014	NA	NA	1.431	0.010	NA	NA
30	89.5	10520	0.015	NA	NA	1.463	0.010	NA	NA
29	92	10712	0.015	0.055	0.035	1.494	0.011	0.570	0.026
28	94.5	10897	0.014	NA	NA	1.424	0.010	NA	NA

Particle size distributions of samples from the Dry Creek site

Sam #	Depth	Age (BP)	12 f	11.75f	11.5f	11.25f	11f	10.75f	10.5f
27	97	11074	0	0	0	0	0.02	0.16	0.18
26	99.5	11245	0	0	0	0	0.01	0.14	0.17
25	102	11410	0	0	0	0	0.02	0.17	0.19
24	104.5	11568	0	0	0	0	0.02	0.16	0.19
23	107	11722	0	0	0	0	0.02	0.18	0.2
22	109.5	11871	0	0	0	0	0.02	0.16	0.18
21	112	12016	0	0	0	0	0.02	0.16	0.19
20	114.5	12158	0	0	0	0	0.02	0.17	0.19
19	117	12296	0	0	0	0	0.02	0.16	0.18
18	119.5	12433	0	0	0	0	0.01	0.14	0.17
17	122	12567	0	0	0	0	0.01	0.13	0.15
16	124.5	12700	0	0	0	0	0.01	0.14	0.17
15	127	12832	0	0	0	0	0.02	0.15	0.17
14	129.5	12964	0	0	0	0	0.01	0.14	0.16
13	132	13096	0	0	0	0	0.02	0.15	0.18
12	134.5	13228	0	0	0	0	0.02	0.16	0.18
11	137	13362	0	0	0	0	0.02	0.15	0.18
10	139.5	13498	0	0	0	0	0.02	0.18	0.2
9	142	13541	0	0	0	0	0.02	0.17	0.19
8	144.5	13627	0	0	0	0	0.02	0.17	0.2
7	147	13714	0	0	0	0	0.02	0.17	0.2
6	149.5	13800	0	0	0	0	0.02	0.19	0.21
5	152	13887	0	0	0	0	0.02	0.18	0.21
4	154.5	13974	0	0	0	0	0.09	0.2	0.22
3	157	14060	0	0	0	0	0.11	0.23	0.24
2	159.5	14147	0	0	0	0	0.11	0.22	0.23
1	162	14233	0	0	0	0	0.12	0.24	0.26

Particle size distributions of samples from the Dry Creek site (cont.)

Sam #	Depth	Age (BP)	10.25f	10f	9.75f	9.5f	9.25f	9f	8.75f
27	22	418	0.17	0.3	0.25	0.23	0.22	0.47	0.37
26	24.5	1023	0.16	0.28	0.24	0.22	0.22	0.47	0.39
25	27	1607	0.18	0.32	0.27	0.25	0.25	0.54	0.44
24	29.5	2168	0.18	0.32	0.27	0.25	0.25	0.55	0.45
23	32	2709	0.19	0.33	0.28	0.26	0.26	0.55	0.45
22	34.5	3229	0.18	0.31	0.26	0.24	0.24	0.51	0.42
21	37	3728	0.18	0.31	0.26	0.24	0.24	0.52	0.43
20	39.5	4208	0.18	0.32	0.27	0.24	0.24	0.51	0.41
19	42	4669	0.17	0.31	0.26	0.24	0.24	0.51	0.42
18	44.5	5112	0.17	0.29	0.25	0.23	0.23	0.48	0.39
17	47	5536	0.15	0.27	0.23	0.21	0.21	0.45	0.36
16	49.5	5943	0.16	0.28	0.24	0.22	0.21	0.45	0.37
15	52	6333	0.16	0.28	0.24	0.21	0.21	0.45	0.37
14	54.5	6707	0.16	0.28	0.23	0.21	0.21	0.45	0.36
13	57	7065	0.17	0.3	0.25	0.23	0.23	0.48	0.38
12	59.5	7407	0.18	0.31	0.25	0.24	0.23	0.49	0.39
11	62	7735	0.17	0.29	0.24	0.22	0.22	0.45	0.36
10	64.5	8049	0.19	0.34	0.29	0.26	0.25	0.52	0.41
9	67	8349	0.19	0.33	0.28	0.25	0.25	0.51	0.41
8	69.5	8635	0.19	0.33	0.28	0.25	0.25	0.51	0.41
7	72	8910	0.19	0.33	0.27	0.25	0.24	0.49	0.39
6	74.5	9172	0.2	0.36	0.3	0.26	0.25	0.51	0.4
5	77	9422	0.2	0.36	0.29	0.26	0.25	0.49	0.38
4	79.5	9662	0.21	0.37	0.3	0.26	0.24	0.45	0.34
3	82	9891	0.24	0.42	0.35	0.3	0.27	0.51	0.38
2	84.5	10110	0.23	0.4	0.33	0.28	0.25	0.47	0.34
1	87	10319	0.25	0.44	0.36	0.32	0.29	0.55	0.41

Particle size distributions of samples from the Dry Creek site (cont.)

Sam #	Depth	Age (BP)	8.5□	8.25□	8□	7.75□	7.5□	7.25□	7□
27	22	418	0.66	0.71	0.89	1.08	1.44	1.79	1.97
26	24.5	1023	0.71	0.76	0.98	1.2	1.62	2.04	2.26
25	27	1607	0.79	0.85	1.09	1.34	1.8	2.26	2.5
24	29.5	2168	0.81	0.87	1.11	1.36	1.82	2.28	2.5
23	32	2709	0.8	0.86	1.09	1.33	1.78	2.23	2.44
22	34.5	3229	0.76	0.82	1.05	1.29	1.73	2.17	2.39
21	37	3728	0.77	0.83	1.06	1.31	1.75	2.2	2.42
20	39.5	4208	0.74	0.79	1.01	1.23	1.65	2.06	2.25
19	42	4669	0.74	0.79	1.01	1.23	1.65	2.07	2.29
18	44.5	5112	0.7	0.75	0.96	1.18	1.59	2	2.22
17	47	5536	0.66	0.71	0.91	1.12	1.5	1.89	2.08
16	49.5	5943	0.66	0.71	0.91	1.12	1.5	1.89	2.08
15	52	6333	0.66	0.7	0.9	1.1	1.48	1.86	2.06
14	54.5	6707	0.64	0.69	0.88	1.09	1.46	1.84	2.02
13	57	7065	0.68	0.73	0.92	1.13	1.51	1.89	2.08
12	59.5	7407	0.7	0.74	0.94	1.14	1.52	1.9	2.08
11	62	7735	0.64	0.68	0.85	1.05	1.4	1.76	1.95
10	64.5	8049	0.72	0.77	0.97	1.12	1.57	1.96	2.15
9	67	8349	0.73	0.78	0.99	1.2	1.61	2.01	2.2
8	69.5	8635	0.73	0.78	0.99	1.21	1.61	2.02	2.22
7	72	8910	0.7	0.75	0.95	1.17	1.57	1.98	2.17
6	74.5	9172	0.7	0.74	0.94	1.15	1.55	1.94	2.14
5	77	9422	0.66	0.7	0.89	1.1	1.48	1.87	2.07
4	79.5	9662	0.58	0.6	0.75	0.92	1.24	1.56	1.72
3	82	9891	0.63	0.64	0.78	0.93	1.21	1.48	1.6
2	84.5	10110	0.57	0.58	0.71	0.84	1.09	1.32	1.43
1	87	10319	0.69	0.7	0.86	1.04	1.39	1.75	1.94

Particle size distributions of samples from the Dry Creek site (cont.)

Sam #	Depth	Age (BP)	6.75□	6.5□	6.25□	6□	5.75□	5.5□	5.25□
27	22	418	2.43	2.69	3.19	3.62	4.14	4.6	5.27
26	24.5	1023	2.8	3.09	3.65	4.09	4.58	4.97	5.54
25	27	1607	3.09	3.4	4	4.45	4.93	5.25	5.76
24	29.5	2168	3.08	3.37	3.94	4.36	4.81	5.13	5.61
23	32	2709	3.01	3.3	3.87	4.3	4.75	5.09	5.58
22	34.5	3229	2.96	3.26	3.85	4.32	4.84	5.24	5.8
21	37	3728	2.99	3.29	3.88	4.35	4.85	5.26	5.83
20	39.5	4208	2.79	3.05	3.59	4.02	4.51	4.92	5.53
19	42	4669	2.85	3.15	3.74	4.2	4.69	5.04	5.51
18	44.5	5112	2.76	3.06	3.64	4.11	4.64	5.07	5.66
17	47	5536	2.58	2.85	3.37	3.8	4.29	4.69	5.24
16	49.5	5943	2.58	2.86	3.39	3.83	4.32	4.71	5.27
15	52	6333	2.56	2.84	3.38	3.82	4.32	4.73	5.31
14	54.5	6707	2.5	2.75	3.25	3.66	4.14	4.56	5.16
13	57	7065	2.58	2.85	3.38	3.81	4.31	4.72	5.32
12	59.5	7407	2.57	2.84	3.36	3.79	4.29	4.71	5.32
11	62	7735	2.41	2.67	3.17	3.58	4.06	4.48	5.09
10	64.5	8049	2.65	2.91	3.45	3.9	4.43	4.89	5.53
9	67	8349	2.71	2.96	3.52	3.96	4.48	4.93	5.57
8	69.5	8635	2.74	3.02	3.56	4	4.51	4.94	5.54
7	72	8910	2.69	2.97	3.54	4.02	4.59	5.09	5.77
6	74.5	9172	2.65	2.93	3.5	4	4.59	5.12	5.84
5	77	9422	2.57	2.86	3.42	3.92	4.53	5.07	5.8
4	79.5	9662	2.15	2.4	2.9	3.38	4.01	4.64	5.5
3	82	9891	1.97	2.2	2.71	3.25	4	4.77	5.77
2	84.5	10110	1.75	1.96	2.4	2.89	3.56	4.28	5.25
1	87	10319	2.44	2.73	3.3	3.8	4.39	4.91	5.62

Particle size distributions of samples from the Dry Creek site (cont.)

Sam #	Depth	Age (BP)	5□	4.75□	4.5□	4.25□	4□	3.75□	3.5□
27	22	418	5.62	6.95	7.18	7.62	7.58	7.21	6.43
26	24.5	1023	5.75	6.95	7.03	7.32	7.16	6.71	5.9
25	27	1607	5.85	6.92	6.84	6.99	6.73	6.21	5.37
24	29.5	2168	5.7	6.75	6.7	6.87	6.65	6.18	5.42
23	32	2709	5.69	6.76	6.73	6.93	6.73	6.29	5.53
22	34.5	3229	5.95	7.06	6.99	7.12	6.82	6.26	5.41
21	37	3728	5.96	7.12	7.06	7.2	6.88	6.29	5.38
20	39.5	4208	5.78	7.02	7.12	7.42	7.23	6.73	5.85
19	42	4669	5.58	6.54	6.4	6.49	6.22	5.77	5.08
18	44.5	5112	5.86	7.02	7	7.17	6.91	6.38	5.56
17	47	5536	5.44	6.54	6.56	6.77	6.58	6.16	5.47
16	49.5	5943	5.47	6.58	6.6	6.82	6.64	6.23	5.53
15	52	6333	5.52	6.67	6.73	7	6.85	6.48	5.79
14	54.5	6707	5.44	6.67	6.82	7.17	7.08	6.7	5.99
13	57	7065	5.56	6.77	6.88	7.2	7.11	6.74	6.03
12	59.5	7407	5.57	6.78	6.9	7.23	7.13	6.76	6.05
11	62	7735	5.38	6.61	6.8	7.19	7.16	6.83	6.15
10	64.5	8049	5.79	6.99	6.99	7.16	6.85	6.27	5.41
9	67	8349	5.83	7.07	7.13	7.37	7.13	6.6	5.74
8	69.5	8635	5.77	6.96	6.99	7.2	6.97	6.44	5.59
7	72	8910	6.05	7.31	7.31	7.47	7.14	6.51	5.57
6	74.5	9172	6.15	7.45	7.45	7.6	7.23	6.56	5.56
5	77	9422	6.11	7.39	7.36	7.45	7.02	6.27	5.23
4	79.5	9662	6.01	7.53	7.74	8.04	7.74	7.06	6.01
3	82	9891	6.34	7.86	7.89	7.94	7.35	6.4	5.18
2	84.5	10110	5.87	7.47	7.75	8.11	7.86	7.27	6.33
1	87	10319	5.93	7.22	7.27	7.47	7.17	6.58	5.67

Particle size distributions of samples from the Dry Creek site (cont.)

Sam #	Depth	Age (BP)	3.25□	3□	2.75□	2.5□	2.25□	2□	1.75□
27	22	418	5.27	3.99	2.71	1.6	0.78	0.23	0
26	24.5	1023	4.75	3.53	2.33	1.31	0.56	0.12	0
25	27	1607	4.26	3.09	1.99	1.08	0.44	0.08	0
24	29.5	2168	4.38	3.28	2.21	1.31	0.65	0.19	0
23	32	2709	4.48	3.35	2.26	1.31	0.61	0.17	0
22	34.5	3229	4.3	3.16	2.08	1.18	0.52	0.13	0
21	37	3728	4.22	3.03	1.93	1.03	0.42	0.08	0
20	39.5	4208	4.65	3.39	2.2	1.22	0.54	0.14	0
19	42	4669	4.19	3.27	2.38	1.61	1.03	0.62	0.37
18	44.5	5112	4.5	3.41	2.39	1.53	0.9	0.47	0.18
17	47	5536	4.53	3.56	2.63	1.83	1.22	0.79	0.49
16	49.5	5943	4.58	3.58	2.61	1.76	1.11	0.65	0.34
15	52	6333	4.81	3.74	2.69	1.77	1.07	0.6	0.33
14	54.5	6707	4.97	3.87	2.79	1.85	1.13	0.65	0.35
13	57	7065	5	3.88	2.76	1.78	1.05	0.55	0.26
12	59.5	7407	5.02	3.9	2.78	1.78	1.02	0.51	0.19
11	62	7735	5.13	3.99	2.86	1.85	1.08	0.55	0.24
10	64.5	8049	4.31	3.22	2.23	1.43	0.88	0.54	0.35
9	67	8349	4.6	3.42	2.31	1.39	0.73	0.32	0.1
8	69.5	8635	4.47	3.3	2.2	1.3	0.68	0.31	0.15
7	72	8910	4.4	3.23	2.15	1.28	0.67	0.29	0.09
6	74.5	9172	4.33	3.11	2.01	1.15	0.57	0.24	0.07
5	77	9422	3.99	2.8	1.76	0.98	0.48	0.24	0.18
4	79.5	9662	4.69	3.4	2.27	1.39	0.82	0.5	0.34
3	82	9891	3.85	2.69	1.81	1.24	0.96	0.87	0.85
2	84.5	10110	5.16	4.01	2.98	2.13	1.48	0.99	0.62
1	87	10319	4.53	3.39	2.37	1.55	0.96	0.58	0.34

Particle size distributions of samples from the Dry Creek site (cont.)

Sam #	Depth	Age (BP)	1.5□	1.25□	1□	0.75□	0.5□	0.25□	0□
27	22	418	0	0	0	0	0	0	0
26	24.5	1023	0	0	0	0	0	0	0
25	27	1607	0	0	0	0	0	0	0
24	29.5	2168	0	0	0	0	0	0	0
23	32	2709	0	0	0	0	0	0	0
22	34.5	3229	0	0	0	0	0	0	0
21	37	3728	0	0	0	0	0	0	0
20	39.5	4208	0	0	0	0	0	0	0
19	42	4669	0.24	0.18	0.17	0.2	0.25	0.32	0.38
18	44.5	5112	0.04	0	0	0	0	0	0
17	47	5536	0.29	0.15	0.08	0.09	0.18	0.33	0.5
16	49.5	5943	0.15	0.02	0	0	0.17	0.34	0.53
15	52	6333	0.21	0.18	0.19	0.2	0.21	0.21	0.2
14	54.5	6707	0.2	0.13	0.11	0.11	0.13	0.17	0.2
13	57	7065	0.12	0.03	0	0	0	0	0
12	59.5	7407	0.04	0	0	0	0	0	0
11	62	7735	0.11	0.09	0.13	0.19	0.24	0.28	0.29
10	64.5	8049	0.26	0.22	0.19	0.16	0.14	0.15	0.16
9	67	8349	0	0	0	0	0	0	0
8	69.5	8635	0.12	0.14	0.17	0.17	0.16	0.13	0.11
7	72	8910	0	0	0	0	0	0	0
6	74.5	9172	0	0	0	0	0	0	0
5	77	9422	0.22	0.3	0.37	0.41	0.41	0.38	0.33
4	79.5	9662	0.28	0.24	0.2	0.16	0.13	0.11	0.1
3	82	9891	0.84	0.78	0.67	0.51	0.36	0.23	0.15
2	84.5	10110	0.35	0.12	0.02	0	0	0	0
1	87	10319	0.15	0.03	0	0	0	0	0

Particle size distributions of samples from the Dry Creek site (cont.)

Sam #	Depth	Age (BP)	-0.25□	-0.5□	-0.75□	-1□	-1.25□	Mean	Mode
27	22	418	0	0	0	0	0	37.76	53.35
26	24.5	1023	0	0	0	0	0	34.19	50.32
25	27	1607	0	0	0	0	0	31.00	47.06
24	29.5	2168	0	0	0	0	0	31.52	47.88
23	32	2709	0	0	0	0	0	32.00	48.65
22	34.5	3229	0	0	0	0	0	31.85	46.29
21	37	3728	0	0	0	0	0	31.52	46.38
20	39.5	4208	0	0	0	0	0	34.03	49.88
19	42	4669	0.41	0.38	0.3	0.15	0	33.72	45.46
18	44.5	5112	0	0	0	0	0	33.97	47.35
17	47	5536	0.61	0.61	0.49	0.26	0	37.37	48.85
16	49.5	5943	0.66	0.68	0.56	0.3	0	37.07	49.17
15	52	6333	0.19	0.17	0.12	0.06	0	37.01	50.50
14	54.5	6707	0.21	0.19	0.14	0.07	0	38.20	52.03
13	57	7065	0	0	0	0	0	36.61	51.80
12	59.5	7407	0	0	0	0	0	36.53	51.75
11	62	7735	0.27	0.23	0.16	0.08	0	39.07	53.47
10	64.5	8049	0.17	0.17	0.13	0.07	0	34.87	46.82
9	67	8349	0	0	0	0	0	34.35	48.56
8	69.5	8635	0.1	0.09	0.01	0	0	34.26	48.28
7	72	8910	0	0	0	0	0	33.83	46.53
6	74.5	9172	0	0	0	0	0	33.71	46.14
5	77	9422	0.28	0.22	0.15	0.07	0	34.54	44.89
4	79.5	9662	0.1	0.09	0.02	0	0	38.44	48.48
3	82	9891	0.11	0.1	0.02	0	0	37.87	13.99
2	84.5	10110	0	0	0	0	0	41.79	49.38
1	87	10319	0	0	0	0	0	35.47	47.40

Particle size distributions of samples from the Dry Creek site (cont.)

Sam #	Depth	Age (BP)	Median	% C1	Std Error % C1	% C2	Std Error C2	Mode C1 phi	Mode C1 microns
27	22	418	44.83	1.00	NA		NA	4.648	39.896
26	24.5	1023	40.72	1.00	NA		NA	4.770	36.664
25	27	1607	37.17	1.00	NA		NA	4.901	33.464
24	29.5	2168	37.74	1.00	NA		NA	4.878	34.003
23	32	2709	38.28	1.00	NA		NA	4.864	34.338
22	34.5	3229	38.12	1.00	NA		NA	4.861	34.419
21	37	3728	37.77	1.00	NA		NA	4.881	33.935
20	39.5	4208	40.54	1.00	NA		NA	4.793	36.069
19	42	4669	40.18	0.98	0.002	0.025	0.002	4.803	35.825
18	44.5	5112	40.47	1.00	NA		NA	4.759	36.923
17	47	5536	44.39	0.97	0.002	0.031	0.002	4.670	39.274
16	49.5	5943	44.04	0.97	0.002	0.032	0.002	4.695	38.609
15	52	6333	43.98	0.99	0.001	0.015	0.001	4.666	39.387
14	54.5	6707	45.37	0.99	0.001	0.012	0.001	4.625	40.526
13	57	7065	43.50	1.00	NA		NA	4.669	39.298
12	59.5	7407	43.42	1.00	NA		NA	4.678	39.056
11	62	7735	46.40	0.98	0.001	0.018	0.001	4.615	40.809
10	64.5	8049	41.54	0.99	0.001	0.013	0.001	4.761	36.878
9	67	8349	40.91	1.00	NA		NA	4.772	36.603
8	69.5	8635	40.80	0.99	0.001	0.009	0.001	4.790	36.157
7	72	8910	40.31	1.00	NA		NA	4.785	36.269
6	74.5	9172	40.17	1.00	NA		NA	4.799	35.920
5	77	9422	41.11	0.97	0.002	0.031	0.002	4.816	35.489
4	79.5	9662	45.63	1.00	NA		NA	4.611	40.915
3	82	9891	44.98	0.96	0.004	0.045	0.004	4.708	38.263
2	84.5	10110	49.62	1.00	NA		NA	4.475	44.956
1	87	10319	42.18	1.00	NA		NA	4.737	37.503

Particle size distributions of samples from the Dry Creek site (cont.)

Sam #	Depth	Age (BP)	Mode C2 phi	Mode C2 microns	Med C1 phi	Std Error Med C1 phi	Med C2 phi	Std Error Med C2 phi	Mean C1 phi
27	22	418			4.885	0.001	NA	NA	4.992
26	24.5	1023			5.003	0.001	NA	NA	5.107
25	27	1607			5.130	0.001	NA	NA	5.230
24	29.5	2168			5.107	0.001	NA	NA	5.207
23	32	2709			5.093	0.001	NA	NA	5.193
22	34.5	3229			5.091	0.001	NA	NA	5.192
21	37	3728			5.111	0.001	NA	NA	5.212
20	39.5	4208			5.026	0.001	NA	NA	5.129
19	42	4669	-0.183	1135.206	5.031	0.001	-0.023	0.048	5.128
18	44.5	5112			4.993	0.001	NA	NA	5.095
17	47	5536	-0.343	1268.107	4.904	0.001	-0.212	0.024	5.006
16	49.5	5943	-0.383	1304.105	4.929	0.001	-0.262	0.024	5.032
15	52	6333	0.010	993.298	4.901	0.001	0.193	0.049	5.004
14	54.5	6707	-0.188	1139.302	4.862	0.001	-0.034	0.048	4.966
13	57	7065			4.905	0.001	NA	NA	5.009
12	59.5	7407			4.914	0.001	NA	NA	5.018
11	62	7735	-0.087	1061.953	4.853	0.001	-0.077	0.048	4.958
10	64.5	8049	-0.049	1034.606	4.992	0.001	-0.139	0.049	5.092
9	67	8349			5.005	0.001	NA	NA	5.108
8	69.5	8635	0.278	824.851	5.021	0.001	0.446	Inf	5.122
7	72	8910			5.018	0.001	NA	NA	5.121
6	74.5	9172			5.032	0.001	NA	NA	5.135
5	77	9422	0.275	826.285	5.048	0.001	0.481	0.025	5.151
4	79.5	9662			4.846	0.001	NA	NA	4.947
3	82	9891	1.055	481.174	4.943	0.001	1.287	0.025	5.046
2	84.5	10110			4.718	0.001	NA	NA	4.826
1	87	10319			4.970	0.001	NA	NA	5.072

Particle size distributions of samples from the Dry Creek site (cont.)

Sam #	Depth	Age (BP)	Std Error Mean C1 phi	Mean C2 phi	Std Error Mean C2 phi	Std Dev C1 phi	Std Error Std Dev C1 phi	Std Dev C2 phi	Std Error Std Dev C2 phi
27	22	418	0.014	NA	NA	1.423	0.010	NA	NA
26	24.5	1023	0.014	NA	NA	1.431	0.010	NA	NA
25	27	1607	0.015	NA	NA	1.456	0.010	NA	NA
24	29.5	2168	0.015	NA	NA	1.482	0.010	NA	NA
23	32	2709	0.015	NA	NA	1.480	0.010	NA	NA
22	34.5	3229	0.014	NA	NA	1.448	0.010	NA	NA
21	37	3728	0.014	NA	NA	1.438	0.010	NA	NA
20	39.5	4208	0.014	NA	NA	1.440	0.010	NA	NA
19	42	4669	0.016	0.064	0.048	1.562	0.011	0.604	0.037
18	44.5	5112	0.015	NA	NA	1.470	0.010	NA	NA
17	47	5536	0.016	-0.140	0.031	1.539	0.011	0.485	0.024
16	49.5	5943	0.015	-0.195	0.026	1.505	0.010	0.447	0.020
15	52	6333	0.015	0.291	0.079	1.516	0.011	0.702	0.057
14	54.5	6707	0.015	0.051	0.066	1.506	0.011	0.581	0.050
13	57	7065	0.015	NA	NA	1.485	0.010	NA	NA
12	59.5	7407	0.015	NA	NA	1.478	0.010	NA	NA
11	62	7735	0.015	0.166	0.055	1.488	0.011	0.619	0.041
10	64.5	8049	0.015	0.240	0.097	1.530	0.012	0.724	0.070
9	67	8349	0.015	NA	NA	1.459	0.010	NA	NA
8	69.5	8635	0.015	0.536	0.088	1.490	0.011	0.638	0.063
7	72	8910	0.014	NA	NA	1.441	0.010	NA	NA
6	74.5	9172	0.014	NA	NA	1.431	0.010	NA	NA
5	77	9422	0.015	0.591	0.059	1.441	0.011	0.807	0.043
4	79.5	9662	0.016	NA	NA	1.580	0.010	NA	NA
3	82	9891	0.017	1.408	0.090	1.487	0.015	0.944	0.054
2	84.5	10110	0.015	NA	NA	1.483	0.010	NA	NA
1	87	10319	0.015	NA	NA	1.507	0.010	NA	NA

APPENDIX B

Geochemistry of Dry Creek Samples

Sam #	Depth	Age (BP)	SiO2 mass%	Al2O3 mass%	CaO mass%	K2O mass%	Na2O mass%	Fe2O3 mass%	MgO mass%	MnO mass%	TiO2 mass%	P2O5 mass%	As ppm	Ba ppm	Co ppm
57	22	418	78.793	10.804	1.323	1.854	1.333	8.135	0.281	0.104	0.845	0.097	16	727	16
56	24.5	1023	75.568	11.519	0.903	2.175	1.238	8.658	0.378	0.171	0.889	0.112	10	737	13
55	27	1607	71.902	13.173	0.613	2.257	1.205	8.365	0.656	0.112	0.955	0.095	13	734	18
54	29.5	2168	75.762	12.851	0.476	2.314	1.238	8.157	0.486	0.064	0.939	0.094	12	710	12
53	32	2709	76.836	13.196	0.446	2.473	1.257	6.948	0.503	0.038	0.944	0.084	12	722	4
52	34.5	3229	75.646	12.448	0.468	2.284	1.234	8.389	0.453	0.063	0.913	0.103	14	681	8
51	37	3728	69.938	13.513	0.593	2.38	1.277	9.415	0.762	0.126	0.918	0.12	13	736	18
50	39.5	4208	73.623	13.235	0.505	2.372	1.216	8.161	0.617	0.101	0.919	0.113	12	706	18
49	42	4669	71.398	13.411	0.492	2.407	1.223	8.419	0.662	0.147	0.926	0.133	12	709	22
48	44.5	5112	72.966	13.166	0.494	2.401	1.224	8.641	0.623	0.104	0.929	0.123	13	724	14
47	47	5536	73.575	13.24	0.517	2.454	1.247	7.944	0.641	0.069	0.906	0.133	13	714	14
46	49.5	5943	72.048	13.553	0.397	2.56	1.214	7.672	0.67	0.088	0.887	0.164	15	688	14
45	52	6333	73.943	12.965	0.375	2.514	1.241	7.719	0.531	0.101	0.883	0.154	15	687	17
44	54.5	6707	75.354	12.977	0.319	2.531	1.235	7.703	0.486	0.087	0.853	0.146	11	658	16
43	57	7065	77.654	12.266	0.328	2.39	1.243	8.022	0.346	0.099	0.873	0.149	12	638	15
42	59.5	7407	75.063	13.13	0.334	2.552	1.262	7.968	0.512	0.104	0.938	0.163	12	708	14
41	62	7735	73.665	13.866	0.29	2.707	1.15	7.016	0.632	0.079	0.909	0.151	12	695	11
40	64.5	8049	76.328	12.582	0.317	2.526	1.238	8.528	0.425	0.087	0.953	0.127	13	700	13
39	67	8349	76.639	14.05	0.344	2.753	1.24	6.692	0.602	0.063	0.975	0.132	11	733	10
38	69.5	8635	72.973	14.218	0.39	2.752	1.19	7.17	0.749	0.074	0.963	0.154	12	757	12
37	72	8910	72.225	13.259	0.422	2.618	1.23	8.924	0.643	0.08	0.958	0.175	18	749	9
36	74.5	9172	70.486	14.846	0.373	2.898	1.139	6.962	0.908	0.068	0.961	0.154	13	774	11
35	77	9422	74.87	13.764	0.489	2.69	1.209	6.945	0.659	0.07	0.948	0.17	17	742	11

Geochemistry of Dry Creek Samples

Sam #	Depth	Age (BP)	Cr ppm	Cu ppm	Mo ppm	Nb ppm	Ni ppm	Pb ppm	Rb ppm	Sc ppm	Sr ppm	Th ppm	U ppm	V ppm	Y ppm	Zn ppm
57	22	418	172	59	2.544	13	61	19	72	18	116	11	2.779	107.904	34	81
56	24.5	1023	282	45	6.208	15	65	13	88	17	97	16	4.509	101.399	41	99
55	27	1607	211	35	4.367	16	37	21	92	18	94	17	2.771	117.529	44	42
54	29.5	2168	228	34	5.179	17	42	17	100	18	88	15	3.213	106.438	43	46
53	32	2709	189	31	5.326	17	41	15	111	16	93	18	3.55	109.685	45	47
52	34.5	3229	203	31	4.138	16	41	22	95	17	85	15	2.237	100.234	43	46
51	37	3728	172	45	2.669	15	35	21	95	17	106	17	3.404	111.314	40	62
50	39.5	4208	166	46	3.793	16	41	18	97	17	90	18	3.062	105.519	42	65
49	42	4669	162	59	4.206	15	39	16	98	16	90	20	4.016	108.131	45	54
48	44.5	5112	178	43	3.99	16	44	17	96	17	89	16	3.076	110.849	42	62
47	47	5536	150	33	3.146	15	41	15	94	17	92	17	3.34	105.051	42	68
46	49.5	5943	131	33	2.487	16	37	23	99	17	89	16	3.363	99.098	47	63
45	52	6333	154	33	3.455	16	41	23	99	16	87	21	2.95	96.038	49	63
44	54.5	6707	131	29	2.276	17	39	14	100	17	81	19	2.503	92.747	46	73
43	57	7065	209	49	4.349	15	49	16	96	18	80	20	3.264	92.193	50	71
42	59.5	7407	161	54	2.502	17	45	17	101	17	83	22	2.209	100.812	55	74
41	62	7735	116	43	2.317	16	39	18	105	17	82	19	3.457	98.124	52	72
40	64.5	8049	316	54	6.818	16	69	22	99	17	78	20	2.23	98.741	52	64
39	67	8349	160	37	3.813	18	40	20	111	17	90	20	3.032	101.397	56	60
38	69.5	8635	134	49	2.626	17	44	17	109	17	91	19	2.747	106.961	54	60
37	72	8910	192	39	5.322	17	49	29	103	17	85	18	2.958	114.357	51	76
36	74.5	9172	110	30	2.777	18	41	18	115	17	90	20	2.14	109.241	51	64
35	77	9422	142	40	3.464	18	59	28	107	17	96	19	3.086	115.929	47	97

Geochemistry of Dry Creek Samples

Sam #	Depth	Age (BP)	SiO2 mass%	Al2O3 mass%	CaO mass%	K2O mass%	Na2O mass%	Fe2O3 mass%	MgO mass%	MnO mass%	TiO2 mass%	P2O5 mass%	As ppm	Ba ppm	Co ppm
34	79.5	9662	75.193	13.03	0.416	2.623	1.195	7.987	0.522	0.06	0.916	0.164	11	664	11
33	82	9891	74.628	13.067	0.347	2.646	1.193	7.946	0.512	0.074	0.907	0.166	13	659	14
32	84.5	10110	76.465	12.68	0.368	2.569	1.16	7.764	0.428	0.092	0.91	0.148	11	704	18
31	87	10319	79.29	13.044	0.302	2.605	1.025	6.059	0.403	0.077	0.931	0.144	9	645	17
30	89.5	10520	75.774	13.204	0.362	2.666	1.179	7.911	0.518	0.08	0.963	0.168	12	686	13
29	92	10712	74.837	12.616	0.427	2.514	1.223	8.694	0.464	0.102	0.915	0.174	12	690	14
28	94.5	10897	75.581	13.4	0.427	2.667	1.243	7.367	0.561	0.092	0.927	0.163	13	745	13
27	97	11074	75.426	12.677	0.47	2.507	1.205	7.957	0.47	0.168	0.928	0.172	12	712	14
26	99.5	11245	74.078	14.055	0.429	2.736	1.163	6.989	0.686	0.083	0.982	0.191	13	711	11
25	102	11410	73.903	13.241	0.394	2.633	1.171	8.526	0.573	0.074	0.98	0.189	13	720	13
24	104.5	11568	76.132	13.089	0.403	2.569	1.191	7.617	0.491	0.076	0.965	0.171	12	680	11
23	107	11722	73	12.654	0.365	2.551	1.149	9.563	0.517	0.122	0.959	0.171	15	687	16
22	109.5	11871	74.02	13.081	0.418	2.625	1.189	8.828	0.555	0.092	0.959	0.172	13	711	12
21	112	12016	73.178	12.915	0.399	2.589	1.172	9.118	0.559	0.09	0.966	0.175	12	709	8
20	114.5	12158	72.678	12.798	0.441	2.59	1.178	9.423	0.568	0.081	0.969	0.187	14	698	13
19	117	12296	72.44	13.365	0.618	2.719	1.275	8.642	0.734	0.073	0.959	0.163	14	834	15
18	119.5	12433	72.773	14.916	0.603	3.022	1.286	6.515	0.987	0.069	0.961	0.154	12	874	15
17	122	12567	75.269	13.774	0.546	2.838	1.267	6.868	0.681	0.074	0.917	0.138	12	812	12
16	124.5	12700	73.095	13.329	0.557	2.745	1.266	8.382	0.675	0.11	0.962	0.166	13	779	14
15	127	12832	73.975	13.121	0.57	2.724	1.269	8.304	0.611	0.106	0.956	0.17	13	775	12
14	129.5	12964	74.848	12.927	0.534	2.732	1.285	8.171	0.553	0.115	0.958	0.157	13	787	14
13	132	13096	73.625	13.511	0.604	2.786	1.295	8.086	0.694	0.087	0.957	0.165	12	811	13
12	134.5	13228	72.238	13.73	0.625	2.858	1.298	8.326	0.776	0.108	0.957	0.176	13	817	15

Geochemistry of Dry Creek Samples

Sam #	Depth	Age (BP)	Cr ppm	Cu ppm	Mo ppm	Nb ppm	Ni ppm	Pb ppm	Rb ppm	Sc ppm	Sr ppm	Th ppm	U ppm	V ppm	Y ppm	Zn ppm
34	79.5	9662	142	40	3.464	18	59	28	107	17	96	20	2.516	100.952	47	108
33	82	9891	132	20	2.874	16	41	19	100	17	85	19	3.541	97.254	50	103
32	84.5	10110	140	29	3.181	17	40	19	102	17	81	17	3.436	93.55	48	92
31	87	10319	137	41	2.66	16	41	18	101	16	83	17	3.243	92.9	53	77
30	89.5	10520	117	32	2.11	18	42	19	107	17	81	17	3.741	100.722	53	91
29	92	10712	167	49	3.771	17	48	23	105	18	83	20	2.223	97.196	54	78
28	94.5	10897	171	60	3.596	16	54	22	98	17	85	15	2.141	99.658	50	78
27	97	11074	133	42	2.827	17	51	19	105	17	91	21	3.424	97.588	53	68
26	99.5	11245	168	58	4.542	16	68	17	99	18	87	21	3.53	104.76	57	69
25	102	11410	122	33	3.109	19	49	21	107	17	88	19	4.227	103.183	54	61
24	104.5	11568	157	28	3.015	18	41	21	100	17	81	19	2.196	94.976	56	58
23	107	11722	144	23	3.072	18	43	18	100	17	85	19	3.782	99.475	51	71
22	109.5	11871	169	33	3.855	16	44	21	95	17	78	18	2.68	101.728	48	76
21	112	12016	200	33	3.858	17	47	21	101	16	83	20	2.708	98.312	52	73
20	114.5	12158	181	25	4.245	17	46	18	98	17	81	18	4.434	99.027	50	95
19	117	12296	188	27	4.444	17	48	20	97	17	82	18	2.095	114.474	43	115
18	119.5	12433	171	45	4.144	16	52	18	103	18	102	19	3.585	120.568	46	100
17	122	12567	132	43	2.249	18	56	15	119	17	113	20	2.353	111.839	41	90
16	124.5	12700	146	46	2.475	17	54	18	110	17	106	17	2.927	113.965	50	87
15	127	12832	165	50	4.026	16	57	22	102	17	98	21	3.984	109.069	50	87
14	129.5	12964	192	51	4.715	16	61	20	102	17	97	18	4.101	106.082	50	89
13	132	13096	205	50	5.297	16	59	19	102	17	96	17	3.266	111.519	49	89
12	134.5	13228	146	48	2.413	16	56	20	102	17	103	18	3.823	113.669	46	92

Geochemistry of Dry Creek Samples

Sam #	Depth	Age (BP)	SiO2 mass%	Al2O3 mass%	CaO mass%	K2O mass%	Na2O mass%	Fe2O3 mass%	MgO mass%	MnO mass%	TiO2 mass%	P2O5 mass%	As ppm	Ba ppm	Co ppm
11	137	13362	71.592	13.817	0.624	2.909	1.296	8.51	0.807	0.1	0.965	0.192	15	831	17
10	139.5	13498	70.696	12.529	1.063	2.415	1.467	8.162	0.756	0.125	0.894	0.141	14	822	20
9	142	13541	71.578	14.117	0.752	2.872	1.387	8.189	0.9	0.106	0.957	0.142	15	826	17
8	144.5	13627	71.754	13.713	0.832	2.773	1.408	8.726	0.844	0.111	0.942	0.141	15	863	13
7	147	13714	70.873	13.421	1.071	2.674	1.474	8.508	0.879	0.119	0.938	0.136	15	885	16
6	149.5	13800	72.189	13.461	1.543	2.479	1.653	8.218	0.937	0.115	0.92	0.147	15	909	12
5	152	13887	71.433	13.335	1.743	2.426	1.834	8.274	0.988	0.17	0.936	0.137	14	924	17
4	154.5	13974	74.352	12.53	2.751	1.949	2.001	7.186	0.865	0.129	0.866	0.172	13	911	13
3	157	14060	77.257	12.076	3.041	1.716	2.065	6.66	0.719	0.121	0.863	0.19	14	937	15
2	159.5	14147	76.973	11.909	3.108	1.717	2.166	6.852	0.704	0.134	0.881	0.182	19	925	12
1	162	14233	75.442	12.355	2.579	1.885	2.055	7.554	0.855	0.136	0.866	0.17	19	930	20

Geochemistry of Dry Creek Samples

Sam #	Depth	Age (BP)	Cr ppm	Mo ppm	Nb ppm	Ni ppm	Pb ppm	Rb ppm	Sc ppm	Sr ppm	Th ppm	U ppm	V ppm	Y ppm	Zn ppm
11	137	13362	176	58	2.896	17	74	21	107	19	18	2.551	112.922	46	103
10	139.5	13498	193	57	4.286	14	84	16	91	19	16	3.109	116.243	42	93
9	142	13541	166	57	3.473	15	74	16	107	18	16	3.078	116.294	44	97
8	144.5	13627	178	62	3.52	16	76	18	102	18	17	1.425	120.139	42	99
7	147	13714	237	65	4.895	14	77	18	100	18	14	1.96	120.034	39	93
6	149.5	13800	199	54	3.919	16	67	14	91	18	14	3.226	123.443	41	92
5	152	13887	258	58	4.722	15	75	14	87	18	14	3.44	128.607	39	87
4	154.5	13974	179	44	2.576	13	60	12	68	17	12	2.647	127.634	39	80
3	157	14060	147	42	1.656	13	65	12	59	17	9	3.459	130.527	38	92
2	159.5	14147	181	45	3.213	13	70	14	60	18	7	0.257	128.023	43	92
1	162	14233	207	73	3.489	13	81	16	66	18	9	3.533	139.442	38	89

APPENDIX C

Major and trace element soil geochemistry from Serpentine Hot Springs. >2 indicates analysis was performed on the >2mm fraction of the soil, 2-4 indicates analysis of the 2-4 mm fraction, and >4 indicates analysis of the >4mm fraction. All other analyses were performed on the < 2mm fraction of the soil.

Sample	Ag (ppm)	Al (%)	As (ppm)	Ba (ppm)	Be (ppm)	Bi (ppm)	C (%)	Ca (%)	Cd (pp,)	Ce (ppm)
S-3A	0.07	6.68	7.8	520	3.21	0.35	7.53	0.61	0.08	84.9
S-3B	0.08	6.44	7.5	500	2.79	0.36	2.99	0.54	0.06	61.8
S-2	0.11	6.94	11.9	850	2.28	0.29	0.71	0.51	0.11	102.5
S-1A	0.13	7.17	10.1	850	2.82	0.3	0.53	0.68	0.23	126.5
S-1B	0.11	7.63	11.1	800	3.45	0.3	0.53	0.64	0.14	127
S-Gruss	0.04	6.24	2.6	410	5.38	0.22	0.43	1.08	0.04	186
S-3A >2	0.04	5.5	2.1	790	1.96	0.07	---	0.3	<0.02	12.5
S-3B >2	0.06	5.71	2.1	890	1.61	0.06	---	0.28	<0.02	4.58
S-2 >2	0.38	5.08	2.1	720	1.79	0.09	---	0.27	<0.02	8.12
S-1A >2	0.09	6.29	1.3	910	2.25	0.07	---	0.36	<0.02	15.95
S-1B >2	0.04	6.47	1.4	920	2.25	0.08	---	0.4	<0.02	15.15
S-Gruss 2-4	0.03	5.63	1.4	660	3.06	0.07	---	0.53	<0.02	24.3
S-Gruss >4	0.01	6.41	1.2	810	3.04	0.11	---	0.5	<0.02	48.5

Major and trace element soil geochemistry from Serpentine Hot Springs. >2 indicates analysis was performed on the >2mm fraction of the soil, 2-4 indicates analysis of the 2-4 mm fraction, and >4 indicates analysis of the >4mm fraction. All other analyses were performed on the < 2mm fraction of the soil.

Sample	Co (ppm)	Cr (ppm)	Cs (ppm)	Cu (ppm)	Fe (%)	Ga (ppm)	Ge (ppm)	Hf (ppm)	Hg (ppm)	In (ppm)
S-3A	8.2	67	9.26	13.2	3.4	17.15	0.12	2	0.07	0.053
S-3B	5.4	65	9.28	11.8	3.29	16.35	0.11	1.9	0.1	0.052
S-2	16.1	87	6.82	26.5	4.29	17.15	0.14	2.2	0.08	0.061
S-1A	13.6	86	8.91	28.4	3.97	17.7	0.17	2.1	0.06	0.064
S-1B	15.3	70	9.98	28.1	4.08	20.5	0.23	2.5	0.06	0.075
S-Gruss	4.5	40	13.05	8.4	2.2	17.9	0.21	2.3	0.07	0.05
S-3A >2	1.4	84	5.21	12	1.03	11.1	0.06	0.8	0.1	0.011
S-3B >2	1	123	4.04	15.5	1.24	10.6	0.05	0.5	0.03	0.006
S-2 >2	1.6	141	4.06	17.5	1.34	9.61	0.06	0.5	0.04	0.006
S-1A >2	1.2	76	4.88	11.4	0.88	12.65	0.07	0.4	0.03	0.005
S-1B >2	1.6	80	4.79	11.7	0.95	12.9	0.05	0.4	0.04	0.006
S-Gruss 2-4	1.4	86	5.84	14.1	1.16	12.3	0.07	0.8	0.12	0.01
S-Gruss >4	1.7	46	8.6	8.7	1.11	14.95	0.08	0.8	0.07	0.02

Major and trace element soil geochemistry from Serpentine Hot Springs. >2 indicates analysis was performed on the >2mm fraction of the soil, 2-4 indicates analysis of the 2-4 mm fraction, and >4 indicates analysis of the >4mm fraction. All other analyses were performed on the < 2mm fraction of the soil.

Sample	K (%)	La (ppm)	Li (ppm)	Mg (%)	Mn (ppm)	Mo (ppm)	N (%)	Na (%)	Nb (ppm)	Ni (ppm)
S-3A	1.88	40.9	51.7	0.64	389	1	0.24	1.56	25.6	14.8
S-3B	1.62	30.1	39.4	0.55	270	1.09	0.15	1.33	23.7	40
S-2	1.78	47.7	47.8	0.96	692	1.08	0.09	1.06	15.5	36.4
S-1A	2.08	60.2	53.2	0.89	640	2.32	0.06	1.37	20.7	40.9
S-1B	1.97	58.6	61.5	0.92	600	0.98	0.06	1.6	23	8.4
S-Gruss	2.41	92.2	66.5	0.4	434	0.9	0.06	2.36	51.6	8.7
S-3A >2	4.61	6.2	17	0.04	102	2.56	---	1.49	4.3	11.4
S-3B >2	4.98	2.6	10.7	0.02	62	3.49	---	1.5	3.7	14
S-2 >2	4.18	4.3	12.8	0.03	100	3.98	---	1.37	2.3	8.5
S-1A >2	5.21	6	14.6	0.04	81	2.3	---	1.78	5	9.2
S-1B >2	5.34	6.2	13.7	0.05	104	2.69	---	1.81	4.1	8.8
S-Gruss 2-4	4.03	10	25.4	0.08	142	2.58	---	1.8	10.5	5.3
S-Gruss >4	5.11	20.8	37.4	0.13	188	1.55	---	1.95	15.3	19.3

Major and trace element soil geochemistry from Serpentine Hot Springs. >2 indicates analysis was performed on the >2mm fraction of the soil, 2-4 indicates analysis of the 2-4 mm fraction, and >4 indicates analysis of the >4mm fraction. All other analyses were performed on the < 2mm fraction of the soil.

Sample	P (ppm)	Pb (ppm)	Rb (ppm)	Re (ppm)	S (ppm)	Sb (ppm)	Sc (ppm)	Se (ppm)	Sn (ppm)	Sr (ppm)
S-3A	570	19	141.5	<0.002	0.02	0.58	9.8	1	5.4	122
S-3B	820	17	118	<0.002	0.03	0.55	9.9	2	5.1	105.5
S-2	770	16.7	109	<0.002	0.01	0.86	14.8	2	3.2	102
S-1A	910	18.6	141	<0.002	0.01	0.82	13.2	2	4.6	124.5
S-1B	780	20.8	151	<0.002	0.01	0.88	15.6	2	5.5	124
S-Gruss	690	21.9	208	<0.002	<0.01	0.28	5.9	2	11.9	174
S-3A >2	80	23.9	249	<0.002	<0.01	0.33	0.7	<1	1.8	178
S-3B >2	50	24.3	230	<0.002	<0.01	0.36	0.4	<1	1.9	188
S-2 >2	70	21.7	217	<0.002	<0.01	0.4	0.5	1	1.8	159.5
S-1A >2	90	27.3	187.5	<0.002	<0.01	0.32	0.5	1	1.9	207
S-1B >2	100	27.3	257	<0.002	<0.01	0.38	0.7	<1	1.6	212
S-Gruss 2-4	170	22.7	231	<0.002	<0.01	0.33	1	1	3.4	177
S-Gruss >4	270	29.2	222	<0.002	<0.01	0.22	1.6	1	3.9	204

Major and trace element soil geochemistry from Serpentine Hot Springs. >2 indicates analysis was performed on the >2mm fraction of the soil, 2-4 indicates analysis of the 2-4 mm fraction, and >4 indicates analysis of the >4mm fraction. All other analyses were performed on the < 2mm fraction of the soil.

Sample	Ta (ppm)	Te (ppm)	Th (ppm)	Ti (%)	Tl (ppm)	U (ppm)	V (ppm)	W (ppm)	Y (ppm)	Zn (ppm)	Zr (ppm)
S-3A	1.93	<0.05	25	0.391	0.83	3.5	91	3	18.9	65	66.3
S-3B	1.88	<0.05	17.7	0.405	0.73	3.4	95	2.3	17.4	50	64
S-2	1.13	0.05	18.9	0.42	0.68	3.5	130	1.7	27.2	96	75.9
S-1A	1.57	<0.05	28.6	0.404	0.84	3.7	113	2.3	30.8	100	75.1
S-1B	1.65	0.06	30.8	0.434	0.94	4.5	117	3.1	30.9	94	92.6
S-Gruss	4.72	<0.05	50.3	0.321	1.13	5.3	37	4.7	45.4	53	64.1
S-3A >2	0.27	<0.05	10.6	0.037	1.16	1.5	6	0.5	3.3	7	19.9
S-3B >2	0.42	<0.05	4.4	0.026	1.23	1.2	6	0.5	3.1	3	12.1
S-2 >2	0.16	<0.05	7	0.022	1.06	1.2	4	0.4	2.3	5	13.7
S-1A >2	0.53	<0.05	6.8	0.031	1.35	1.4	5	0.5	5.5	7	11.9
S-1B >2	0.32	<0.05	5.6	0.032	1.3	1.3	6	0.6	3.7	8	12.6
S-Gruss 2-4	0.93	<0.05	11.1	0.06	1.13	1.8	6	1	9	12	18.6
S-Gruss >4	1.16	<0.05	20	0.091	1.57	3.1	9	1.5	11.3	19	23.6

REFERENCES

Abbott, M.B., Finney, B.P., Edwards, M.E., Kelts, K.R., 2000. Lake-level reconstruction and paleohydrology of Birch Lake, central Alaska, based on seismic reflection profiles and core transects. Quaternary Research 53, 154–166.

Ager, T.A., 1983. Holocene vegetational history of Alaska. In: Wright, H.E. (Ed.), Late Quaternary Environments of the United States, Volume 2: The Holocene, University of Minnesota, Minneapolis, MN, pp. 128–141.

Ager, T.A., 2003. Late Quaternary vegetation and climate history of the central Bering land bridge from St. Michael Island, western Alaska. Quaternary Research 60, 19–32.

Anderson, P.M., Brubaker, L.B., 1994. Vegetation history of northcentral Alaska: A mapped summary of late-quaternary pollen data. Quaternary Science Reviews 13, 71–92.

Anderson, P.M., Lozhkin, A.V., Eisner, W.R., Kozhevnikova, M.V., Hopkins, D.M., Brubaker, L.B., Colinvaux, P.A., 1994. Two late Quaternary pollen records from south-central Alaska. Géographie physique et Quaternaire 48, 131–143.

Ashley, G.M., 1978. Interpretation of polymodal sediments. The Journal of Geology 411–421.

Bagnold, R.A., Barndorff-Nielsen, O., 1980. The pattern of natural size distributions. Sedimentology 27, 199–207.

Barber, V.A., Finney, B.P., 2000. Late Quaternary paleoclimatic reconstructions for interior Alaska based on paleolake-level data and hydrologic models. Journal of Paleolimnology 24, 29–41.

Begét, J.E., Hawkins, D.B., 1989. Influence of orbital parameters on Pleistocene loess deposition in central Alaska. Nature 337, 151-153.

Bertran, P., 1993. Deformation-induced microstructures in soils affected by mass movements. Earth Surface Processes and Landforms 18, 645–660.

Bertran, P., Texier, J.-P., 1995. Fabric Analysis: Application to Paleolithic Sites. Journal of Archaeological Science 22, 521–535.

Bertran, P., Texier, J.-P., 1999. Facies and microfacies of slope deposits. CATENA 35, 99–121.

Bigelow, N., Begét, J., Powers, R., 1990. Latest Pleistocene increase in wind intensity recorded in eolian sediments from central Alaska. Quaternary Research 34, 160 168.

Bigelow, N.H., Edwards, M.E., 2001. A 14,000 yr paleoenvironmental record from Windmill Lake, Central Alaska: Lateglacial and Holocene vegetation in the Alaska range. Quaternary Science Reviews 20, 203–215.

Bigelow, N.H., Powers, W.R., 2001. Climate, vegetation, and archaeology 14,000–9000 cal yr BP in central Alaska. Arctic Anthropology 38, 171–195.

Dansgaard, W., Johnsen, S.J., Clausen, H.B., Dahl-Jensen, D., Gundestrup, N.S., Hammer, C.U., Hvidberg, C.S., Steffensen, J.P., Sveinbjörnsdottir, A.E., Jouzel, J., 1993. Evidence for general instability of past climate from a 250-kyr ice-core record. Nature 364, 218.

DiPietro, L.M., Driese, S.G., Nelson, T.W., Harvill, J.L., 2017. Variations in late Quaternary wind intensity from grain-size partitioning of loess deposits in the Nenana River Valley, Alaska. Quaternary Research 87, 258–274.

Erlandson, J.M., Moss, M.L., 1996. The Pleistocene-Holocene Transition along the Pacific Coast of North America. In: Straus, L.G., Eriksen, B.V., Erlandson, J.M., Yesner, D.R. (Eds.), Humans at the End of the Ice Age. Springer, pp. 277–301.

Erlandson, J.M., Walser, R., Maxwell, H., Bigelow, N., Cook, J., Lively, R., Adkins, C., Dodson, D., Higgs, A., Wilber, J., 1991. Two early sites of Eastern Beringia: Context and chronology in Alaskan interior archaeology. Radiocarbon 33, 35-50.

Folk, R.L., Ward, W.C., 1957. Brazos River bar [Texas]; a study in the significance of grain size parameters. Journal of Sedimentary Research 27, 3–26.

Gal, R., 2002. Providence and frugality: Tools for high latitude living. In: Paper presented at the 29th Annual Meeting of the Alaska Anthropological Association. Alaska: Anchorage.

Goebel, T., Buvit, I, 2011. Introducing the Archaeological Record of Beringia. In: Goebel, T., Buvit, I. (Eds.), From the Yenisei to the Yukon: interpreting lithic assemblage variability in Late Pleistocene/Early Holocene Beringia. Texas A&M University Press, College Station, TX, pp. 1-32.

Goebel, T., Powers, R., Bigelow, N., 1991. The Nenana complex of Alaska and Clovis origins. In: Bonnichsen, R., Turnmire, K. (Eds.) Clovis origins and adaptations. Oregon State University, Corvallis, OR. pp. 49–79.

Gore, A.K., Graf, K.E., 2018. Technology and Human Response to Environmental Change at the Pleistocene-Holocene Boundary in Eastern Beringia: A View from Owl Ridge, Central Alaska. In: Robinson, E., Sellet, F. (Eds.), Lithic Technological Organization and Paleoenvironmental Change, Studies in Human Ecology and Adaptation. Springer International Publishing, pp. 203–234.

Graf, K.E., Bigelow, N.H., 2011. Human response to climate during the Younger Dryas chronozone in central Alaska. Quaternary International 242, 434–451.

Graf, K.E., Buvit, I., 2017. Human dispersal from Siberia to Beringia: Assessing a Beringian Standstill in light of archaeological evidence. Current Anthropology 58, S583-S603.

Graf, K.E., Goebel, T., 2009. Upper Paleolithic toolstone procurement and selection across Beringia. In: Adams, B., Blades, B. (Eds.), Lithic materials and Paleolithic societies. Wiley-Blackwell, pp. 55–77.

Graf, K.E., Blong, J., Goebel, T., 2010. A concave-based projectile point form new excavations at the Owl Ridge site, central Alaska. Current Research in the Pleistocene 27, 88–91.

Graf, K.E., DiPietro, L.M., Krasinski, K.E., Gore, A.K., Smith, H.L., Culleton, B.J., Kennett, D.J., Rhode, D., 2015. Dry Creek Revisited: New Excavations, Radiocarbon Dates, and Site Formation Inform on the Peopling of Eastern Beringia. American Antiquity 80, 671–694.

Guthrie, R.D., 2003. Rapid body size decline in Alaskan Pleistocene horses before extinction. Nature 426, 169–171.

Guthrie, R.D., 2006. New carbon dates link climatic change with human colonization and Pleistocene extinctions. Nature 441, 207.

Hamilton, T.D., Goebel, T., 1999. Late Pleistocene peopling of Alaska. In: Bonnichsen, R., Turnmire, K.L. (Eds.), Ice Age peoples of North America: Environments, origins, and adaptations of the first Americans. Oregon State University Press, Corvallis, OR, pp. 156-199.

Harding, J.P., 1949. The use of probability paper for the graphical analysis of polymodal frequency distributions. Journal of the Marine Biological Association of the United Kingdom 28, 141–153.

Hoffecker, J.F., Powers, W.R., Goebel, T., 1993. The colonization of Beringia and the peopling of the New World. Science 259, 46–53.

Holmes, C.E., 2001. Tanana River Valley archaeology circa 14,000 to 9000 BP. Arctic Anthropology 154–170.

Hu, F.S., Brubaker, L.B., Anderson, P.M., 1996. Boreal ecosystem development in the northwestern Alaska range since 11,000 yr BP. Quaternary Research 45, 188–201.

Kaufman, D.S., Ager, T.A., Anderson, N.J., Anderson, P.M., Andrews, J.T., Bartlein, P.J., Brubaker, L.B., Coats, L.L., Cwynar, L.C., Duvall, M.L., 2004. Holocene thermal maximum in the western Arctic (0–180 W). Quaternary Science Reviews 23, 529–560.

Kaufman, D.S., Axford, Y.L., Henderson, A.C.G., McKay, N.P., Oswald, W.W., Saenger, C., Anderson, R.S., Bailey, H.L., Clegg, B., Gajewski, K., Hu, F.S., Jones, M.C., Massa, C., Routson, C.C., Werner, A., Wooller, M.J., Yu, Z., 2016. Holocene climate changes in eastern Beringia (NW North America) – A systematic review of multi-proxy evidence. Quaternary Science Reviews.

Kokorowski, H.D., Anderson, P.M., Mock, C.J., Lozhkin, A.V., 2008. A re-evaluation and spatial analysis of evidence for a Younger Dryas climatic reversal in Beringia. Quaternary Science Reviews 27, 1710–1722.

Lewkowicz, A.G., Clarke, S., 1998. Late-summer solifluction and active layer depths, Fosheim Peninsula, Ellesmere Island, Canada. In: Proceedings of the 6th International Conference on Permafrost. Centre d'études Nordiques, Université Laval. pp. 641–666.

Lloyd, A.H., Edwards, M.E., Finney, B.P., Lynch, J., Barber, V.A., Bigelow, N.H., 2006. Holocene development of the Alaskan boreal forest. In: Chapin, F.S., Oswood, M.W., Van Cleve, K., Viereck, L.A., Verbyla, D.L. (Eds.), Alaska's Changing Boreal Forest. Oxford University Press, New York, pp. 62–78.

Mann, D.H., Hamilton, T.D., 1995. Late Pleistocene and Holocene paleoenvironments of the North Pacific coast. Quaternary Science Reviews 14, 449–471.

Matsuoka, N., 1996. Soil moisture variability in relation to diurnal frost heaving on Japanese high mountain slopes. Permafrost and Periglacial Processes 7, 139–151.

Matsuoka, N., Hirakawa, K., 2000. Solifluction resulting from one-sided and two-sided freezing: field data from Svalbard. Polar Geoscience, 13, 187-201.

Middleton, G.V., 1976. Hydraulic interpretation of sand size distributions. The Journal of Geology 405–426.

Muhs, D.R., Bettis, E.A., 2003. Quaternary loess-paleosol sequences as examples of climate-driven sedimentary extremes. Special Papers-Geological Society of America 53–74.

Muhs, D.R., Budahn, J.R., 2006. Geochemical evidence for the origin of late Quaternary loess in central Alaska. Canadian Journal of Earth Sciences 43, 323–337.

Muhs, D.R., Ager, T.A., Bettis, E.A., McGeehin, J., Been, J.M., Begét, J.E., Pavich, M.J., Stafford, T.W., De Anne, S.P., 2003. Stratigraphy and palaeoclimatic significance of Late Quaternary loess–palaeosol sequences of the Last Interglacial–Glacial cycle in central Alaska. Quaternary Science Reviews 22, 1947–1986.

Muhs, D.R., Ager, T.A., Skipp, G., Beann, J., Budahn, J., McGeehin, J.P., 2008. Paleoclimatic significance of chemical weathering in loess-derived paleosols of subarctic central Alaska. Arctic, Antarctic, and Alpine Research 40, 396–411.

NPS, 2018. https://www.nps.gov/dena/learn/nature/climate.htm

Petit, J.R., Jouzel, J., Raynaud, D., Barkov, N.I., Barnola, J.-M., Basile, I., Bender, M., Chappellaz, J., Davis, M., Delaygue, G., Delmotte, M., Kotlyakov, V.M., Legrand, M., Lipenkov, V.Y., Lorius, C., PÉpin, L., Ritz, C., Saltzman, E., Stievenard, M., 1999. Climate and atmospheric history of the past 420,000 years from the Vostok ice core, Antarctica. Nature 399, 429–436.

Péwé, T.L., Wahraftig, C., Weber, F.R., 1966. Geologic map of the Fairbanks quadrangle, Alaska. USGS.

Phippen, P., 1988. Archaeology at Owl Ridge: A Pleistocene-Holocene Boundary Age Site in central Alaska. M.A. Thesis, University of Alaska, Fairbanks.

Plaskett, D.C., 1976. Preliminary report: A cultural resources survey in an area of the Nenana and Teklanika rivers of Central Alaska. Submitted to Alaska Division of Parks, Anchorage

Potter, B.A., 2005. Site structure and organization in Central Alaska: Archaeological investigations at Gerstle River. Ph.D. Thesis. University of Alaska, Fairbanks.

Potter, B.A., 2008. Radiocarbon chronology of central Alaska: Technological continuity and economic change. Radiocarbon 50, 181–204.

Potter, B.A., Holmes, C.E., Yesner, D.R., 2013. Technology and economy among the earliest prehistoric foragers in interior eastern Beringia. Paleoamerican Odyssey. Texas A&M University Press, College Station, TX, pp 81–103.

Powers, W.R., Hoffecker, J.F., 1989. Late Pleistocene settlement in the Nenana valley, central Alaska. American Antiquity 263–287.

Pye, K., 1995. The nature, origin and accumulation of loess. Quaternary Science Reviews 14, 653–667.

Pye, K., Zhou, L.-P., 1989. Late Pleistocene and Holocene aeolian dust deposition in north China and the northwest Pacific Ocean. Palaeogeography, Palaeoclimatology, Palaeoecology 73, 11–23.

Rupp, T.S., Chapin, F.S., Starfield, A.M., 2000. Response of subarctic vegetation to transient climatic change on the Seward Peninsula in north-west Alaska. Global Change Biology 6, 541–555.

Schaefer, C.E.R., Ker, J.C., Gilkes, R.J., Campos, J.C., Da Costa, L.M., Saadi, A., 2002. Pedogenesis on the uplands of the Diamantina Plateau, Minas Gerais, Brazil: a chemical and micropedological study. Geoderma 107, 243–269.

Straus, L.G., Eriksen, B.V., Erlandson, J.M., Erlandson, J., Yesner, D.R., 1996. Humans at the End of the Ice Age: The Archaeology of the Pleistocene-Holocene Transition. Springer Science & Business Media.

Stuart, A.J., Kosintsev, P.A., Higham, T.F.G., Lister, A.M., 2004. Pleistocene to Holocene extinction dynamics in giant deer and woolly mammoth. Nature 431, 684.

Taylor, K.C., Lamorey, G.W., Doyle, G.A., Alley, R.B., Grootes, P.M., Mayewski, P.A., White, J.W.C., Barlow, L.K., 1993. The ‘flickering switch’ of late Pleistocene climate change. Nature 361, 432–436.

Thorson, R.M., 1975. Late Quaternary history of the Dry Creek area, central Alaska. Ph.D. thesis, University of Alaska, Fairbanks.

Thorson, R.M., Bender, G., 1985. Eolian deflation by ancient katabatic winds: a late Quaternary example from the north Alaska Range. Geological Society of America Bulletin 96, 702–709.

Thorson, R.M., Hamilton, T.D., 1977. Geology of the Dry Creek Site; a stratified Early Man site in interior Alaska. Quaternary Research 7, 149–176.

Tsoar, H., Pye, K., 1987. Dust transport and the question of desert loess formation. Sedimentology 34, 139–153.

Van Vliet-Lanoe, B., 1985. Frost effects in soils. In: Boardman, J. (Ed.), Soils and quaternary landscape evolution, John Wiley and Sons, pp. 117-158.

Vandenberghe, J., 2013. Grain size of fine-grained windblown sediment: A powerful proxy for process identification. Earth-Science Reviews 121, 18–30.

Vepraskas, M.J., 2001. Morphological features of seasonally reduced soils. In: Vepraskas, M.J., Richardson, J.L. (Eds.), Wetland soils: Genesis, Hydrology Landscapes, and Classification, CRC Press, Boca Raton, FL, pp. 163–82.

Viau, A.E., Gajewski, K., Sawada, M.C., Bunbury, J., 2008. Low- and high-frequency climate variability in eastern Beringia during the past 25 000 years. Canadian Journal of Earth Sciences 45, 1435-1453.

Weltje, G.J., Prins, M.A., 2003. Muddled or mixed? Inferring palaeoclimate from size distributions of deep-sea clastics. Sedimentary Geology, Climate Impact on Sedimentary Systems 162, 39–62.

West, F.H. (Ed.), 1996. American Beginnings: The Prehistory and Palaeoecology of Beringia. University of Chicago Press, Chicago, IL.

Wygal, B.T., 2009. Prehistoric colonization of southcentral Alaska: human adaptations in a post glacial world. Ph.D. Thesis, University of Nevada, Reno.

Wygal, B.T., 2018. The peopling of eastern Beringia and its archaeological complexities. Quaternary International 466, 284–298.

Wygal, B.T., Goebel, T., 2011. Deglaciation and the Archaeology of Trapper Creek, Southcentral Alaska. Current Research in the Pleistocene 28, 136.

Wygal, B.T., Heidenreich, S.M., 2014. Deglaciation and Human Colonization of Northern Europe. Journal of World Prehistory 27, 111–144.

Yesner, D.R., 2001. Human dispersal into interior Alaska: antecedent conditions, mode of colonization, and adaptations. Quaternary Science Reviews 20, 315–327.

Younie, A.M., Gillispie, T.E., 2016. Lithic Technology at Linda's Point, Healy Lake, Alaska. Arctic 69, 79-98.

Zimov, S.A., Chuprynin, V.I., Oreshko, A.P., Chapin, F.S., Reynolds, J.F., Chapin, M.C., 1995. Steppe-Tundra Transition: A Herbivore-Driven Biome Shift at the End of the Pleistocene. The American Naturalist 146, 765–794.